Master's thesis

NTNU
Norwegian University of Science and Technology
Faculty of Engineering
Department of Structural Engineering

Lars Dalhaug
Torgeir Tveraaen

Effect of fiber and post-tensioned reinforcement on pile supported ground slabs

Master's thesis in Civil and Environmental Engineering
Supervisor: Terje Kanstad
June 2022

NTNU
Kunnskap for en bedre verden

Lars Dalhaug
Torgeir Tveraaen

Effect of fiber and post-tensioned reinforcement on pile supported ground slabs

Master's thesis in Civil and Environmental Engineering
Supervisor: Terje Kanstad
June 2022

Norwegian University of Science and Technology
Faculty of Engineering
Department of Structural Engineering

NTNU

Kunnskap for en bedre verden

Department of Structural Engineering
Faculty of Engineering
NTNU – Norwegian University of Science and Technology

ACCESSIBILITY

OPEN

MASTER THESIS 2022

SUBJECT AREA:	DATE:	NO. OF PAGES:
Concrete Structures	08.06.2022	87 + 57

TITLE:

Effect of fiber and post-tensioned reinforcement on pile supported ground slabs

Innvirkning av fiber- og spennarmering på peleunderstøttede fundamentplater

BY:

Lars Dalhaug

Torgeir Tveraaen

SUMMARY:
A pile supported ground slab behaves similarly in ULS as flat slabs, with punching shear failure and flexural failure as the main problems. In SLS however, cracking is the main challenge. By including fiber and post-tensioned reinforcement, these issues can be avoided. Different combinations of conventional, PT and fiber reinforcement are therefore investigated in this thesis. ULS is the main emphasis, but SLS performances and aspects during execution are also discussed.

A real pile supported ground slab from a construction site in Trondheim serves as a basis for designing several different reinforcement solutions in this thesis. This slab is analyzed regarding to ULS, and the methods used are equivalent frame method and yield line theory. Yield line theory is used to a small extent in several countries but serves many advantages. Therefore, to better evaluate if yield line theory is a suitable method, it is compared to EFM. EFM is in this thesis based on an LFEA and NB 33. Yield line proves to be an effective method to reduce the reinforcement amount. The LFEA gives axial forces in the piles and serves as a basis for the punching shear calculations. To include fiber reinforcement, it is necessary to apply the proposed new Eurocode. The current Eurocode is also used, and the two Eurocodes are compared. All the investigated reinforcement solutions have sufficient punching shear capacity according to both Eurocodes. The solutions including fibers have the highest capacity.

PT reinforcement is found to be efficient for reducing the necessary reinforcement amount, even when reducing the slab thickness. The fiber reinforced solutions achieve sufficient capacity, especially in shear, but require the largest amount of steel. The results show that a fiber only solution is feasible and would be a time effective solution. A combination of PT and fiber reinforcement is beneficial for ULS and SLS performance. Furthermore, such a reinforcement solution will also be time-efficient to produce.

RESPONSIBLE TEACHER: Terje Kanstad

SUPERVISOR(S): Terje Kanstad

CARRIED OUT AT: Department of Structural Engineering

Abstract

A pile supported ground slab behaves similarly in ULS as flat slabs, with punching shear failure and flexural failure as the main problems. In SLS however, cracking is the main challenge. By including fiber and post-tensioned reinforcement, these issues can be avoided. Different combinations of conventional, PT and fiber reinforcement are therefore investigated in this thesis. ULS is the main emphasis, but SLS performances and aspects during execution are also discussed.

A real pile supported ground slab from a construction site in Trondheim serves as a basis for designing several different reinforcement solutions in this thesis. This slab is analyzed regarding to ULS, and the methods used are equivalent frame method and yield line theory. Yield line theory is used to a small extent in several countries but serves many advantages. Therefore, to better evaluate if yield line theory is a suitable method, it is compared to EFM. EFM is in this thesis based on an LFEA and NB 33. Yield line proves to be an effective method to reduce the reinforcement amount. The LFEA gives axial forces in the piles and serves as a basis for the punching shear calculations. To include fiber reinforcement, it is necessary to apply the proposed new Eurocode. The current Eurocode is also used, and the two Eurocodes are compared. All the investigated reinforcement solutions have sufficient punching shear capacity according to both Eurocodes. The solutions including fibers have the highest capacity.

PT reinforcement is found to be efficient for reducing the necessary reinforcement amount, even when reducing the slab thickness. The fiber reinforced solutions achieve sufficient capacity, especially in shear, but require the largest amount of steel. The results show that a fiber only solution is feasible and would be a time effective solution. A combination of PT and fiber reinforcement is beneficial for ULS and SLS performance. Furthermore, such a reinforcement solution will also be time-efficient to produce.

Sammendrag

En peleunderstøttet fundamentplate oppfører seg på samme måte som flatdekke i ULS, der gjennomlokking og bøyemomentbrudd er hovedproblemene. I SLS er det derimot forskjell, der sprekkdannelse ofte er hovedutfordringen for fundamentplater. Ved å benytte fiber og etteroppspent armering, kan disse utfordringene unngås. Ulike kombinasjoner av konvensjonell, etteroppspent og fiberarmering er derfor undersøkt i denne oppgaven. ULS er i hovedfokus, men egenskaper knyttet til SLS og utførelse er også undersøkt.

En peleunderstøttet fundamentplate fra et byggeprosjekt i Trondheim blir brukt som grunnlag for å prosjektere ulike armeringsløsninger i denne oppgaven. Denne platen er analysert med hensyn til ULS, og metodene som er brukt er ekvivalent rammemetode og bruddlinjeteori. Til tross for flere fordeler, er bruddlinjeteori benyttet i liten grad, blant annet i Norge. I denne oppgaven er rammemetoden basert på lineær elementanalyse og NB 33. Bruddlinjeteori viser seg å være en effektiv metode for å redusere armeringsmengden. Den lineære elementanalysen gir også aksialkrefter i pelene, som brukes til å regne ut gjennomlokking. For å kunne inkludere fiberarmering i disse beregningene, er den foreslåtte nye Eurokoden benyttet. Den nåværende Eurokoden er også benyttet, og disse to Eurokodene er sammenlignet. Alle de undersøkte armeringsløsningene har tilstrekkelig gjennomlokkingskapasitet ifølge Eurokodene. Løsningene som innebærer fiberarmering, gir de høyeste kapasitetene.

Etteroppspent armering viser seg å være effektivt til å redusere nødvendig armeringsmengde, selv ved redusert platetykkelse. Løsningene med fiberarmering oppnår tilstrekkelig kapasitet, og gir svært god kapasitet i skjær. Disse løsningene fører riktignok til det største forbruket av armering. Resultatene viser at løsningen med kun fiber er en mulig og svært tidseffektiv løsning. En kombinasjon av etteroppspent og fiberarmering er fordelaktig for både ULS og SLS. En slik armeringsløsning vil også være tidseffektiv.

Preface

This master thesis has been written with the Department of Structural Engineering at the Norwegian University of Science and Technology as a part of the study program Civil and Environmental engineering. It is the culmination of five years' study to obtain a master's degree.

During the twenty weeks through which the work on this thesis has lasted, we have encountered challenges, but also the highs of overcoming these. It has been a long and demanding, but also very educational process.

Our main motivation behind this project was to learn more about how to design concrete structures with regards to aspects such as economic impact, material savings and practical appliance. Through our investigation into these parameters, a deeper understanding of how innovative solutions such as fiber and post-tensioned reinforcement affect a concrete structure was gained.

We would like to thank our supervisor Terje Kanstad for answering our countless questions and providing endless encouragement, this thesis would not be the same without his guidance. Steinar Trygstad of Dr. Ing. Steinar Trygstad AS also deserves our gratitude for supplying input and insight from his project on Øvre Nyhavna in Trondheim, upon which this thesis is based.

Table of contents

1 Introduction

Concrete is the most used building material in the world, and slabs are among the structures in which the most concrete is used. In recent decades, the environmental impact of concrete structures has become increasingly important. Thus, choosing concrete designs based on parameters reaching beyond mechanical capacity and structural properties is an essential part of the modern design process.

A concrete structure must fulfill demands for both SLS and ULS in order to function satisfactorily. For SLS, properties like deflection and crack widths are of particular interest. The most important of these properties vary depending on the type of structure which is being designed. For most flat slabs, deflections will be of importance. However, for ground slabs exposed to hostile environments or intensive use, crack width might be considered more crucial. In the literature as well as most design processes, flat slabs have been given extensive attention. This is mainly because flat slabs comprise a large percentage of the concrete in many construction projects and, consequently, provide the largest reward when optimized. Ground slabs, however, are less extensively examined, although they present interesting opportunities for new designs. Thus, this thesis investigates a pile supported flat slab in ULS design.

This investigation consists of an assessment of two methods for ULS analysis, namely the Equivalent Frame Method (EFM) and the yield line theory. Punching shear procedures from the current EC2 and the proposed new EC2 are also examined. Several different reinforcement solutions, consisting of conventional, post-tensioned (PT) and fiber reinforcement, are compared using these ULS analyses. In this thesis, SLS calculations is excluded, due to restraints in time and resources. Furthermore, all analyses and assessments are made with cast-in-situ concrete in mind.

For ULS, a pile supported ground slab acts similarly to a flat slab. The moment capacity and punching shear capacities for these structures are important to control. This can be done with both elastic and plastic calculation methods. Elastic calculations might lead to conservative solutions since it does not allow the concrete to crack. This might however be desirable for properties regarding SLS. A linear finite element analysis (LFEA) facilitates such solutions by producing elastic load actions. Plastic calculations, on the other hand, tend to be less conservative and might also be easier to implement, depending on the method. EFM is a method where a slab is divided into different strips. The design moments are constant over each strip but vary between the strips. The ratios between the design moments are given in publications. NB 33, for instance, has its own factors. EFM is also possible to use based on an LFEA, where the moments are spread over the strips. An even faster and less conservative method is yield line theory. This is based on equilibrium between internal work done in the yield lines, and external work contributed by the loads. This is an upper bound method, meaning the results are either correct or on the unsafe side, so additional precautions need to be taken. The obtained reinforcement solution is orthotropic, and the necessary reinforcement amount is low. For EFM, the necessary reinforcement amount tends to be higher and more varied over the slab. As for moment distributions, punching shear is also possible to calculate both with elastic and plastic analysis. The punching shear capacity procedures are well established for conventional reinforcement in current Eurocode 2. Prestressed reinforcement is also

accounted for. The calculation procedures will however change when the new Eurocode 2 gets implemented. This is, among other things, due to an increased usage of fiber reinforced concrete (FRC), which needs to be accounted for.

Conventional, prestressed and fiber reinforcement all have great properties, and some disadvantages. Conventional reinforcement is well-established and has been used for many years with success. However, using prestressed and/or fiber reinforcement instead or combined with rebars might reduce material consumption. Other advantages may also be gained. They have for instance great crack reducing properties and perform well in shear. Fibers are very effective when it comes to production time. Prestressed reinforcement, on the other hand, is very suitable for leaner constructions, which again leads to lower material consumption.

These reinforcement types are possible, and sometimes preferable, to combine. Hence, this thesis examines different reinforcement solutions. The investigated solutions are Conventional reinforcement (A); Conventional and PT (B); Conventional and PT with decreased thickness (C); Conventional, PT and fibers (D); PT and fibers (E); and fibers (F). These are examined for ULS mainly, with moment capacity and punching shear capacity as the main emphasis. EFM and yield line theory are both used, mainly to be able to compare all solutions, since EFM is not applicable for solution F. Also, yield line theory is an effective method which keeps the material consumption at a low level but is still used to a small extent in several countries. Thus, to compare yield line theory with EFM is of interest. For punching shear assessment, the current Eurocode 2 does not cover fiber reinforcement, although the new Eurocode 2 allows this. There are further differences in the punching shear capacity calculations of the two versions of EC2. For better comparisons between the reinforcement solutions, these differences are investigated, and the current and new EC2 are therefore compared. Beyond this, several aspects regarding SLS and conditions regarding production time, economy and environmental issues are discussed, in order to evaluate the reinforcement solutions on a broader basis.

Abbreviations

Some of the most frequently used terms and references are abbreviated in the full text to enhance the reading experience. These abbreviations are listed and explained below. In addition, all terms are explained in the context in which they are used.

EFM	Equivalent Frame Method
FK	Focus Konstruksjon
PT	Post tensioned
SCC	Self-compacting concrete
NB 33	Norsk Betongforenings publikasjon nr. 33
NB 38	Norsk Betongforenings publikasjon nr. 38
EC2:2004	NS-EN 1992-1-1:2004, current Eurocode
EC2:2021	NS-EN 1992-1-1:2021, proposed new Eurocode
LFEA	Linear Finite Element Analysis
CMA	Compressive Membrane Action
FRC	Fiber Reinforced Concrete

2 Theory overview

This chapter provides an overview of the different aspects of pile supported concrete ground slabs in the scientific literature, in addition to central methods for analyzing such slabs and different effects which may alter a ground slab's behavior. Furthermore, different reinforcement types and combinations of reinforcement types will be discussed.

A short historical overview of flat slabs is provided, as well as an introduction to the main issues concerning both flat slabs and pile supported slabs. It is stated in Eurocode 2 that flat slabs may be designed with methods such as finite element analysis (FEA), yield line analysis or equivalent frame method analysis (EC2, I.1.1). In this thesis, yield line and equivalent frame analysis will be used and is, therefore, discussed in this chapter. In recent decades, new reinforcement types have been introduced into concrete structures in general. For slabs, due to their geometry and usually large volume, steel fiber reinforcement has been increasingly used (Destree, 2009). Therefore, steel fiber reinforcement, in addition to reinforcement types such as prestressing and conventional bars, will be presented in this chapter.

2.1 Flat slabs

Concrete is a dense material with negligible tensile strength (Oikonomou-Mpegetis, 2013, p. 35). These material properties mean that concrete structures need reinforcement to handle tensile stresses. Historically, this has made concrete slabs dependent on the use of beams for support and deflection control. This changed around 1910, when the first pioneering construction of buildings with floors of slabs supported only on columns started appearing (Fürst & Marti, 1997). Design methods based on theory of elastic plates were developed in the 1920s, and this way of constructing such slab systems, known as flat slabs, then became the dominant method.

Flat slabs are essentially a large concrete plate supported by columns, where the columns are connected to the plate on its underside. This makes the slab continuous and without openings or "humps" where the columns attach. The plate thus consists of a series of slab segments resting on four columns, named bays. Figure 1 shows a flat plate bay suspended between four columns.

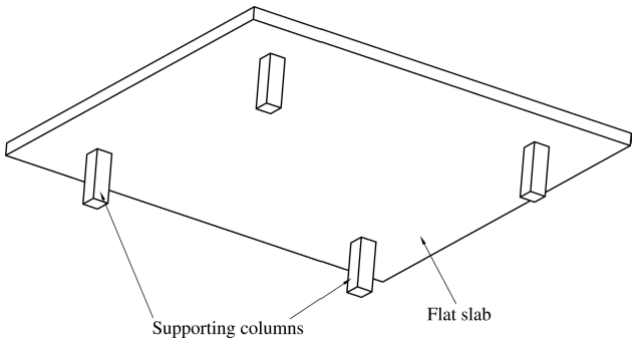

Figure 1: Layout of a flat slab bay resting on columns (Sahab et al., 2005).

In buildings constructed of reinforced concrete that are several stories high, floor systems of flat slabs have several benefits (Sahab et al., 2005). They allow for fast and efficient construction, provide an economical story-height, and facilitate flexible and modifiable area usage etc. These advantages have led to most high-rise buildings being constructed using such flat slab systems in recent decades. Cost-optimization of concrete structures and, as a result, a more efficient construction process with less environmental impact has been a work in progress as this building method has increased in popularity (Sarma & Adeli, 1998). Floor systems of flat slabs can be designed as regular and symmetrical systems, with standardized column spacings and rectangular slab segments of constant size. Thus, an automated optimization process is possible, with economic and material savings increasing with the size of the project. As computing power has improved and the use of algorithms has become more widespread, these efforts have resulted in more effective models for optimizing the design of floor systems (de Albuquerque et al., 2012).

Flat slabs consist of plate segments divided into panels, or bays, suspended between columns, and are generally slender structures. Deflections of flat slabs are generally 20-40% larger than for equivalent beam supported slabs (Hagberg et al., 2004, p. 8). Thus, deflection of bays in SLS is a major problem that needs to be handled during design of such structures. Calculating these deflections is challenging, and there have been many attempts to produce efficient and precise calculation tools for this problem (Van Gorder, 2012). Since flat slabs rest on columns, they are exposed to large, concentrated loads close to the column faces. These large, concentrated loads act in addition to flexure. Thus, punching shear failure near columns is a major risk in ULS for such systems (Abbood & Al-Bayati, 2021). The last major design issue that must be addressed for flat slabs is flexural resistance.

2.2 Pile supported slabs

Ground floor slabs have the primary function of transferring the imposed loads from the structure into the ground. In some cases, this load is too large for the ground to withstand. This is especially true for structures such as industrial warehouse floors, which are exposed to heavy live loads during their entire service life (Concrete Society, 2016). Thus, piles driven into the ground are needed to ensure sufficient load bearing capacity. This is achieved either by utilizing friction between the piles and the soil, or by anchoring the piles to rock (Oikonomou-Mpegetis, 2013, p. 29). A layout of pile heads and ground, or sub-base, for a pile supported slab is exemplified in Figure 2, and Figure 3 illustrates how a slab rests on a pile head.

Figure 2: Layout of pile heads and sub-base underneath a pile supported slab (Hulett, 2011).

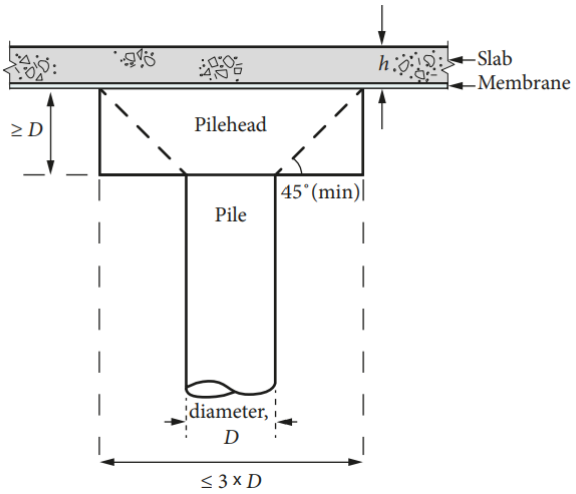

Figure 3: Detail of slab resting on a level pile head, an ideal method of construction for reduced restraint (Concrete Society, 2016).

Pile supported slabs share many attributes with flat slab floor systems in, for instance, office buildings (Hulett, 2011). Since pile supported slabs rest on piles and the ground underneath gives no or negligible support at large loads, they behave similarly to flat slabs. Thus, both types of structures are designed using methods developed for flat slabs. A key difference, however, is that pile supported slabs, especially in industrial buildings such as warehouses, are exposed to the environment. Suspended floors are covered by a ceiling on the underside and raised floors on top. Therefore, cracking in SLS is not necessarily observed on suspended floors, as opposed to on ground floors. Furthermore, in industrial floors with surface cracking, loads from trucks and other machinery may cause abrasion and accelerated deterioration of the floor. Thus, crack width control in SLS is particularly important when designing pile supported ground

floors. To handle this issue, The Concrete Society recommends using enlarged pile heads in addition to designing and constructing pile heads with great care (2016, p. 42). Furthermore, details such as joints and slip membranes must limit shrinkage restraint as much as possible, and the concrete mix should be designed to avoid large shrinkage potential.

Pile supported slabs are not suspended between columns in the same manner as flat slabs. Thus, deflections are not usually a problem, but may still cause significant problems in SLS. Usually, flexure of plate segments due to heavy loads is the main cause of deflections in flat slabs, whereas in pile supported slabs, settlement of the ground or the piles may play a major role in deflection development (Concrete Society, 2016).

2.3 Membrane action

Membrane action, or compressive membrane action (CMA), is a known phenomenon in continuous reinforced concrete slabs (Peel-Cross et al., 2001). It occurs when a slab deflects and cracks in the tensile zone. During deflection, the neutral axis moves towards the concrete's compressive edge and the ends try to expand. If the ends are laterally restrained, the expansion is prevented. This restraint induces arching forces that make the slab stiffer and increase the load bearing capacity. Figure 4 illustrates the phenomenon.

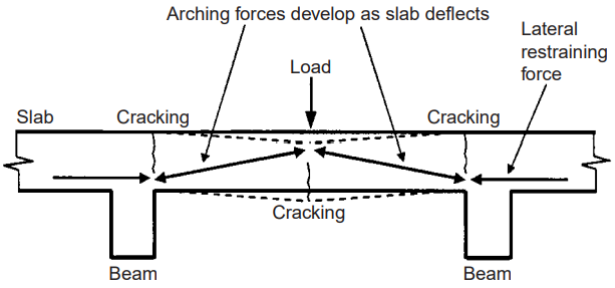

Figure 4: Arching forces caused by lateral restrained ends in a deflected concrete slab (Peel-Cross et al., 2001).

This effect can in some cases give considerably higher load capacity than the design capacity obtained for instance from yield line theory analysis. The amount of capacity increase depends, among other things, on the concrete's compressive strength, span to depth ratio and the amount of lateral restraint available (Peel-Cross et al., 2001). The increase in capacity is larger for suspended and pile supported slabs than in ground bearing slabs (Eyre, 2006). This is due to the lateral restraint offered by the piles or columns. In slabs, CMA occurs as a ring of arching forces around the deflected area. This means loading close to edges or joints will only produce a small contribution from this effect. Thus, large, jointless slabs are the structures benefitting the most from CMA.

2.4 Deflections

As previously mentioned, deflections might be a problem in SLS for pile supported slabs. A soil investigation should be conducted in order to determine parameters for calculation of long- and short-term deflection of the piles in the soil (Concrete Society, 2016). The soil gives some resistance at small loads, which may help limit deflections at SLS-level loading. If the slab develops excessive cracking however, its capacity to transfer loads deteriorates to the point where unacceptable deformations of some segments of the pile

supported slab occur. This type of problem can also arise from insufficient load transferring capacity in joints.

In the US, ACI guidelines limit allowed deflections to L/360 (Ojo, 2021), and in Europe, Eurocode 2 uses L/250 (CEN, 2004). Here, L represents the span length. It is common that measures such as sufficient slab thickness and limiting span lengths by reducing pile spacing will result in deflections that satisfy at least the European limits (Concrete Society, 2016). If more detailed documentation on deflections is required, it is usually done through a FEA. In these situations, effects such as reduced elastic modulus and settlement of piles should be included. The deflection of a slab floor system is complex, where each bay's deflection is affected by the deflection of adjacent bays. A deflection calculation should therefore be considered as an estimate rather than as an exact value (Ojo, 2021). In general, sophisticated computer programs that account for several factors such as cracking, tension stiffening, creep, shrinkage and load history may give good results compared to physical testing (Hirsch, 2009).

2.5 Cracking

In addition to handling the intended loads, avoiding surface cracking is the primary design objective when designing a pile supported slab (Concrete Society, 2016). Cracking can cause large problems with aesthetics, and, in some cases, excessive cracking may influence the structural soundness of a slab related to functionality and durability. These issues can have financial consequences even if the load capacity of the slab is not significantly reduced, due to extensive repairs being necessary (Oikonomou-Mpegetis, 2013). Cracking is most commonly associated with lateral restraint against shrinkage, though early loading can also play a major role (Concrete Society, 2016). Since pile supported slabs are often cast in large segments, where joints may be far in between or even non-existent, the risk of cracking from shrinkage restraint can be substantial. Sometimes however, large loads and early loading might cause cracking as well. Usually, restraint-cracks are small and impose no threat to structural soundness. In certain situations, however, restraint-cracks may occur in areas with sustained loading. These circumstances are especially likely to occur in industrial floors, where trucks and heavy aisles impose loads daily directly on the slab and may force a full stop in all operations to conduct repairs. This might be expensive and should, therefore, be avoided. A concrete mix with less shrinkage, frictionless surfaces, joints, pile head design and reinforcement design are some measures which can be taken to handle shrinkage (Concrete Society, 2016; Oikonomou-Mpegetis, 2013). When designing pile supported slabs, it is important to design for limiting the extent of cracking, and not limiting crack-widths (Hulett, 2011). This is because many very fine cracks are difficult to repair, as opposed to fewer and wider cracks, and they might drastically increase the deterioration rate of the slab. This is especially relevant for industrial floors, where the fine cracks are directly exposed to loading.

In addition to these measures, limiting the bending moments over the pile heads in SLS will reduce the extent of cracking. In order to accurately calculate crack widths as a function of loading, a non-linear finite element analysis (NLFEA) must be conducted (Concrete Society, 2016). In such an analysis, effects like redistribution of stresses and progressive yielding should be included. However, this is not always necessary. If the guidelines listed above are followed, this should prevent problems with cracking. Furthermore, design in ULS with, for instance, yield line analysis can give some assurance of satisfactory slab performance. This type of analysis is only applicable on a

fully cracked slab, and the location of major cracks must be known beforehand. If this is known, the crack pattern can be designed for, and repair measures can be included. Another design measure that can be taken is to design the slab elastically over the pile heads. This may result in expensive solutions but ensures that the applied moment to moment capacity ratio is low. The resistance to cracking is improved by adding fibers into the concrete which bridge cracks (Oikonomou-Mpegetis, 2013), or by prestressing the slab to remove tensile stresses by imposing compressive stresses (Concrete Society, 2016; Ojo, 2021).

2.5.1 Water-tightness in concrete slabs

Annex H in the new version of Eurocode 2, expected to be released in 2022, provides guidance on water-tightness in concrete structures (CEN, 2021).This guidance is for structures that must be tight enough to avoid leakage either from water kept within storage, or from water on the outside such as ground water. Annex H classifies concrete structures into tightness classes according to leakage requirements. For each tightness class there are provided tightness criteria, from general crack limiting procedures given in NS-EN 1992-1-1:2021, clause 9.2 for the most lenient tightness class, to special measures needed to satisfy the strictest tightness class. Among the general guidelines that are provided in Annex H are examples of how to adequately compose the concrete mix for water-tightness, designing members with sufficient thickness and use of adequate reinforcement for crack distribution and crack-width limitation. It is worth noting that use of fiber reinforced concrete or post-tensioned concrete are highlighted as more efficient alternatives to using large amounts of conventional reinforcement in order to control cracking.

2.6 Yield line theory

In this chapter, the background for yield line theory is explained. This includes the physical principles behind this theory, in addition to advantages, disadvantages and limitations for the method.

2.6.1 Principles of the yield line theory

The yield line theory might be used to investigate failure mechanisms at the Ultimate Limit State (Ojo, 2021). This means that the imposed load approaches the failure load. When this happens, the cracks will grow where the moments are highest, and the reinforcement in these areas will begin to yield. The slab collapses when the full yield line pattern occurs and the reinforcement in these regions yield. It is a fast and simple method to use but it requires a good understanding of the formations of yield line patterns, as well as the assumptions behind the theory.

For yield line theory to work, it is assumed that the slab consists of rigid bodies between the yield lines. This is a close approximation when the deformations are big. At smaller deformations however, when the elastic deformations are significant, this does not give a true depiction of the behavior (Oikonomou-Mpegetis, 2013). The yield line analysis will in these cases overestimate rotations since the neglected elastic deformation is significant at small displacements. The yield line method does therefore not predict the response up to the first crack very well. Also, to achieve plastic deformation, sufficient ductility is important. This is achieved by using relatively small amounts of reinforcements in both the positive and negative yield lines. The ratio between these yield lines must therefore be between 0.5 and 2 (Løset, 2021). Another assumption made in yield line theory is that the moment of resistance is constant. For fiber reinforced concrete, however, the

moment of resistance will in reality decrease with increased crack width. This is important to consider to avoid an overestimation of the capacity.

The yield line theory is based on the principle of balance of internal and external work (Kennedy & Goodchild, 2004). In other words, this means that the work done internally by plane segments rotating along yield lines equals the work done externally by the load deforming the structure. The yield lines are straight lines that occur at the most stressed areas of the slab, where the reinforcement yields. These lines are axes of rotation, or continuous plastic hinges. When calculating, it might be necessary to investigate several yield line patterns. The yield line pattern which gives the lowest corresponding load, or the highest corresponding moments, will be the correct one. The design of the slab should therefore be based on this critical pattern. Figure 5 shows an example of a slab with two possible yield line patterns. How the yield lines will form, depends on the geometry and boundary conditions of the slab. Figure 6 and Figure 7 show how the yield line patterns are affected by these conditions.

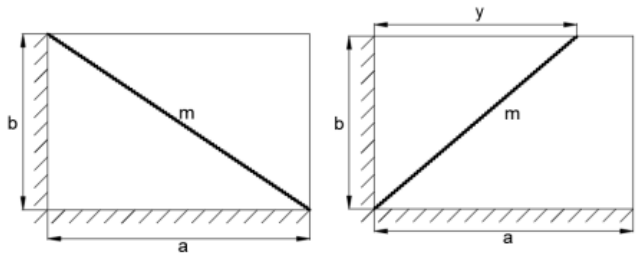

Figure 5: Two different yield line patterns for the same slab (Løset, 2021).

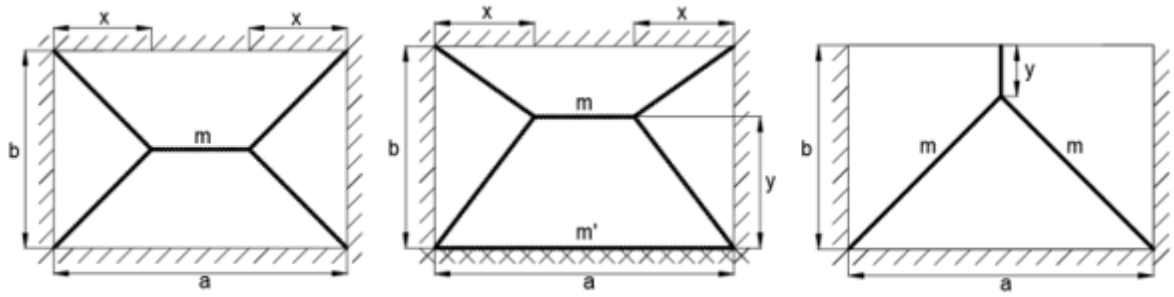

Figure 6: Yield line patterns affected by the geometry and boundary conditions of the slab (Løset, 2021).

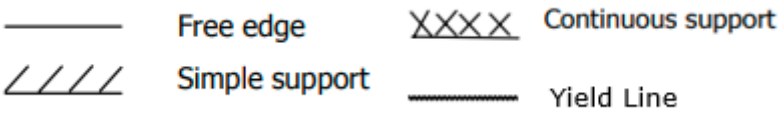

Figure 7: Drawing notation.

There are different ways to apply this theory. The work method and use of standard formulae are the most frequently used applications. Standard formulae are a fast method to use. Different slabs have their own sets of formulae, so for standard slabs, this method works well. The formulae might however become complicated for some cases.

The work method is the most used method. It is based on the same principle, but there are no formulae to follow. Both the internal and external work must be calculated, and the equilibrium must be solved. The internal work, or the work done in the yield lines, is usually written as the moment of resistance times the angle between the rigid bodies, times the length of the yield line. The internal work in all yield lines is then summed up. The external work is the work done by external loads. For a point load, this would be the load times the vertical displacement. For a uniformly distributed load, it is the deflected volume times the load. The external work for all regions is then summed up. Knowing that internal work equals external work, it is possible to find either the load required for the slab to yield, or the moment of resistance at which the slab yields. This method can be simply expressed by the following formulae (Kennedy & Goodchild, 2004, p. 23):

$$External\ energy\ expended\ by\ loads\ moving = Internal\ energy\ dissipated\ by\ rotations$$

$$Expended = Dissipated$$

$$E = D$$

$$\sum(N * \delta)_{\ all\ regions} = \sum(m * l * \theta)_{all\ regions}$$

Here, N denotes the external load acting on a region, δ is the deformation caused by the external load in the region, m is the moment of resistance of the slab along a yield line (per meter length), l is the length of the given yield line, θ is the rotation of a region about a yield line. Diagonal yield lines are split into two orthogonal directions and treated individually, then these individual contributions are summed together. These parameters are illustrated in Figure 8.

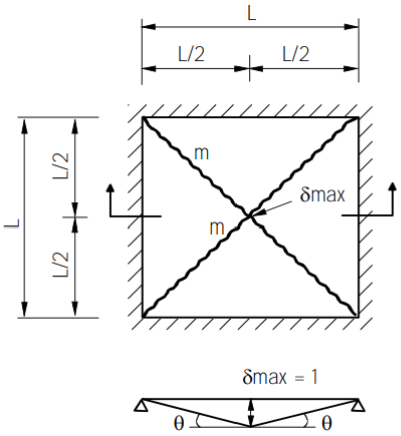

Figure 8: Illustration of yield lines and deflection from an external load in the work method (Kennedy & Goodchild, 2004, p. 25).

2.6.2 Advantages and limitations

There are several advantages by using yield line theory. Firstly, it is a simple and fast method. By using this method, the designed slabs are also more economic and sustainable. This is because it considers failure mechanisms at ultimate limit state and is an upper bound method according to the theory of plasticity. Since it is an upper bound method, the amount of reinforcement is quite low, and the slabs are relatively thin.

There are also some limitations or disadvantages with this method. Because it assumes a failure mechanism, it is not suitable for serviceability issues like crack widths or deflections. As it is an upper bound theory, it might be unsafe. The method also demands

a good understanding of the structure's behavior, since it is necessary to determine the location of the yield lines that will develop.

2.6.3 Upper bound theory

The yield line theory is an upper bound theory according to the theory of plasticity. This means that solutions calculated according to this theory are either correct or «unsafe», which means that the calculated capacity might be higher than the real capacity. In most calculations, the yield line solution will be within 10% of the mathematically correct solution, and it is therefore common to increase the yield line solution with 10% to be on the safer side (Kennedy & Goodchild, 2004). This is called the "10% rule". In addition, it should be noted that slabs might experience compressive membrane action and strain hardening of reinforcement, which will give increased capacities. Even though the calculations might be theoretically "unsafe", the mentioned effects and the 10% rule tend to make the calculations safe, and the yield line theory can therefore be used (Kennedy & Goodchild, 2004). In addition to this, the complexity of slabs on an irregular grid of columns causes an increase of 15% to the calculated moment of resistance to be a necessary margin of safety (Kennedy & Goodchild, 2004, p. 121).

2.6.4 Application on pile supported slabs

For flat slabs supported on a rectangular grid of columns, as well as pile supported slabs, a folded plate mechanism is the most common failure mode (Kennedy & Goodchild, 2004, p. 88). This mechanism is driven by positive yield lines at midspan and negative yield lines over columns running in parallel to each other. The rotation axis is along the negative yield lines over the columns, and maximum deflection occurs at the positive yield lines. This failure mode is prone to occur simultaneously in both directions at once, as a combined folded plate mechanism, as illustrated in Figure 9. Whether or not the folded plate mechanism occurs in both directions has no impact on the ultimate load.

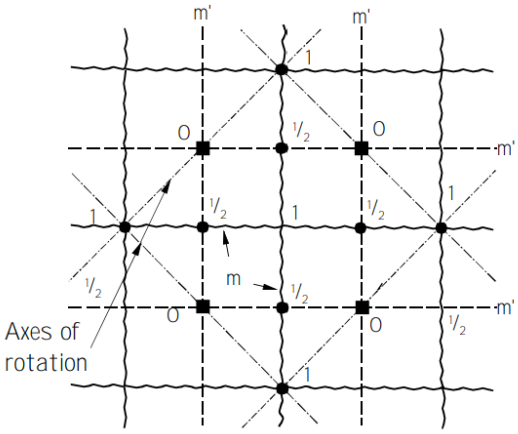

Figure 9: Positive and negative yield lines in folded plate mechanism, the numbers indicate deflection (Kennedy & Goodchild, 2004, p. 89).

Conical collapse mode is another flexural failure that can occur in flat- and pile supported slabs. It consists of negative yield lines forming radially from the column center, and positive yield lines creating a circular shape around the column. The slab segments deflect uniformly between these cones. Figure 10 illustrates this failure mode in a flat slab.

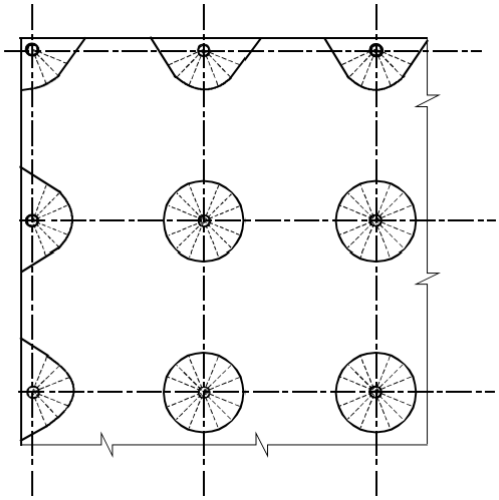

Figure 10: Conical collapse mode around columns in a flat slab (Kennedy & Goodchild, 2004, p. 89).

According to Hulett, many designers assume a yield line pattern that does not correspond to the crack patterns which are often observed in pile supported slabs (2011). This leads to smaller effective span widths, and poorer slab performance than assumed. A recommended yield line pattern provided by Hulett is illustrated in Figure 11. Nevertheless, several full-scale tests of pile supported slabs found that failure occurred along yield lines consistent with the folded plate mechanism (Aidarov et al., 2021; Ojo, 2021, pp. 128–129).

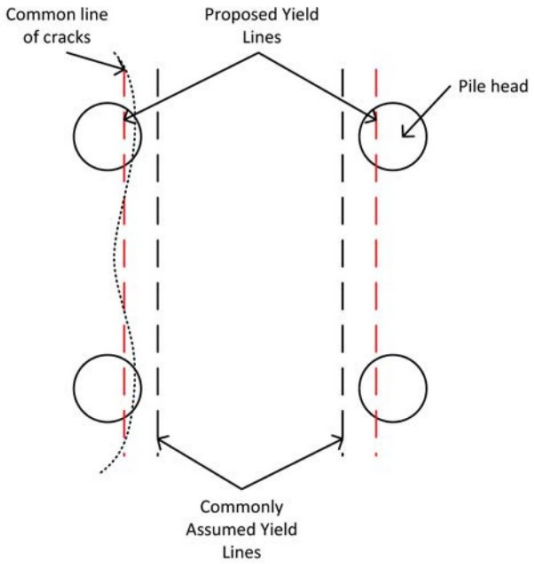

Figure 11: Recommended yield line pattern for pile supported slabs (Hulett, 2011, p. 2).

2.7 Equivalent Frame Method

The equivalent frame method (EFM) is a method for analyzing two-way slabs such as flat slabs and pile supported slabs, given that they are orthogonally reinforced. EFM divides a three-dimensional frame into a series of two-dimensional frames (Ojo, 2021, p. 9). This means that a two-way slab is split into so-called plate strips, which are analyzed in turn.

This allows for an analysis based on loads in each orthogonal direction and the stiffness of the two-dimensional strips' cross-sections.

EFM is one of the few methods for analysis of two-way slabs mentioned in Eurocode 2, and in the US, EFM is the only allowable method for analysis of prestressed slabs (Ojo, 2021). Paragraph EC2, I.1.2 describes rules for flat slab analysis using the equivalent frame method (CEN, 2004). The Eurocode 2 describes this method as dividing the slab into frames longitudinally and transversely and distributing the moment along these frames' width. Furthermore, the slabs should be divided into column- and middle strips. This is because maximum positive bending moment is concentrated in the middle of slab segments, and the maximum negative bending moment is concentrated over columns. Figure 12 illustrates the division of slabs into middle- and column strips.

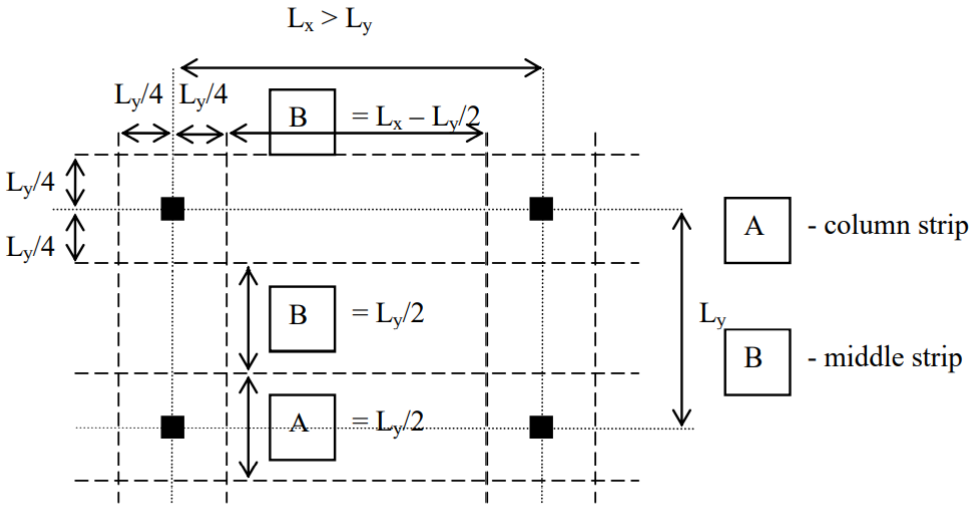

Figure 12: Illustration of the recommended division of slabs into column- and middle strips using the EFM (Sørensen & Øverli, 2013).

Table 1 presents the recommended bending moment apportionment between middle- and column strips given in Eurocode 2.

Table 1: Simplified allocation of bending moments between column- and middle strips after Eurocode 2, total negative and positive bending moments allocated between strips should add up to 100%.

	Negative moments	Positive moments
Column strip	60-80%	50-70%
Middle strip	40-20%	50-30%

Since EFM assumes a uniformly distributed moment over a given section of the equivalent frame, it typically underestimates the negative bending moments concentrated over supports. T. O. Ojo found this to be true in his experiments on post-tensioned flat slabs loaded with a uniformly distributed load (Ojo, 2021). His analysis was in accordance with the ACI guidelines. To address this deviation from elastic theory, the guidelines formed by the Norwegian Concrete Association divides a two-way slab into a finer system of slab strips. As opposed to the division illustrated in Figure 12, their publication NB 33 has three types of column strips and two types of field strips (Hagberg et al., 2004). The sum of the strips in field and over columns is still half the span length,

as in Eurocode 2 and ACI 318. This finer partitioning of slab stripes enables the analysis to more closely emulate the moment distribution found in an elastic analysis, especially over the columns. Figure 13 illustrates this finer distribution. Here, m_{SS}^1 and m_{SS}^2 are the support moments in the inner and outer column strips, respectively, m_{SF} is the support moment in the field strip, m_{FS} is the field moment in the column strip and m_{FF} is the field moment in the field strip. All moments are in kNm/m, and these are usually determined through an analysis using elastic theory, although yield line theory analysis and an analysis using moment-coefficients based on empirical tests may also be used. The latter is standardized in the ACI Building Code (Hagberg et al., 2004, p. 14).

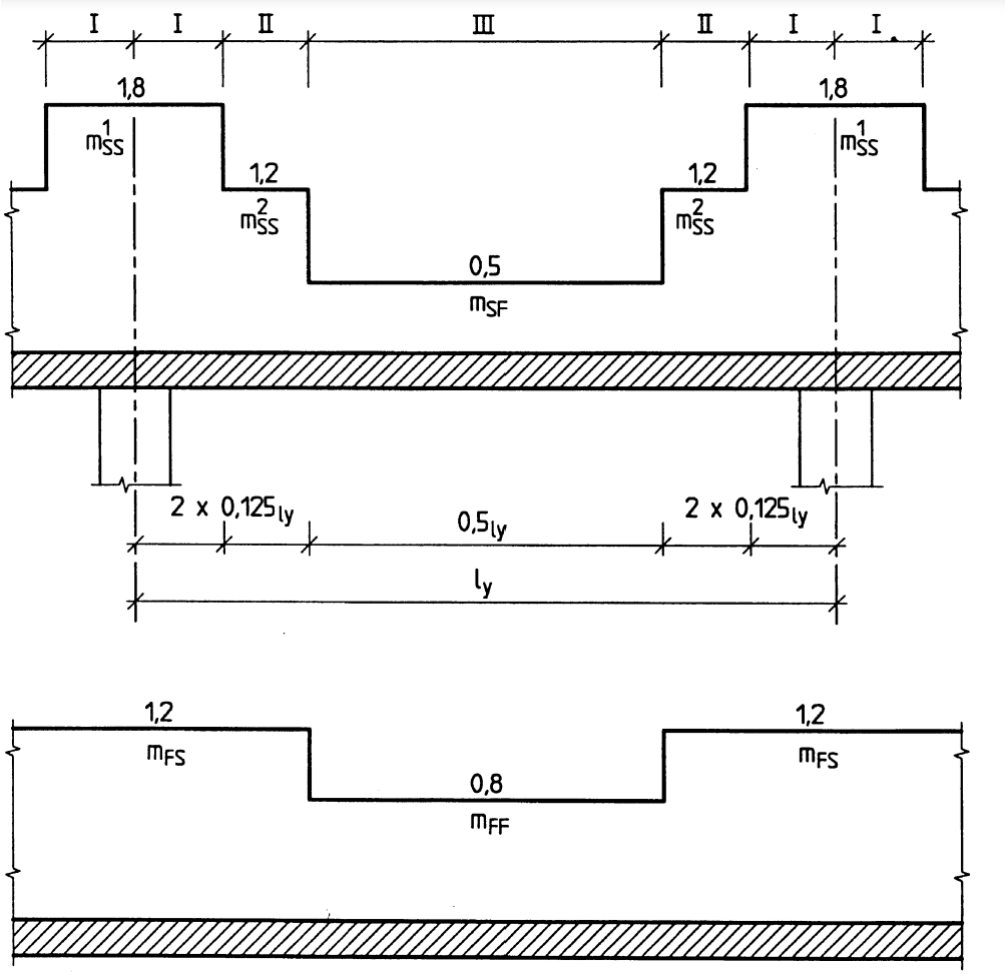

Figure 13: The moment distribution in column strips (above) and field strips (below), according to NB 33 (Hagberg et al., 2004, p. 15).

When the moment distribution is calculated according to the system described above, one can determine the necessary reinforcement area in each segment of the slab, given a concrete quality and slab thickness (Hagberg et al., 2004). This is generally done by satisfying:

$$M_{Ed} \leq M_{Rd}$$

Where M_{Ed} is the design moment acting on the slab, found from the previously determined moment distribution, and M_{Rd} is the design moment capacity of the slab. For a cross-section reinforced with conventional reinforcement, this is expressed as:

$$M_{Rd} = 0.275 * f_{cd} * bd^2$$

Assuming a normal reinforced cross-section. Where f_{cd} is the design concrete compressive strength, b is the breadth of the cross-section one designs (usually calculated per meter breadth for slabs), and d is the reinforcement depth in the cross-section. These equations, as well as equilibrium between the concrete compressive force reactant in the concrete compressive zone and the tensile force from the reinforcement, give the internal lever arm as:

$$z = \left(1 - 0.17\frac{M_{Ed}}{M_{Rd}}\right) * d$$

The equilibrium then gives the necessary reinforcement area as:

$$A_s = \frac{M_{Ed}}{z * f_{yd}}$$

Here, A_S is the reinforcement area, and f_{yd} is the design yield strength of the reinforcement steel.

2.8 Punching shear

Punching shear failure is caused by a concentrated transverse load in combination with flexural stresses (Ramos & Lucio, 2008). In flat slabs, the highest concentrated loads often occur at column-slab interfaces (pile-slab interfaces for pile supported slabs). This failure mode forms a truncated cone along diagonal tensile cracks and punching shear failure is a brittle failure mechanism. These cracks lead to a failure perimeter around the area of the concentrated load. A typical punching shear failure around a column is illustrated in Figure 14, with the truncated cone shape and typical crack pattern. The main problem with this failure mode is its brittle nature and the risk of progressive failure associated with it (Fernández Ruiz et al., 2010; Ramos & Lucio, 2008). The punching shear capacity of concrete structures is influenced by concrete quality, reinforcement amount, the size of the load area (column or pile head) and the definition of the critical control perimeter.

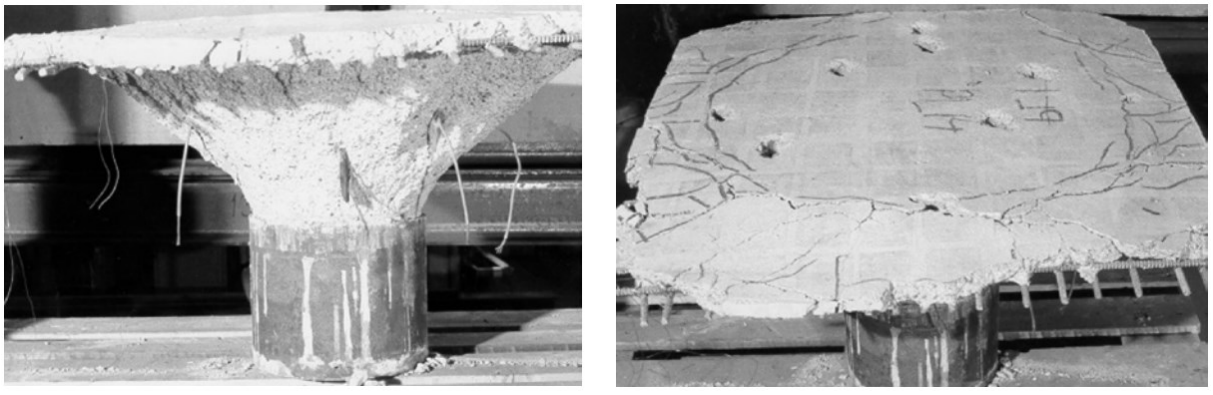

Figure 14: Punching shear failure with truncated cone and failure cracks (Sørensen & Øverli, 2013, p. 130).

The most common way of controlling slabs for punching shear failure is to calculate shear stresses at a critical distance from pile heads or columns. The critical distance varies between different codes, where the Eurocode 2 uses two times the average reinforcement depth, $2d$ (CEN, 2004). Section 6.4 in the Eurocode describes the punching shear control method. Figure 15 illustrates the model provided in Eurocode 2 for checking

punching shear capacity. The basic control section is surrounded by the basic control perimeters. This perimeter depends on the shape of the loaded area, and is given as:

$$u_1^{circular} = \pi(D + 4d); u_1^{rectangular} = 4\pi * d + 2c_1 + 2c_2$$

Where the circumference of the control perimeter, u_1, should be minimized; D is the diameter of a circular load area; d is the effective depth of the slab given as the average of the orthogonal effective depths; c_1 and c_2 are the side lengths of a rectangular load area.

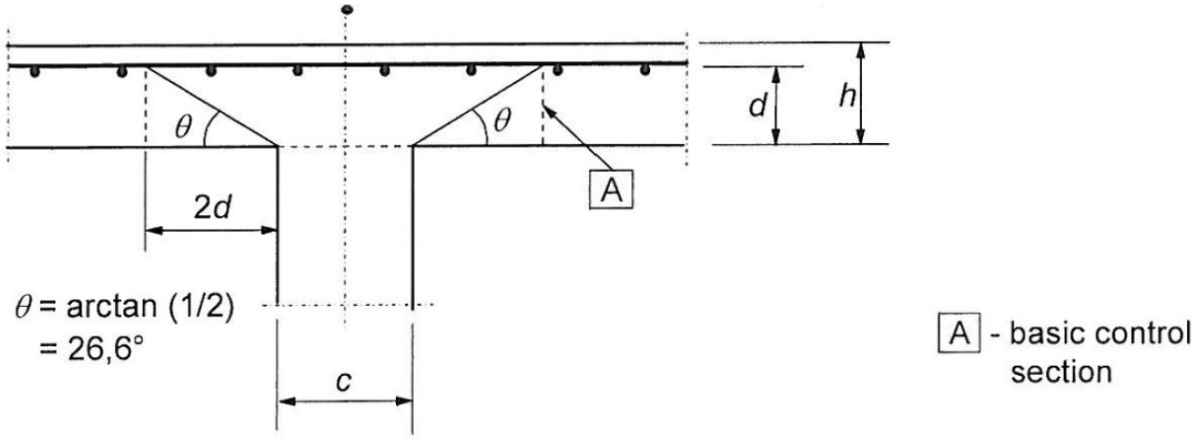

Figure 15: The verification model for punching shear presented in Eurocode 2 (CEN, 2004).

The design shear stress from the acting shear force, v_{Ed}, at a slab-column connection given in EC2 is:

$$v_{Ed} = \frac{\beta V_{Ed}}{u_1 d}$$

Here, β is a factor that accounts for moment transfer and V_{Ed} is the design punching shear load. The moment transfer factor is given as:

$$\beta = 1 + k\frac{M_{Ed}}{V_{Ed}} * \frac{u_1}{W_1}$$

The factor k accounts for the effect of the column's rectangularity; M_{Ed} is the design moment in the control section; V_{Ed} is the design punching shear load in the control section; W_1 is a factor accounting for the shear distribution in the control perimeter.

For a rectangular column we have:

$$W_1 = \frac{c_1^2}{2} + c_1c_2 + 4c_2d + 16d^2 + 2\pi dc_1$$

Where c_1 is the column length parallel to the eccentric load; c_2 is the column length perpendicular to the eccentric load. For structures that are laterally supported and have spans with lengths differing by 25% or less, simplified values for the moment transfer factor may be used. These factors depend on column type:

$$\beta_{internal} = 1.15;\ \beta_{edge} = 1.4;\ \beta_{corner} = 1.5$$

The design punching shear stress capacity of a slab, $v_{Rd,c}$, is given as:

$$v_{Rd,c} = C_c k (100 \rho f_{ck})^{\frac{1}{3}} \geq 0.035 k^{\frac{3}{2}} \sqrt{f_{ck}} = v_{Rd,min}$$

Where $C_c = \frac{0.18}{\gamma_c}$; $k = 1 + \sqrt{\frac{200}{d}} \leq 2.0$ is a size effect factor; $\rho \leq 0.02$ is the ratio of bonded steel in tension to concrete area; f_{ck} is the characteristic cylinder concrete compressive strength. For slabs with prestressing, there is an added capacity contribution given by the axial stress contribution from the tendons:

$$k_1 * \sigma_{cp}$$

Here, $k_1 = 0.1\ (compression)\ or - 0.3\ (tension)$, and σ_{cp} is the normal stress acting on the concrete cross-section.

There have been many comparisons between the punching shear capacity given by the method in Eurocode 2 and test results. Silva et al. gathered data from tests of in total 40 slabs, 37 of which were prestressed (2007). They found that this methodology gives large differences between prestressed slabs and ordinarily reinforced slabs, with considerably more conservative capacities for prestressed slabs. Abbood and Al-Bayati compared the test results of 118 steel fiber reinforced flat slabs with the provisions in, amongst others, Eurocode 2 (2021). Since the current EC2 does not include the strength contribution of steel fibers in punching shear capacity calculations, they found the theoretical punching shear capacity to be conservative. The authors concluded that steel fibers increase punching shear capacity of flat slabs at internal columns significantly and finds the current provisions in standards lacking.

The combination of moment transfer due to flexion of slab segments in addition to concentrated shear loads makes improvement of slab-column connections necessary in many cases (Hagberg et al., 2004, p. 9). This can be done by increasing the area through which the loads get transferred between the slab and column. Such measures can greatly improve moment capacity adjacently to the columns, in addition to increasing shear capacity. Two such solutions are illustrated in Figure 16. Other design decisions that increase punching shear capacity is to increase slab depth and to provide more reinforcement in areas of high concentrated loads.

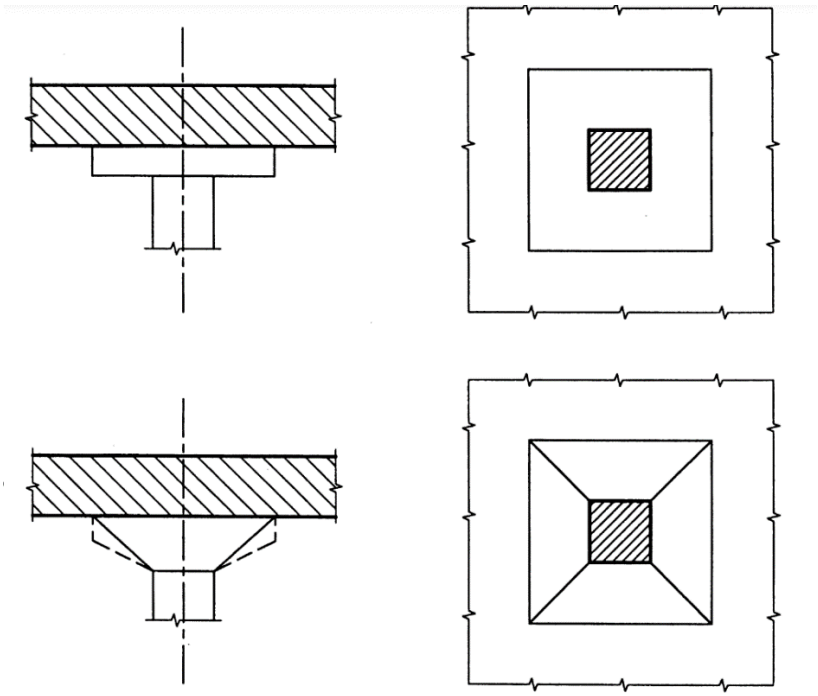

Figure 16: Examples of solutions to improve load capacity of slab-column connections (Hagberg et al., 2004, p. 9).

Ojo conducted tests of several flat slabs, and one of them experienced punching shear failure at the face of a column (2021). He concluded that the reason this particular slab was the only one in the test program which experienced punching shear failure, was that the other slabs had either steel fiber reinforcement, a banded-banded tendon distribution, or both. Thus, it seems that both the inclusion of fiber reinforcement and more PT reinforcement near columns help increase the punching shear capacity of flat slabs. This is because the fibers in concrete are oriented in all directions, making them active in the direction of the shear stresses and contributing to bridging the cracks (Abbood & Al-Bayati, 2021). PT reinforcement is inclined at column-slab connections, improving both shear capacity and moment transfer at these points (Ramos & Lucio, 2008).

2.8.1 Proposed new Eurocode 2

During the past few years, a revised edition of EC2:2004 has been under development. The new Eurocode 2 is expected to be finished within the next couple of years. How punching shear is handled in the new EC2 differs from the current calculation method on several points (CEN, 2021). Section 8.4 provides the method for punching shear design, and, according to 8.4.1(2), there are five checks in the punching shear capacity verification procedure:

$$i)\ \tau_{Ed} \leq \tau_{Rdcmin};\ ii)\ \tau_{Ed} \leq \tau_{Rdcmin};\ iii)\ \tau_{Ed} \leq \tau_{Rdmax};\ iv)\ \tau_{Ed} \leq \tau_{Rdcs};\ v)\ check\ at\ b_{0.5out}$$

If check *i*) is satisfied, further punching shear detailing may be omitted; *ii*) verifies whether shear reinforcement is necessary or not; *iii*) provides the maximum punching shear resistance that may not be exceeded; *iv*) controls whether the cross-section with shear reinforcement has sufficient capacity; and *v*) is a control of the outer perimeter where shear reinforcement is no longer needed. In EC2:2021, the design shear stress in the critical section is defined as:

$$\tau_{Ed} = \frac{\beta_e V_{Ed}}{b_{0.5} d_v}$$

Here, β_e accounts for shear force concentration and may be approximated according to Table 8.3; V_{Ed} is the design shear force acting on the load area; $b_{0.5}$ is the length of the control perimeter, set at $0.5d_v$ rather than $2d_v$ as in the current EC2; d_v is the aggregate effective reinforcement depth.

The design punching shear resistance is in 8.4.3(1) given as:

$$\tau_{Rdc} = \frac{0.6}{\gamma_V} * k_{pb} * \left(100\rho_l f_{ck} * \frac{d_{dg}}{d_v}\right)^{\frac{1}{3}} \leq \frac{0.6}{\gamma_V} * \sqrt{f_{ck}}$$

We have that $\gamma_V = 1.4$ is a partial factor for shear design given in Table 4.3; k_{pb} is the punching shear gradient enhancement coefficient, given by $1 \leq k_{pb} = 3.6 * \sqrt{1 - \frac{b_0}{b_{0.5}}} \leq 2.5$; ρ_l is the ratio of bonded flexural reinforcement in the area considered, which is taken as the column width plus $3d_v$ to each side; d_{dg} describes the failure zone roughness; f_{ck} is the characteristic compressive strength of the concrete. In structures with post-tensioned reinforcement, the capacity may be increased by the factor $k_{pp} = \sqrt{1 + 1.2 * \frac{b_{0.5}\sigma_d}{\mu_p d_v * \sqrt{f_{ck}}}}$. Here, σ_d is the average normal stress resulting from the prestressing forces, and μ_p is a coefficient that considers the shear force gradient and the bending moment inside the control perimeter.

There is also a minimum shear stress resistance, provided in 8.2.1(4):

$$\tau_{Rdcmin} = \frac{11}{\gamma_V} * \sqrt{\frac{f_{ck} * d_{dg}}{f_{yd} * d}}$$

Where f_{yd} is the design yield strength of the reinforcement.

If punching shear reinforcement is required, 8.4.4(1) gives the punching shear resistance of a reinforced slab as:

$$\tau_{Rdcs} = \eta_c * \tau_{Rdc} + \eta_s * \rho_w * f_{ywd} \geq \rho_w * f_{ywd}$$

Where we have $\eta_c = \frac{\tau_{Rdc}}{\tau_{Ed}}$; $\rho_w = \frac{A_{sw}}{s_r s_t}$ is the shear reinforcement ratio; f_{ywd} is the design yield strength of the shear reinforcement; and:

$$\eta_s = \frac{d_v}{150\phi_V} + \sqrt{15 * \frac{d_{dg}}{d_v}} * \left(\frac{1}{\eta_c k_{pb}}\right)^{\frac{3}{2}} \leq 0.8$$

In 8.4.4(3), a maximum shear resistance in a cross-section with shear reinforcement is given as:

$$\tau_{Rdmax} = \eta_{sys} * \tau_{Rdc};\ \eta_{sys} = 1.15 * \frac{d_{sys}}{d_v} + 0.63 * \left(\frac{b_0}{d_v}\right)^{\frac{1}{4}} - 0.85 * \frac{s_0}{d_{sys}}$$

Figure 8.23 in the proposed new EC2 defines s_0 and d_{sys}; and b_0 is the length of a control section at the column face.

Finally, 8.4.4(4) defines the outer perimeter where shear reinforcement is no longer required as:

$$b_{0.5out} = b_{0.5} * \left(\frac{d_v}{d_{vout}\eta_c}\right)^{\frac{3}{2}}$$

Where d_{vout} is the outer shear-resisting effective depth, defined in Figure 8.24.

2.9 Fiber reinforcement

Due to its many benefits, fiber reinforcement has been increasingly common in concrete structures the last few decades (Destree, 2009). Among the largest benefits are savings in cost and time. This subchapter presents the properties of fiber reinforcement used in calculation, and some calculation methods developed for fiber reinforced concrete structures which is provided in current guidelines.

2.9.1 Properties

Fiber reinforcement is small fibers that are mixed into fresh concrete. The fibers can vary in size, geometry and materials (Marcalikova et al., 2020). For bigger structures, they are typically 35-60 mm long with hooked ends and are made of steel. One of the main reasons to use fiber reinforcement, is the reduced need for conventional reinforcement. This will reduce on-site reinforcement work, which will lead to reduced construction time and reduced costs (Oikonomou-Mpegetis, 2013). Less conventional reinforcement will also lead to better overview and control, which again may lead to fewer errors.

Other advantages with fiber reinforcement are the increased capacity of the slab and crack width reduction (Marcalikova et al., 2020). With smaller cracks, the slab will also be less vulnerable for several deterioration mechanisms. Because the fibers are small and distributed, their contribution is largest when the cracks are small. Small cracks may be achieved by allowing for a larger number of cracks. This way, the even distribution of the fibers is also utilized better, because the cracks also get distributed. Thus, the way the slab fails affects how much the fibers will contribute to the capacity of the slab.

As previously mentioned, the recommended design approach from The Concrete Society is to allow for fewer and wider surface cracks in pile supported slabs (2016, p. 34). This contrasts with conventionally reinforced pile supported slabs, where crack width limitation is a viable option. The reason for this discrepancy is, in addition to a lack of crack width calculation methods, that steel fiber reinforced concrete (SFRC) floors may experience excessive fine cracking if measures are not taken. This type of cracking is not easily treatable and accelerates deterioration. In order to avoid this, the designer needs to limit shrinkage and the bending moment above piles. This design recommendation defies intuition for SFRC, which is to allow the fibers to bridge many small cracks and maximize the fiber contribution. However, since this approach is beneficial with regards to repair and maintenance cost, and steel fibers still contribute to pile supported slab constructions, SFRC floors have been one of the largest drivers in increasing the usage of fiber reinforcement in concrete.

Fiber reinforcement does not initially contribute much to the flexural bending strength and is not as good as conventional reinforcement in tension (Kanstad et al., 2020). But after the first cracks appear, the fibers will begin to contribute to the capacity of the slab (Kanstad et al., 2011). This is because of the residual flexural tensile strength and is one of the main functions of fiber reinforcement. This is achieved after the first cracks are

formed, when the fibers are located across the cracks, preventing further crack propagation. This way, the fiber reinforcement may contribute to the shear and tensile capacity. The fact that the fibers may be located across the cracks is what makes fiber reinforcement beneficial. Cracks may form with an angle to the conventional reinforcement, and in locations where there is no conventional reinforcement. Fibers in these areas will contribute to the construction's capacity as smaller cracks are formed. However, it might be difficult to predict the orientation and location of the fibers. It is, for instance, possible that the fibers are oriented in parallel with the cracks, instead of across them. If this happens, the fibers will not contribute to minimize the crack widths. If the casting is done incorrectly, the fibers may concentrate in a few areas of the structure, creating an uneven distribution of fibers. This might happen under the vibration process and could be avoided using self-compacting concrete. It is important that the crew casting the concrete is aware of these possible errors. The location and orientation of the fibers are most predictable in small and simple constructions, like a beam.

In addition to these general fiber properties, there are also some properties that vary depending on the type of fiber. Fibers used as reinforcement can be made of steel, glass, synthetic or natural materials (Kanstad et al., 2011). Steel fibers are most common and have some of the same properties as conventional reinforcement, since it is made of the same material. This means that the reinforcement is quite strong and ductile but might deteriorate due to corrosion. Basalt fibers, however, have high corrosion resistance (Mohaghegh et al., 2015). This could be useful, especially in marine structures. Because the fibers are evenly distributed in the concrete, some of the fibers will have too little cover to be sufficiently protected from corrosion. In structures such as these, high corrosion resistance would be advantageous. The ductility and load capacity on the other hand are not as good for fibers made of basalt as it is for steel fibers. The ductility has a big influence on parameters such as the residual flexural tensile strength for different crack widths. While steel fibers maintain their residual tensile strength with increasing crack widths, basalt fibers will lose this strength as the crack width increases. Because the standard test uses 2.5 mm crack width, the basalt fibers have lost some tensile strength, giving less optimal parameters, when they in reality have higher capacity for small crack widths. Regardless the crack width, steel fibers tend to have higher capacity. Another weakness with basalt is that the fibers may be destroyed or damaged in the mixing process. This is important to consider when choosing mixer and aggregates.

The quantity of fibers in the concrete mix will also influence the properties of the concrete. More fibers will result in higher capacity and better resistance against big cracks (Marcalikova et al., 2020). This is shown in Figure 17. There is, however, a limit at which there is no further utility in adding more fibers. The fresh concrete properties will also worsen if the amount of fiber reinforcement is too high. It might affect the pumpability and make the concrete separate. The critical fiber amount, and how it affects both fresh and hardened concrete, depends on parameters from size of the aggregates to the casting method (Vikan, 2007).

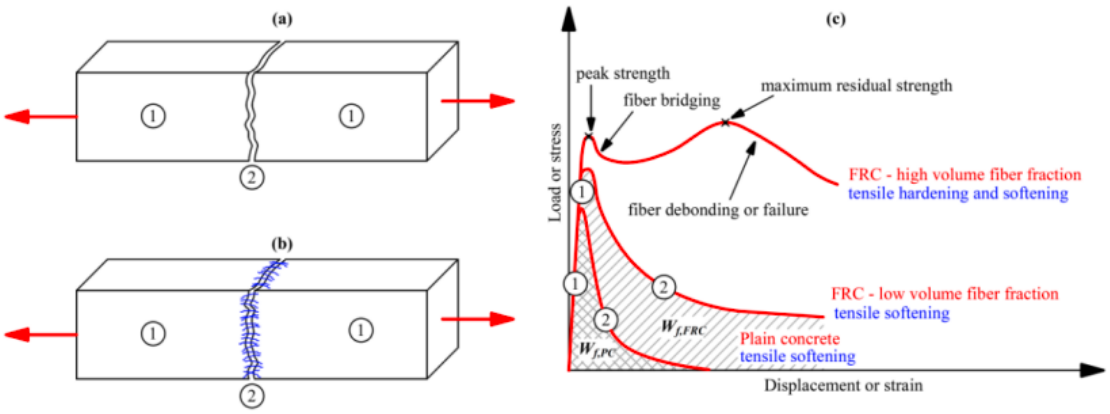

Figure 17: Illustration of how the fibers contribute to higher residual strength (Marcalikova et al., 2020).

2.9.2 Calculation parameters according to NB 38

Capacity calculations for fiber reinforced concrete is based on the residual flexural tensile strength to a given concrete mix, and is not codified in a consistent and uniform manner (Oikonomou-Mpegetis, 2013). One internationally established test method for determining residual flexural tensile strength is provided in NS-EN 14651 (Standard Norge, 2008). This is a three-point load test for small concrete beams with fiber reinforcement and a sawed notch. The procedure given in this standard is for metallic fibers but is also used for basalt fibers. In this thesis, the calculation methods for fiber reinforced concrete structures use the parameters from the test described in NS-EN 14651 and follows the procedure outlined in The Norwegian Concrete Association's publication NB 38 (Kanstad et al., 2020).

Residual flexural tensile strength is written as

$f_{R,i} = 6 * \frac{M_{Ri}}{b*h^2}$, where $M_{Ri} = \frac{F_{Ri}*L}{4}$.

Characteristic residual flexural tensile strength is written as $f_{Rk,i} = f_{R,i} - k * s$, where s is the standard deviation and $k = 1.7$ for a test that follows the requirements in NB 38.

Mean and characteristic residual flexural tensile strength at 2.5 mm crack mouth opening displacement are then used and written as: $f_{R,3m}$ and $f_{R,3k}$. These parameters are then used to find design residual flexural tensile strength:

$$f_{R,3kber} = \min\left(f_{R,3k}; 0.6 * f_{R,3m}\right)$$

$$f_{Ftuk} = 0.37 * f_{R,3kber}$$

$$f_{Ftud} = \frac{f_{Ftuk}}{\gamma_{SF}}$$

When the design residual flexural tensile strength has been determined for the relevant concrete mix, this value is used in calculations of punching shear capacity and bending moment capacity for fiber reinforced concrete. Fiber reinforcement is often combined with other reinforcement types, and most of these calculations are therefore explained in the section for combined reinforcement.

In constructions with fiber reinforcement where punching shear is a possible failure mechanism, the shear capacity should be controlled at a distance $\frac{d}{2}$ from the vertical force (Kanstad et al., 2020). This is shown in Figure 18 and Figure 19. For concrete with fiber reinforcement, there are some additional parameters to consider in comparison with conventionally reinforced concrete, but the principle is the same. For concrete with only fiber reinforcement, the punching shear capacity is:

$$\tau_{Rd,cf} = f_{Ftud}$$

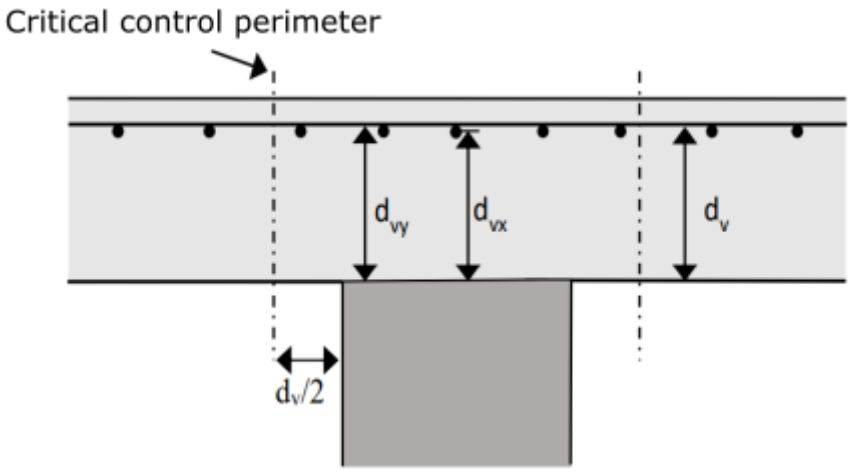

Figure 18: Critical control perimeter cross section, modified from Kanstad et al. (2020).

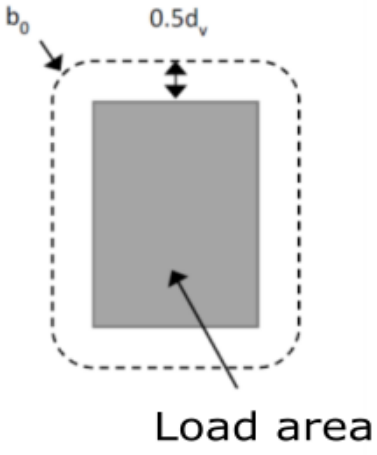

Figure 19: Length of the control perimeter, modified from Kanstad et al. (2020).

2.10 Post-tensioning

As previously mentioned, reinforcement is necessary in concrete in order to handle tensile stresses. In addition to traditional reinforcement bars, prestressed reinforcement in concrete has become increasingly popular the past decades (Ojo, 2021). The advantages of prestressing, including reduced slab thickness and smaller deflections, has made prestressed concrete in constructions such as slabs popular since the 1960s (Bondy, 2006).

There are different ways to execute a prestressed concrete structure (Ojo, 2021). One way is to use bonded prestressing bars. Traditional reinforcement is also bonded. The difference is that for prestressed reinforcement, the bars are applied an axial load before the concrete hardens. The same principle is used for post-tensioned structures. The difference is that PT reinforcement is unbonded, which means there is low friction between the reinforcement and the concrete. This is achieved by placing the PT tendons in a plastic duct and covering them with grease. This way, the axial force is applied after the concrete has hardened and obtained the required strength. One of the most common methods is mono-strand unbonded tendons (Trygestad, 2005). This method is easy to apply on the construction site. For both bonded and unbonded prestressed reinforcement, the axial force is applied before the dead load and the live loads.

The main advantage of prestressed reinforcement is its efficiency in counteracting the deflection and forces from the dead load and the live loads on the structure (Nawy, 2010, p. 3). Traditional reinforcement is only effective after the loads are applied and the slabs are deflected. At this point, cracks might occur in the concrete, and the deflection requirements may have been exceeded. For prestressed concrete, however, this deflection is counteracted by the prestressed reinforcement. Figure 20 and Figure 21 illustrate this. This method allows for leaner structures and/or longer spans. This will result in structures that are more economic and lighter. Lighter structures will again result in more economic structures.

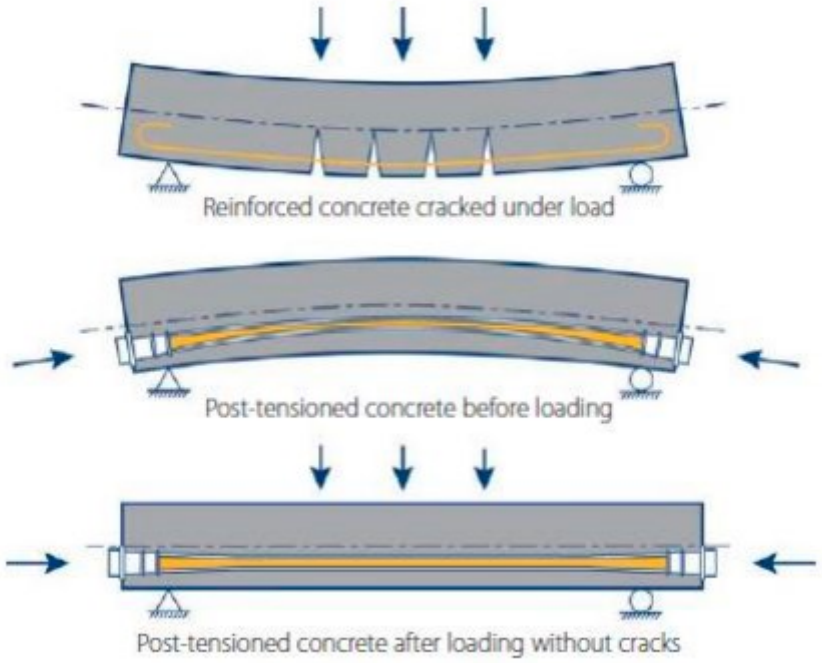

Figure 20: Principle of post-tensioning (Ojo, 2021).

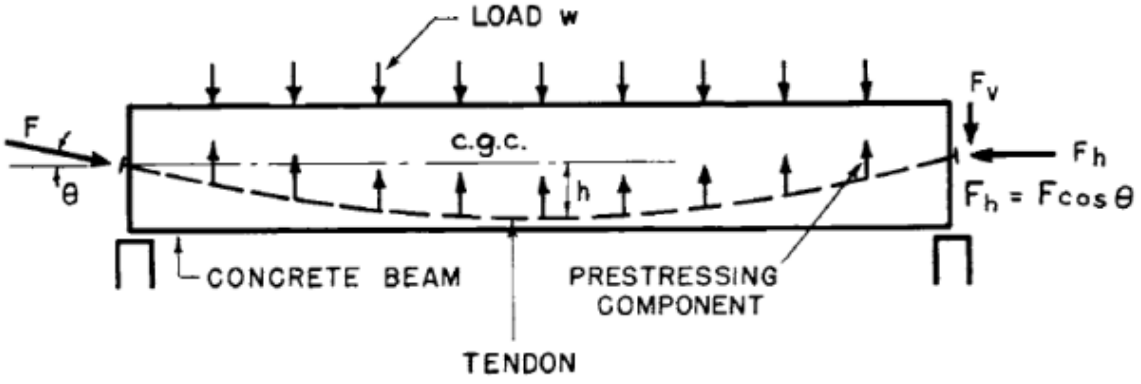

Figure 21: Load balancing for post-tensioned structures (Ojo, 2021).

Today, the common way to design prestressed structures is with the load balancing approach. This approach was invented in 1963 and made the design of prestressed concrete structures comparable to traditional reinforcement design in complexity (Ojo, 2021). Figure 21 illustrates how this principle works. The prestressed tendons keep concrete in compression by applying compression on the tensile part of the concrete structure (Trygestad, 2005). The stresses induced by the prestressed tendons are meant to counteract the stresses induced by external loads. This is done by making the tendon layout follow the bending moment diagram from the external loads. For an evenly distributed load, the moment diagram will be parabolic. To counteract this bending moment, the prestressed tendon layout should therefore also be parabolic. This is illustrated in Figure 21. The parabolic tendons, when tensioned, impose evenly distributed vertical loads on the concrete structure. These prestressing loads are opposite of the external loads. There is, however, a limit to how large the axial force should be. It is normal that the vertical force from the tendons equalize 65% to 80% of the dead load (Ojo, 2021). When designing the prestress force, it is important to take the usage of the structure into account, and consider how to limit cracks and deflections in the best possible way (Trygestad, 2005).

For shear capacity calculations, the Eurocode 2 includes the contribution of the axial force from prestressed tendons (CEN, 2004). It does not, however, give special consideration to prestressed tendons in other ways. For instance, the Eurocode 2 applies the same cover depth rules for post-tensioned tendons as for traditional reinforcement. The cover depth mainly functions to protect the reinforcement against corrosion. Since the post-tensioned reinforcement is already protected by grease and a plastic duct, however, the conventional cover depth rules may be superfluous. Even though the Eurocode 2 does not consider this, the corrosion resistance is a great advantage with post-tensioned reinforcement.

2.10.1 Bending moment capacity

Following the same procedure as for concrete without prestressed reinforcement, the design bending moment distributions presented in Figure 13 are the basis for moment capacity checks. The moment capacity criterion, $M_{Ed} \leq M_{Rd}$, is the same. For prestressed concrete, the moment capacity is given as:

$$M_{Rd} = 0.8\alpha(1 - 0.4\alpha) * f_{cd} b d^2$$

Here, f_{cd} is the design concrete compressive strength; b is the width of the cross-section under consideration; d is the reinforcement depth; α is the relative height of the concrete compressive zone, and can be calculated as:

$$\alpha = \frac{nf_{pd}A_p + f_{yd}A_s}{0.8f_{cd}bd}$$

We have that n is the number of prestressed tendons in the cross-section under consideration; f_{pd} is the design yield strength of a prestressed tendon; A_p is the area of a prestressed tendon; f_{yd} is the design yield strength of conventional reinforcement; A_s is the area of conventional reinforcement. Thus, by knowing the amount of conventional reinforcement, if there is any, and solving $M_{Ed} = M_{Rd} = 0.8\alpha(1 - 0.4\alpha) * f_{cd}bd^2$, we get the relative compressive zone height as:

$$0.32\alpha^2 - 0.8\alpha + \frac{M_{Ed}}{f_{cd}bd^2}$$

The equation giving α may then be solved for the necessary number of prestressed tendons to achieve sufficient moment capacity:

$$n = \frac{0.8\alpha f_{cd}bd - f_{yd}A_s}{f_{pd}A_p}$$

2.10.2 Prestressing losses

When applying stress to the prestressing tendons and subsequently cutting and anchoring the tendons, a loss of prestressing force is expected (Ojo, 2021). These losses have different origins and may be categorized into immediate losses and time-dependent losses (CEN, 2004). This means that the calculated maximum force applied to tendons during tensioning, $P_{max} = A_p * \sigma_{pmax}$, is reduced over time as the losses affect the tendons.

The immediate losses are subdivided into three types in EC2.5.10.5. The first is a result of instantaneous deformation of the concrete structure to which a prestressing force is applied. This loss is, naturally, largest for the first tendons to be stressed and smallest for the last to be stressed. The loss may be calculated as:

$$\Delta P_{el} = A_p E_p * \sum \left(\frac{j * \Delta\sigma_c(t)}{E_{cm}(t)} \right)$$

Here, A_p and E_p is the prestressing steel area and E-modulus, respectively; $\Delta\sigma_c(t)$ is the stress variation of tendons at time t; $j = \frac{n-1}{2n}$ is a coefficient; $E_{cm}(t)$ is the mean concrete E-modulus at time t.

The second instantaneous loss is friction losses, arising from the friction between the tendon and its duct as the tendon is stressed. The loss is expressed as:

$$\Delta P_{mu} = P_{max}\left(1 - e^{-\mu(\theta + kx)}\right)$$

Where P_{max} is the maximum allowable prestressing force applied to a tendon; μ is a friction coefficient given in EC2.Table 5.1; θ is the sum of angular displacements; k is the unintentional angular displacement for internal tendons; x is the distance from the active end of the tendon.

The final immediate loss is due to draw-in of anchorage devices and deformation of the anchorage after the tensioning is complete. This loss is estimated as a distance, in millimeters, of tendon slippage at the anchor.

EC2.5.10.6 subdivides the time dependent losses into three. These losses are the result of creep and shrinkage in the concrete, and relaxation in the steel tendons. A simplified method of estimating these three losses as one is provided in the Eurocode:

$$\Delta P_{c+s+r} = A_p * \frac{\epsilon_{cs} E_p + 0.8\Delta\sigma_{pr} + \frac{E_p}{E_{cm}} * \phi(t, t_0) * \sigma_{cQP}}{1 + \frac{E_p A_p}{E_{cm} A_c} * \left(1 + \frac{A_c}{I_c} * z_{cp}^2\right) * \left(1 + 0.8 * \phi(t, t_0)\right)}$$

We have that ϵ_{cs} is the estimated shrinkage strain; $\Delta\sigma_{pr}$ is the stress variation in the tendons due to relaxation; $\phi(t, t_0)$ is the creep coefficient; σ_{cQP} is the stress in the concrete adjacent to the tendons, resulting from self-weight and other loads; A_c is the area of the concrete section; I_c is the second moment of area of the concrete section; z_{cp} is the distance between the concrete's center of gravity and the tendons.

Because of long-term deformation of the entire concrete member, an increase in tendon stress for ULS analysis may be added. According to EC2.5.10.8(2), this additional stress is $\Delta\sigma_{pULS} = 100MPa$. This, in addition to the losses, gives a final prestressing force of

$$P = P_{max} - \Delta P_{tot} + \Delta\sigma_{pULS} * A_p$$

Which is used for calculations in ULS.

2.11 Combinations of fibers and other types of reinforcement

As explained above, there exists different types of reinforcement. Each of these types have their own advantages and disadvantages. These must be considered and evaluated with regards to the usage of the structure when the designer decides the reinforcement solution. Expenditure of time and overall cost will always be important, but there will also be other parameters to consider. Environmental issues and challenges considering the local environment, such as corrosion problems, also need consideration. For each of these challenges, some reinforcement choices are better than other. Fiber reinforcement is, for instance, fitting when crack control is important. The designer needs to decide what type of reinforcement has the most appropriate properties. In many cases, a combination of different types of reinforcement will be most appropriate. When calculating reinforcement solutions that contain fibers and other reinforcement types, the methods and equations are not the same as for conventional reinforcement. Adapted equations are necessary, and these are presented in this chapter. For punching shear design however, the calculations with fibers should be conducted according to EC2:2021, which are presented in the section for punching shear.

2.11.1 Bending moment capacity

The calculation method for moment capacity for concrete with different types of reinforcement given in NB 38 is based on axial equilibrium between the resultants from the concrete's compression zone, the contribution from the fiber reinforcement and the contribution from the rebars (Kanstad et al., 2020). This equilibrium can be used to find the relative height of the concrete's compressive zone, x, and can be written as

$$T_c = S_f + S_p + S_s$$

Here, T_c is the resultant from the concrete's compression zone; S_f is the contribution from the fiber reinforcement; S_p is the contribution from prestressed tendons and S_s is the contribution from the traditional reinforcement. The resultants can be written as

$$T_c = 0.8x * b * f_{cd}; S_f = (h - x) * b * f_{Ftud}; S_p = \sum(A_p * \sigma_{pm0}); \; S_s = f_{yk} * A_s$$

The resultant from the prestressed tendons is based on Eurocode 2, section 5.10, and the resultant from the traditional reinforcement is based on the assumption that the reinforcement will yield. Moment equilibrium about T_c will give the moment capacity of the cross section:

$$M_{Rd} = S_f * (0.5h + 0.1x) + S_p * (d - 0.4x) + S_s * (d_s - 0.4x)$$

Figure 22 presents the different resultants and illustrates the basis for the equilibrium equations, according to NB 38.

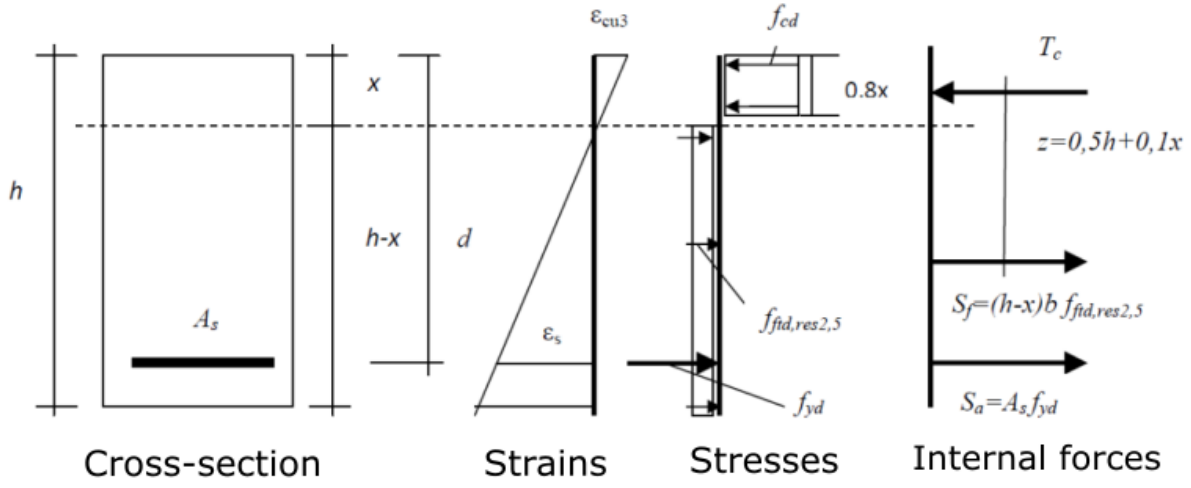

Figure 22: Stress distribution as basis for equilibrium equations, modified from Kanstad et al. (2011).

2.11.2 Distribution of tendons

As previously described, it is possible to combine different types of reinforcement. But, in addition to reinforcement type, there are further issues to consider. An example of this is choosing the distribution and placement of the reinforcement. This is primarily an issue for prestressed reinforcement, and this becomes increasingly important when prestressed reinforcement is combined with other reinforcement types. The distribution will have an impact on the yield line mechanism, and how the cracks will develop. This, in turn, will impact the effect from the fibers in fiber reinforced concrete, because they are most effective against small cracks. Therefore, the fibers are more effective for many small cracks, rather than few large cracks.

It is also important to consider other conditions. The reinforcement is more effective in some places than others. Therefore, it is economically beneficial to distribute the reinforcement in a way that utilizes the reinforcement the most (Hagberg et al., 2004). Figure 23 shows different options for tendon distribution. It is important that the tendons are distributed in column- and field strips, so that they follow the moment distribution. Therefore, option II on the figure is the most ideal. This might, however, lead to practical problems on the construction site. If too many tendons pass through the columns, there

will be many tendons and little space, making it difficult to execute on-site. For practical reasons, alternative IV is most common. When considering punching shear, it is preferable to let the tendons pass through the column strips. This is explained in larger detail in the punching shear section.

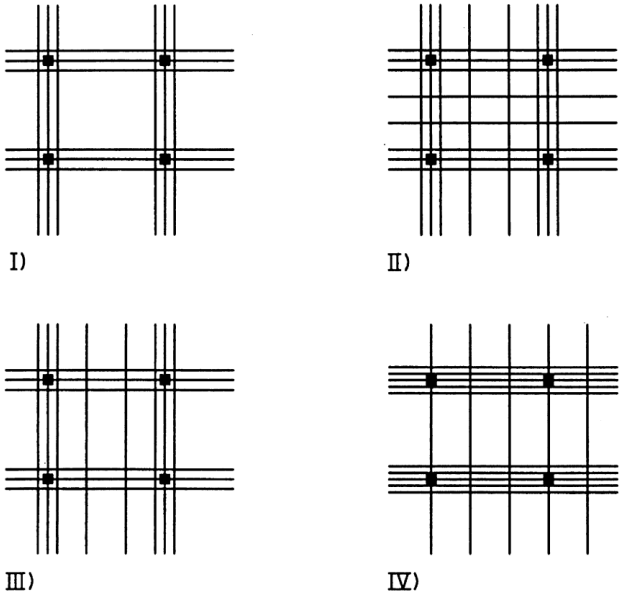

Figure 23: Different distribution options for prestressed tendons in flat slabs (Hagberg et al., 2004).

3 Analysis and design of pile supported slab

This chapter describes the various methods that are used to analyze, design and compare reinforcement solutions for the pile supported slab this thesis examines. First, an overview of the general methods that are applied is provided. Then, a calculation example is presented in which the steps for modelling and determining load actions are shown and described. In the design process, several theories for analysis are utilized. The pile supported slab on which this thesis is centered is then presented and illustrated, and the design procedure is described. Finally, the different reinforcement solutions which this thesis investigates are listed and described.

3.1 Overview of methodology

In this thesis, a pile supported slab is modeled and analyzed. This analysis provides the load actions and the distributions of these and based upon this the necessary reinforcement amounts are calculated. Then, reinforcement solutions are chosen and examined. A comparison between the different reinforcement solutions is then made. This comparison is based on the results of necessary reinforcement calculations, but other factors such as cost, time requirements and practicality are also discussed. The two methods of analysis, the EFM and the yield line theory, are also compared. Furthermore, punching shear calculations according to the current and the proposed new Eurocodes are compared. The analyses contain three main components: a linear-elastic finite element analysis (LFEA) of the slab with its imposed loads for load action calculation, as well as equivalent frame method (EFM) and yield line theory for designing the reinforcement solutions. These components are first presented and discussed through a calculation example. In addition to the yield line solution, this example shows how the linear-elastic analysis and EFM gives comparable results. For the pile supported slab the linear-elastic solution is adjusted to take account for more plastic behavior in ULS. The width of each strip in this adjustment is the same as for EFM according to NB 33. This way, the linear elastic analysis and equivalent frame method are merged, and these results are compared to the yield line solutions.

3.1.1 Analysis

The computer program Focus Konstruksjon (FK), developed by Focus Software, is used to model the construction. Furthermore, FK is used to conduct an LFEA of the slab and provide load actions based on elastic theory. FK is a program developed in order to provide an intuitive and user-friendly option for modelling constructions, applying load combinations and execute finite element analyses (Focus Software, 2021). It allows for different cross-sections, materials and boundary conditions. Furthermore, it helps the user generate load combinations based on Eurocode 1990, generates a variety of graphically represented results, and produces reports for documentation. For analysis of 3D concrete slabs, FK has an option for quickly modelling the slab by choosing concrete quality and slab thickness. Then, the slab's geometry is outlined by the user. A mesh is then generated in order to conduct the analysis, where either a triangular or quadrilateral mesh can be chosen. As opposed to 2D-methods such as the EFM or yield line theory, an LFEA provides a complete overview of load actions such as deformations and cracking.

Thus, using FK to obtain elastic load actions is an efficient way to analyze slabs with complex geometry such as D3-2.

EFM is, as previously mentioned, a well-established method for analysis of two-way slabs. When using EFM on a pile supported slab, one first analyzes the slab as a continuous beam to determine the elastic design moments in spans and over columns. This is done separately for the x- and y-directions, so that the slab is analyzed as two 2D frames. Then, the design moments in spans and over columns are spread over a width equal to the span width of the slab in the respective directions. This distributed bending moment is then multiplied with the appropriate factor, ranging from 0.5 to 1.8, producing the moment distributions shown in Figure 12. When this distribution is produced for all relevant spans and columns in each direction, moment equilibrium in the slab cross-section determines necessary reinforcement amount for the strips. For slabs with non-regular pile layout, the bending moments may be determined with an LFEA. For this thesis, EFM and LFEA are merged to a method where the steps from EFM are used, and the values from the middle of each step are adjusted from an LFEA.

Yield line theory is the last method used for analysis of slab D3-2. For standard cases where load situation, geometry and boundary conditions are known, tabulated standard formulae to determine the load capacity may be used. Furthermore, the geometry of the failure mechanism as well as deflections are given by standard formulae. When a folded plate mechanism occurs, the x- and y-directions is analyzed separately, as for EFM. The design method then consists of determining the design yield line moment for a continuous one-way slab in each orthogonal direction. The design maximum moment that is determined through the analysis, becomes the basis for determining necessary reinforcement amounts for different sections of the slab in both directions. For slabs with irregular pile layout or boundary conditions that makes the folded plate mechanism impossible, standard formulae for two-way slabs with varying boundary conditions provides an efficient design approach. A folded plate mechanism might occur for the example, but slab D3-2 must be considered as a two-way slab.

3.1.2 Comparison

After analyzing and designing the pile supported slab with different reinforcement solutions, a comparison is conducted. First, the different methods for analysis are compared. Among the factors considered in the comparison are the assumptions involved in the calculations, how easy the methods are to use, the similarity of the load actions found with the methods and the necessary reinforcement amount.

Furthermore, a comparison of the results obtained through each method is made for the different reinforcement solutions. This comparison mainly centers on the calculated necessary reinforcement amounts. In addition, comparisons on average usages of steel for the solutions, calculated with both methods, are presented.

Punching shear capacity is calculated according to both EC2:2004 and EC2:2021, for all reinforcement solutions where the formulae allow. A comparison of the different solution’s punching shear results is done, as well as a comparison of the two procedures.

Lastly, an effort is made to compare the reinforcement designs with regards to other factors than what has been calculated. These factors include practical, durability and economical aspects.

3.2 Calculation example

This section presents a calculation example similar to the calculations for slab D3-2. It includes only calculations of the design moments, and not the reinforcement layout, in order to illustrate the methodology in a clear and simple manner. The example will first be introduced with geometry and loads. Then, an LFEA using FK is executed. The results of this are then compared to the results achieved using the method presented in NB 33, as well as the results from yield line theory.

3.2.1 Geometry and load actions

Figure 24 shows a concrete slab with spans of 5 meters in x-direction and 7 meters in y-direction. Slab thickness is $h = 300mm$.

Characteristic loads:

Self-weight: $g = 7.5kN/m^2$

Uniformly distributed live load: $p = 5kN/m^2$

Long term live load: $p_{perm} = 2kN/m^2$

Load factors in ULS: Self-weight 1.2; Live loads 1.5

Materials: C45/55 and B500NC

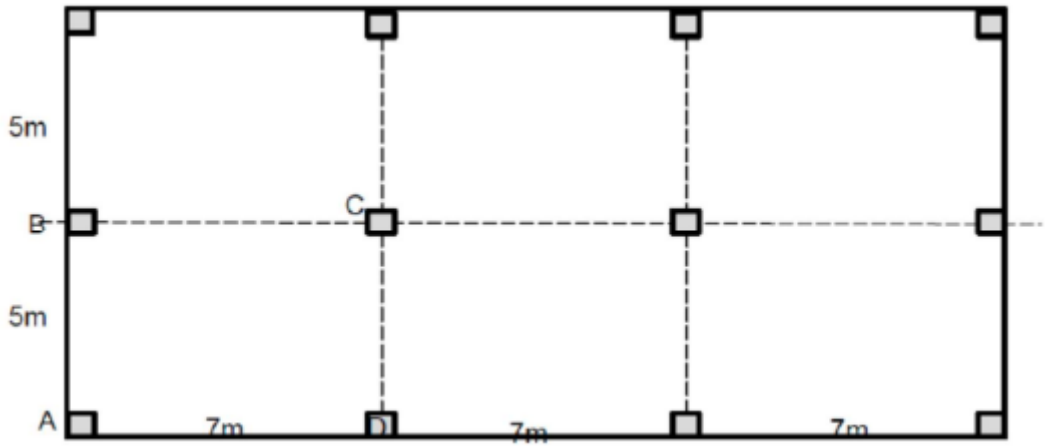

Figure 24: Geometry of the concrete slab.

3.2.2 Concrete slab in FK

The concrete slab is designed with the geometry and loads as given above. Figure 25 shows the slab in FK. The first step is to choose the right material, which is C45 for this example. Then, the columns are placed and given appropriate boundary conditions. The slab is then attached to the columns. The minimum reinforcement may now be generated. The next step is to choose the load actions given in the example. For this, a uniformly distributed surface load is used, with load factors and 40 % of the live loads assumed permanent. The next step is to choose an appropriate mesh. The slab is then ready to get verified and analyzed. When the analysis is done, the results are ready.

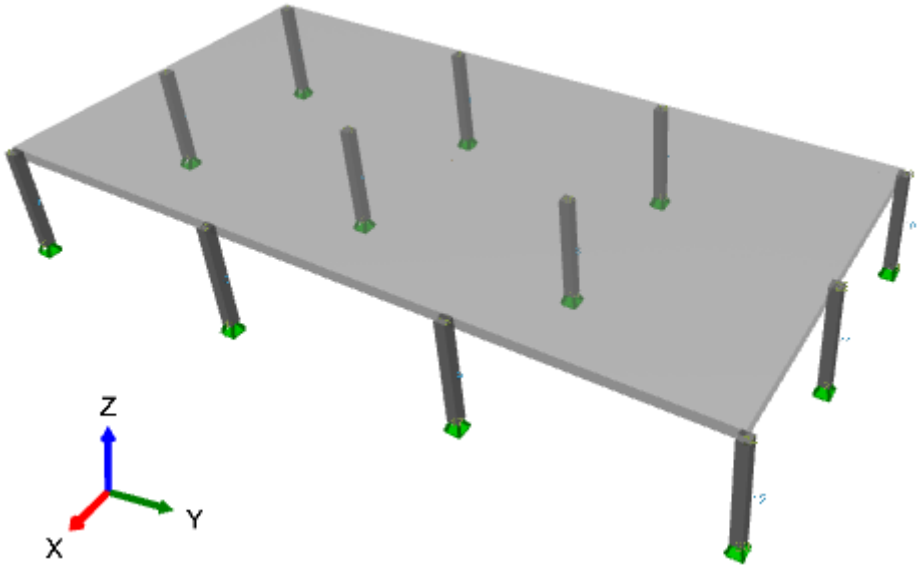

Figure 25: The concrete slab in FK.

For the EFM, the procedure is as explained in Section 2.7. Strips, or beams, are established in each direction. These strips have the same length as the slab in the given direction and have supports where the columns are located. The width of the beam is considered equal to the span width. For the y-direction for instance, a 21 meters long and five meters wide beam is considered, simply supported every seventh meter. This means that the uniformly distributed load with the units of kN/m^2 should be multiplied with the width of five meters. The new distributed load is given in kN/m. The design moments are then calculated with beam theory, and the maximum moments are located at the support and in the middle of the fields. These moments are found by using the most unfavorable load situations, and then divided by the span width of five meters. At this point, there are three different moments to consider. One moment at the supports, one in the outer fields and one in the middle field. These moments are then multiplied with the factors given in NB 33, which are 0.5, 1.2 and 1.8 for the columns and 0.8 and 1.2 in the fields. The procedure for the x-direction is identical. The differences are the number and length of the spans, and the width of the considered beam. This beam has only two spans of five meters each, but the width of seven meters.

The results produced by using FK are compared to the results obtained by the EFM in Figure 26. The results from FK are also adjusted in the graphs, to better compare to the EFM. The adjustment is done by making steps for the same coordinates as for EFM, and the moment in these steps is taken from the FK solution for the coordinates in the middle of these steps. This adjustment is appropriate because the moment will decrease locally when the first crack appears and get smeared over a larger concrete area. Also, the column will provide an evenly distributed negative load over its width, and the moment will be distributed over a larger area than the FK solution expresses. As shown in Figure 26 there is some similarity between EFM and the adjusted moments from FK, but also some distinct differences. The moments around the columns are similar for EFM and FK. The exception is the point located just above the columns. FK gets a significantly higher moment than EFM in this location. The adjusted moments from FK are, on the other hand, more comparable. The EFM does however give the highest moments in the field. In

the y-direction there is a significant difference between these methods. In the x-direction however, they are more comparable. But in both directions, the EFM gives higher moments than FK in the fields. These observations agree with what is described by Sørensen & Øverli (Sørensen & Øverli, 2013). It also indicates that using a linear elastic analysis in FK is an appropriate method which may be combined with EFM according to NB 33. This is especially the case over the columns. In the fields, NB 33 tends to overestimate the moments slightly.

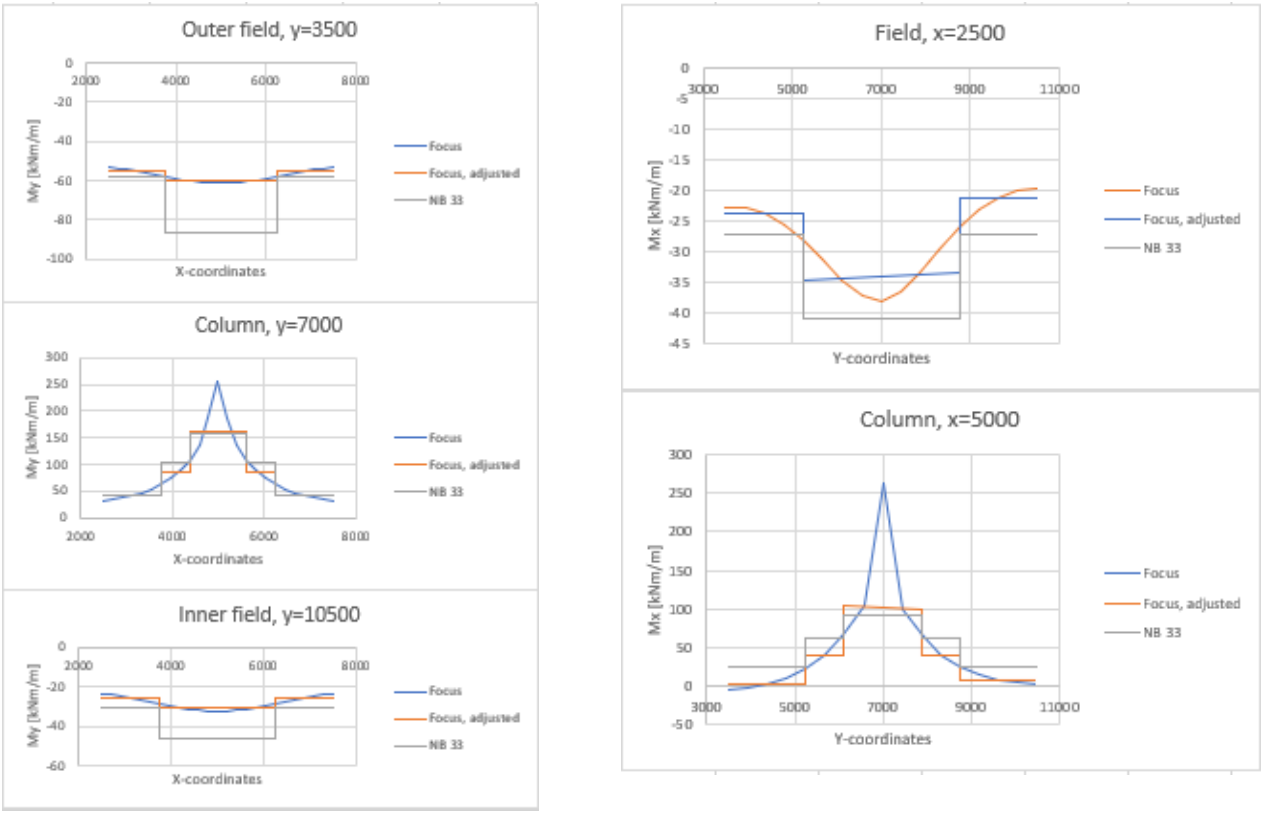

Figure 26: Moments according to FK compared to the method in NB 33.

3.2.3 Yield line theory solution

As explained in Section 2.6, it is expected that by using yield line theory, the calculated design moments should be equal to, or smaller than, the moments obtained in the methods explained above. For this example, there are several yield line patterns that should be checked. Because this is just an example, some simplifications are made during the calculation process. For instance, there will be no iterations to find the exact location of the yield lines in cases where the yield lines are located an unknown distance from one of the edges. It is also assumed that the moment resistance in the top of the slab is three times the moment in the bottom, $\frac{m'}{m} = 3$. This does not necessarily give the best solution but is considered sufficient for this example.

The most relevant yield line patterns are checked either by the work method, or the use of formulae depending on what is more convenient. Figure 27 shows the assumed yield lines for this slab.

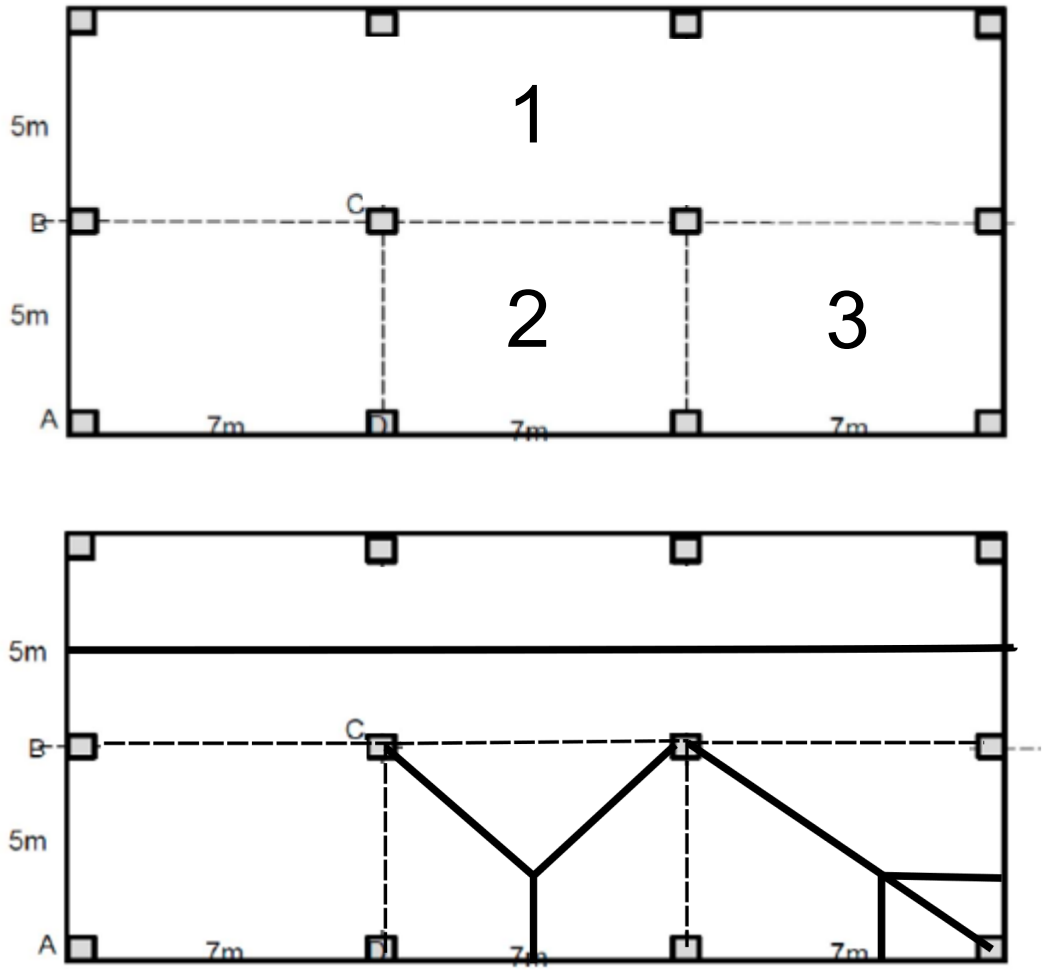

Figure 27: The most relevant yield line patterns.

Case 1 is a folded plate mechanism. The formula and situation obtained from (Kennedy & Goodchild, 2004) is

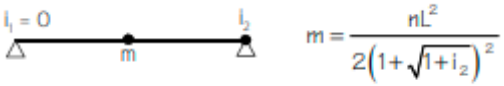

because there is only moment at one of the supports.

For this case:

$$n = g * 1{,}2 + p * 1{,}5 = 7{,}5 * 1{,}2 + 5{,}0 * 1{,}5 = 16{,}5\ kN/m^2$$

$$L = 5m$$

$$i_2 = 3$$

$$m = \frac{16{,}5 * 5^2}{2 * \left(1 + \sqrt{1+3}\right)^2} = 22{,}92 kNm/m$$

For case 2, it is also possible to use formulae obtained from Kennedy & Goodchild (2004). Because of no line loads, the formula might be written as:

$$n' = n$$

$$a' = \frac{2b}{\sqrt{1+i_1}+\sqrt{1+i_3}} = \frac{2*7}{\sqrt{1+3}+\sqrt{1+3}} = 3{,}5$$

$$b' = \frac{2a}{\sqrt{1+i_2}} = \frac{2*5}{\sqrt{1+3}} = 5$$

$$m = \frac{n'*a'*b'}{8*\left(1+\frac{b'}{a'}+\frac{a'}{b'}\right)} = \frac{16{,}5*3{,}5*5}{8*\left(1+\frac{5}{3{,}5}+\frac{3{,}5}{5}\right)} = 11{,}54\ kNm/m$$

For case 3 it is assumed that each side of the small rectangle is 40% of the sides of the bigger rectangle. The geometry of the small rectangle then becomes $2.8 * 2\ m$. For this case, it is necessary to use the work method, following the procedure in Section 2.6.1.

The external work for a slab with an evenly distributed load is the load times the volume of the deflection. This section could be divided into:

One rectangle with $b * h = 4.2 * 2\ m$

One rectangle with $b * h = 2.8 * 2\ m$

Two triangles with $b * h = 4.2 * 3\ m$

Two triangles with $b * h = 2.8 * 2\ m$

The external work is then $W_e = 238.7 * w$

The internal work is also calculated as explained in the theory section. The internal work in this case is $W_i = w * m * 18.31$

$W_e = W_i$ gives $m = 13.04\ kNm/m$

Other possible yield line patterns are shown in Figure 28. However, since the load is evenly distributed and the folded plate mechanism resulted in almost twice as high moments as the other cases, it is likely that the folded plate mechanism will occur. Besides, the patterns in Figure 28 will also lead to more internal work, which will reduce the moment. The moments that the slab should be designed for is therefore the results from case 1, $m = 23kNm/m$ and $m' = 3m = 69\ kNm/m$.

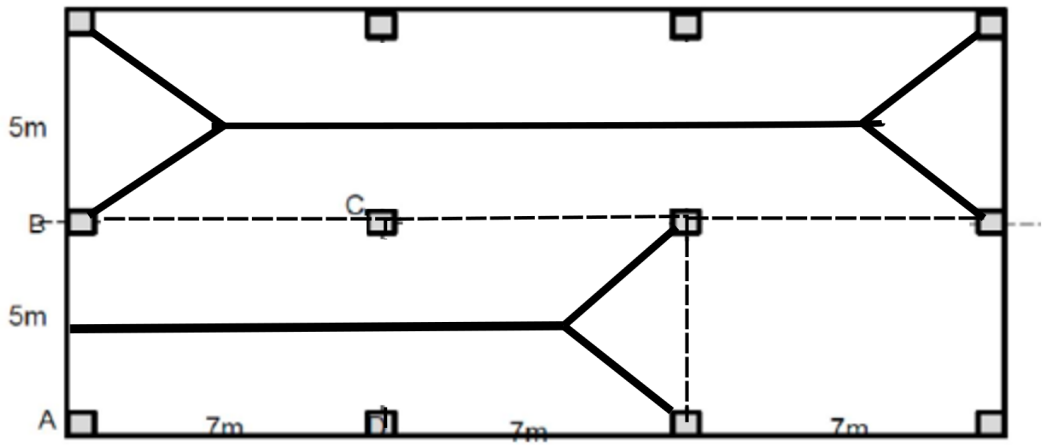

Figure 28: Other possible yield lines.

3.2.4 Conclusion

This example shows the difference between the methods presented in this thesis. The yield line method gives the same design moment all over the slab, whereas the EFM and FK divide the slab into sections. The values in Figure 26 shows moments given by FK and EFM. The field moment for M_x in this figure is from the same section in the slab as the yield line was investigated and is therefore comparable. The values for M_x over the column in Figure 26 are comparable with m'.

Based on this figure, and that yield line theory resulted in $m = 23\ kNm/m$, it is clear that yield line theory gives a lower design moment. This agrees with the theory. For $m' = 69\ kNm/m$, however, the situation is different. Based on the figure, the total negative moment is higher for yield line theory. This indicates that $\frac{m'}{m} = 3$ is not the most optimal solution. With a lower ratio, the positive moment obtained from yield line theory would have been closer to the FK and EFM solution. So would the negative moment as well.

The differences in fundamental principles of these methods become clear through this example. FK exaggerate the moments over the columns, because of elastic theory. By using the FK moments in the middle of each EFM step, the new FK adjusted moments are, for the most part, comparable to the moments achieved by using EFM and NB 33. This is especially true for the negative moments. The use of yield line theory results mostly in lower design moments. Because the reinforcement is homogenous, however, there will be parts of the slab with unnecessarily large amounts of reinforcement. So, despite lower design moments, the total reinforcement area is not necessarily smaller than by using the other methods. However, for a more optimal $\frac{m'}{m}$ ratio, it would have been clearer that yield line theory results in a small amount of reinforcement. It is also important to remember that the slab has not been checked for fan mechanisms or punching shear, which could have led to other design moments and reinforcement demands.

3.3 Slab D3-2

In this thesis, a pile supported slab from a local construction site in Trondheim, named slab D3-2, is analyzed in accordance with the procedure described in the example above. Six reinforcement solutions are considered, where three solutions contain steel fibers, and three solutions include post-tensioned tendons. Thus, the figures used to illustrate the slab, taken from the computer program Focus Konstruksjon (FK), are used to conduct the linear elastic analysis from which elastic bending moments are obtained. In this chapter, the plate's geometry and load situation are described. Then, the procedures for analysis and design of reinforcement solutions according to EFM, yield line theory and punching shear methodology are presented. Lastly, a summary of the six reinforcement solutions which are evaluated is presented. This summary includes explanations of some of the specific detailing and calculation choices that are necessary to make in order to handle each solution in an effective manner.

3.3.1 Geometry and load situation

The slab consists of C35 concrete and is executed as two connected areas with different thicknesses. The largest area, intended for commercial use, is 275 mm thick. The smaller area, in which the elevator and staircase are located, is 335 mm thick. Underneath the walls and columns that are on top of the slab, a lowered concrete area is located which is 200 mm thick and up to 900 mm wide. The intention of this extra area is to help deal with punching shear. It also ensures that connecting reinforcement from the adjacent structures, such as walls, into the slab is feasible on-site. This layout of the slab-wall connection also contributes with some bending stiffness at the slab's edges. Slab D3-2 spans 20 meters in the x-direction and 16 meters in the y-direction at its largest. Since the slab constitutes the ground floor in an apartment building, considerations regarding floor layout in the higher floors have led to an irregular pile layout for the slab. This is because piles are needed wherever columns from the floors above are led into the slab, so that the concentrated column loads are led directly into the ground. Furthermore, issues with driving steel piles through 20 meters of quick clay down to solid rock has led to some of the piles becoming scrap piles that are unable to fulfill their intended functions. Revisions related to this has led to further irregularities in the layout of piles. Thus, the plate has a complex geometry, as illustrated in Figure 29 and Figure 30. Furthermore, the pile layout and lowered areas underneath columns and walls mean that no extra line- or concentrated loads are imposed on the plate.

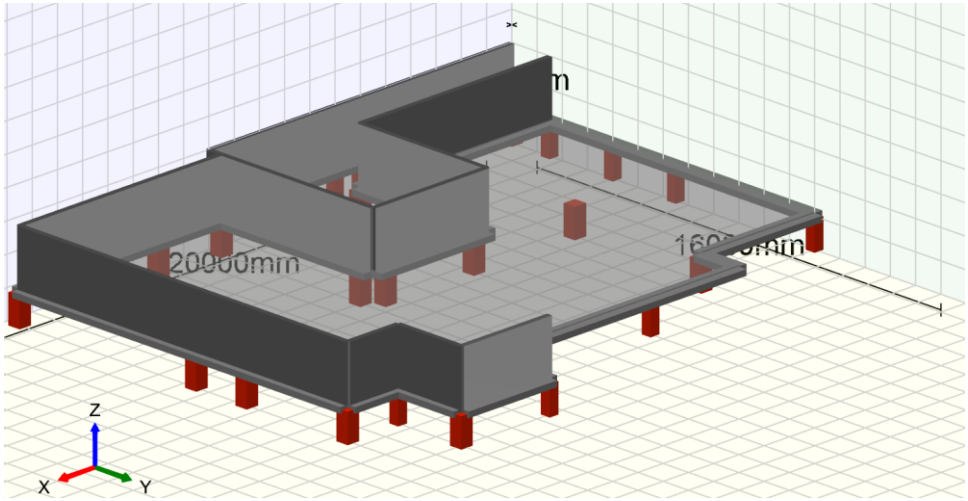

Figure 29: Geometry of slab D3-2, from a skewed angle.

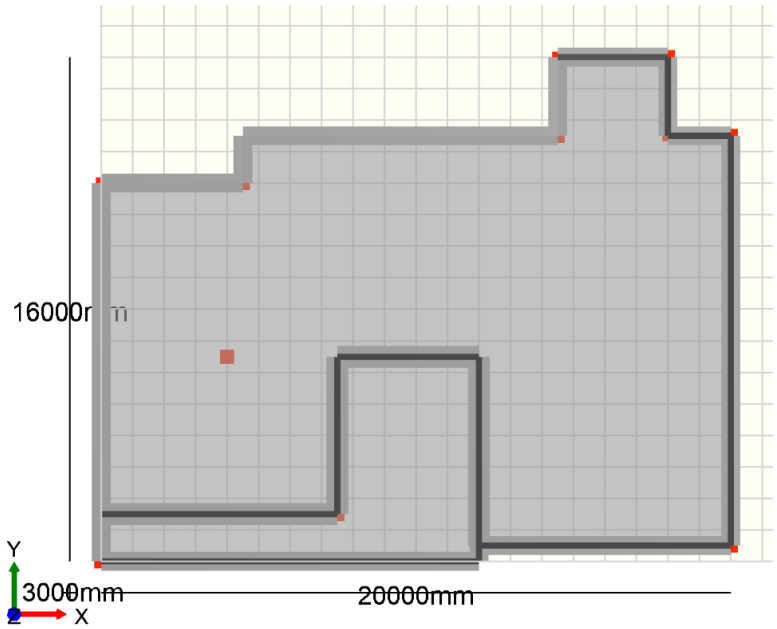

Figure 30: The geometry of slab D3-2, from a bird's eye view.

The connection between the piles and D3-2 is executed with pile heads made of a welded steel plate embedded in the middle of the lowered area under the slab. The steel plates vary in thickness between 30 and 50 mm, and are quadratic with side lengths of either 350 or 450 mm. In FK, this is modelled as steel columns with a length of 1000 mm and the dimensions of the respective pile heads. The steel columns in the model are assumed to be fully fixed in the bottom, with stiff connections to the slab.

The slab is loaded with a live load from usage of the commercial area of $p = 4\ kN/m^2$ and an imposed dead load of $g_{outer} = 2.5\ kN/m^2$, in addition to the slab's self-weight of $g_{self} = 6.875\ kN/m^2$. These loads are uniformly distributed across the entire slab, and give the following design load case:

$$q_{Ed} = 1.2 * (g_{outer} + g_{self}) + 1.5 * p = 17.25\ kN/m^2$$

In the analysis of the slab, it is assumed that the entire live load acts on the whole slab and is not distributed unfavorably. Furthermore, a triangular mesh is generated for the elastic analysis. The slab with loads is shown in Figure 31, and Figure 32 illustrates the mesh.

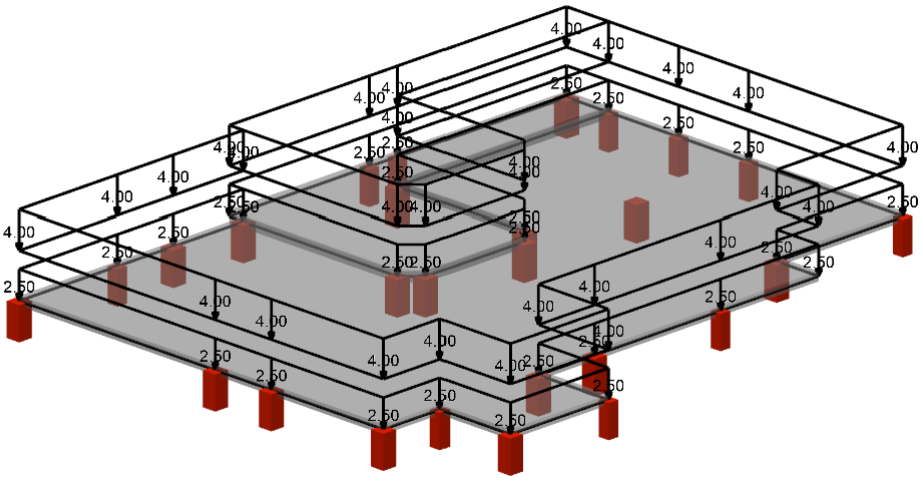

Figure 31: Slab D3-2 with external loads.

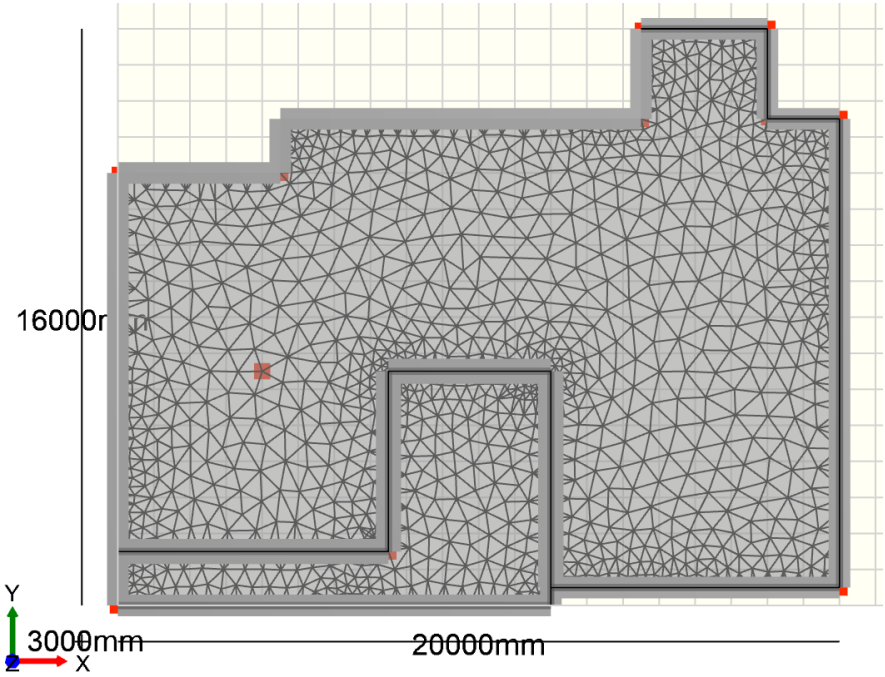

Figure 32: Triangular mesh generated by FK.

3.3.2 Elastic analysis

Bending moments in x- and y-directions are obtainable from the results of the elastic analysis in FK. The distributions of these moments are illustrated in Figure 33 and Figure 34.

Figure 33: Distribution of M_x from FK.

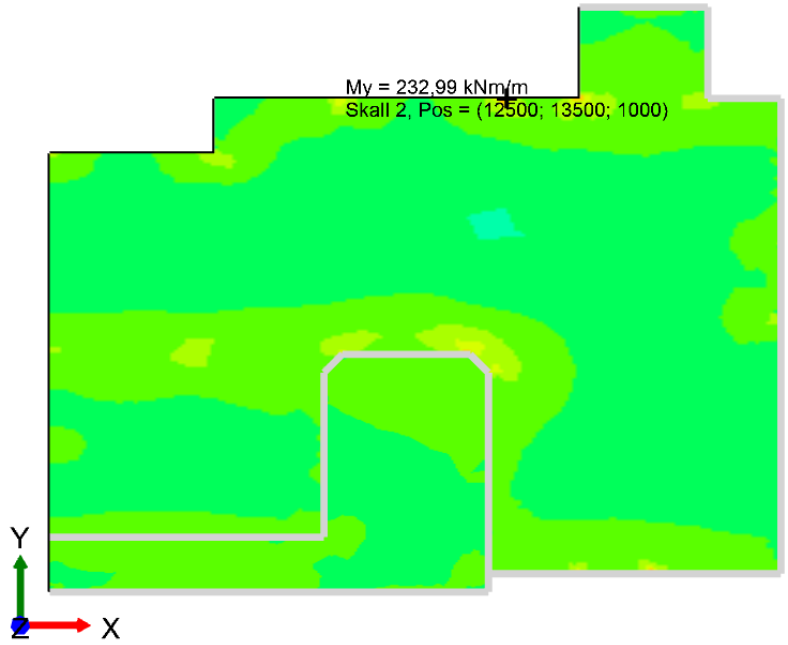

Figure 34: Distribution of M_y from FK.

On these figures, yellow and orange coloring indicates large bending moments with tension at the top part of the cross-section. The light blue color indicates the largest bending moments with tension in the bottom. Based on these moment distributions, areas of special interest within the slab may be identified. This overview guides the choice of critical sections for further analysis with EFM and yield line theory. The spans and columns with the largest bending moments get chosen as the field- and column strips which are used in an analysis with EFM. Furthermore, suitable areas between columns that have large moments get analyzed with yield line theory by checking the

critical failure mechanism for this slab. Thus, obtaining elastic load actions from an LFEA such as this ensures an efficient design process when a slab has a complicated and non-symmetrical geometry (Hagberg et al., 2004, p. 4).

3.3.3 EFM

Based on the moment distributions illustrated in Figure 33 and Figure 34, the sections defined in Figure 35 and Figure 36 are chosen for analysis with EFM.

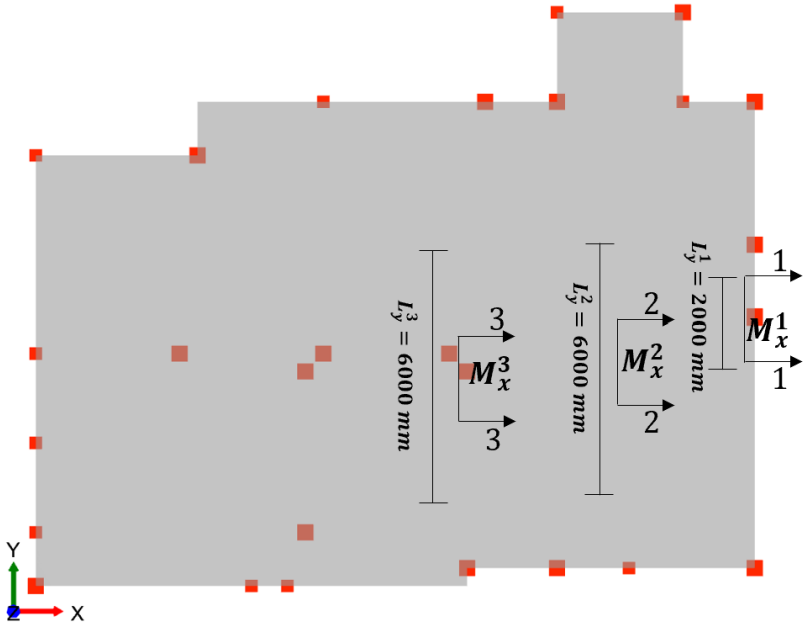

Figure 35: Sections determined after the distribution of Mx.

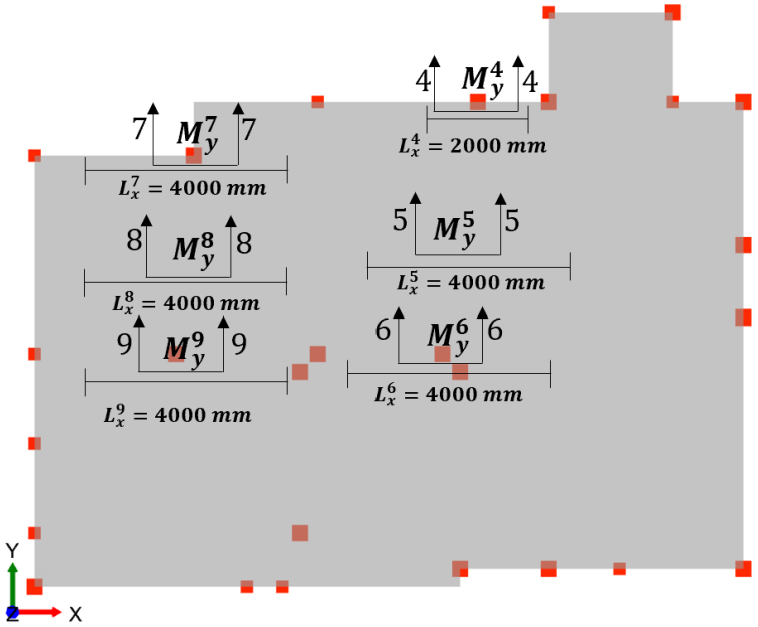

Figure 36: Sections determined after the distribution of My.

From the elastic analysis in FK, the design moment over each strip's width is extracted. The widths are determined conservatively as the largest span between piles in the section's vicinity. Then, following the same procedure as in the example presented

above, the moment distributions are adjusted into strips in accordance with the method described in Section 2.7. Thus, an adjusted moment distribution as illustrated in Figure 37 is created.

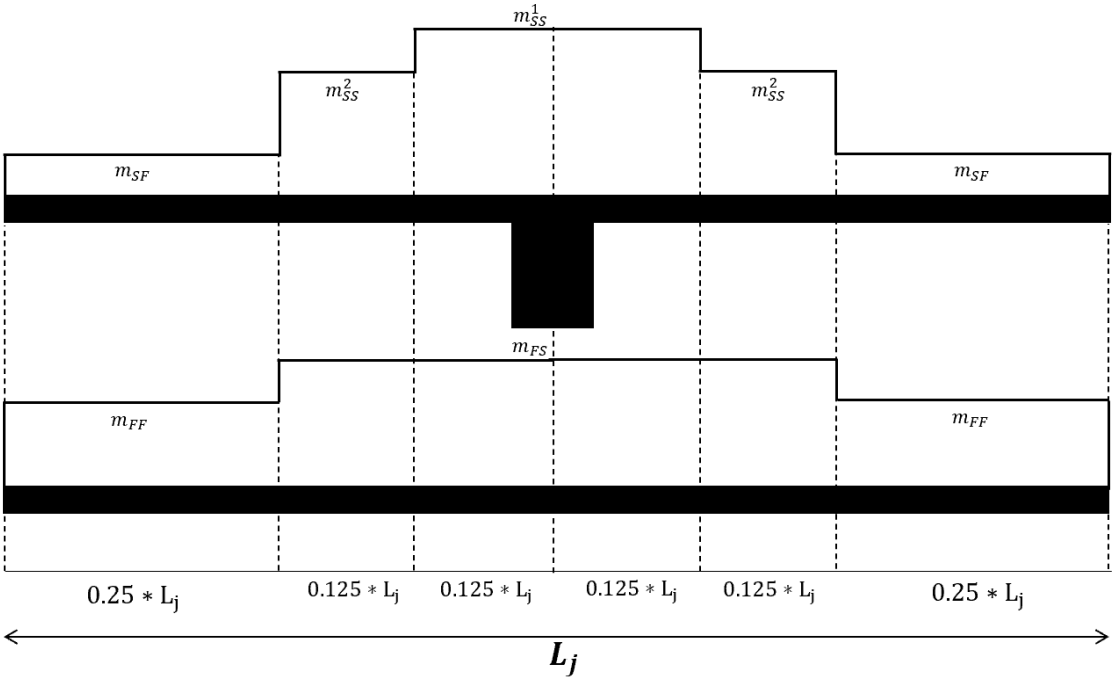

Figure 37: Illustration of the adjusted moment distributions created in this thesis, following the procedure from the calculation example.

Here, L_j is the span length defining the width of the section under analysis. With this system in place, the moment which is distributed into strips may be calculated for all sections. Then, necessary reinforcement areas are calculated using these design moments and equilibrium equations for moment capacity. Ultimately, this gives a comprehensive reinforcement solution for the critical sections of the slab. In order to maintain adherence to the objective of emphasizing a comparison of calculation results, the necessary and chosen reinforcement amounts are only obtained for the critical sections. Thus, no reinforcement layout is produced for the slab in its entirety, and neither is there any reinforcement detailing calculations made for the critical sections.

3.3.4 Yield line theory

The foundation upon which the yield line theory analysis is made is, as for EFM analysis, the bending moment distributions presented in Figure 33 and Figure 34. The distribution of large bending moments, both positive and negative, guide the identification of areas in which critical yield line patterns may arise. This, in combination with the largest spans in slab D3-2, and the given boundary conditions, makes one yield line pattern appear to be the critical one. As the scope of this thesis is to illuminate the differences between several reinforcement solutions, a detailed and iterative calculation process to determine the critical yield line pattern is not carried out. Therefore, the probable critical yield line pattern is chosen, and calculations are conducted. The pattern's geometry, as well as the relevant calculation parameters, are presented in Figure 38.

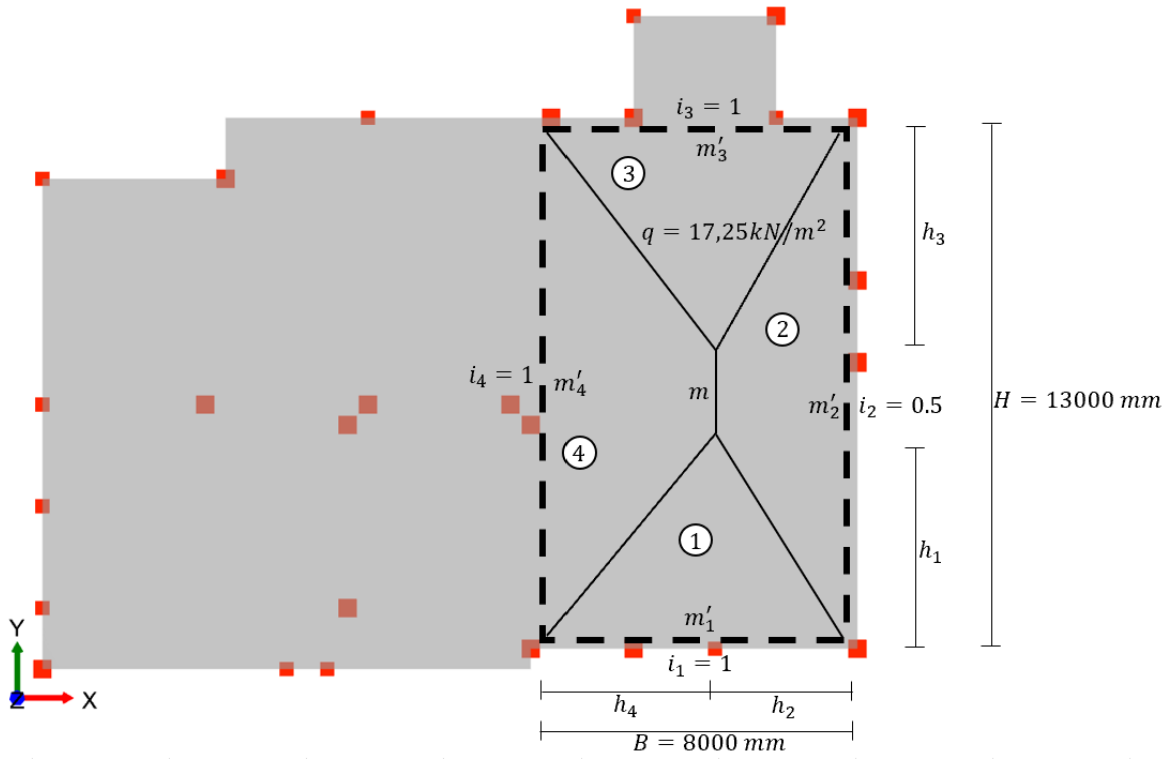

Figure 38: The critical yield line pattern in slab D3-2.

Where m is the moment along the negative yield line; m' is the moment along the positive yield line; $i_i = \frac{m_i'}{m}$ is the fixity ratio of an edge; $1{,}2{,}3{,}4$ are the areas between the yield lines acting as stiff slab segments; h_1, h_2, h_3, h_4, B, H define the yield line pattern's geometry; $q = 17.25\ kN/m^2$ is the evenly distributed load acting on the slab.

The section of slab D3-2 contained in the yield line pattern illustrated above is a two-way slab with supports on four sides. As in the analysis of case 2 in the calculation example presented above, this particular yield line pattern may also be calculated using standard formulae obtained from Kennedy & Goodchild (2004). The formulae for a yield line pattern akin to this are found in Tables 3.6a and 3.6b, and for a slab with no line loads give:

$$b_r = \frac{2B}{\sqrt{1+i_2}+\sqrt{1+i_4}}; h_r = \frac{2H}{\sqrt{1+i_1}+\sqrt{1+i_3}}$$

Which are the reduced sides of a simply supported two-way slab with the same midspan moments as the slab with fixed supports and sides B and H. Furthermore:

$$m = \frac{q * b_r * h_r}{8 * \left(1 + \frac{h_r}{b_r} + \frac{b_r}{h_r}\right)}\ and\ m_i' = i_i * m$$

Which is the moment obtained by the yield pattern. Finally, the geometry is defined by:

$$h_1 = \sqrt{6 * (1+i_1) * \frac{m}{q}}; h_2 = \frac{b_r}{2} * \sqrt{1+i_2}; h_3 = \sqrt{6 * (1+i_3) * \frac{m}{q}}; h_4 = \frac{b_r}{2} * \sqrt{1+i_4}$$

As mentioned in Section 2.6.4, a slab with an irregular pile layout should be designed for a moment 15% larger than what is provided by the calculation. Thus, the design moment is:

$$m_{Ed} = 1.15 * m; m'_{Ed,i} = i_i * m_{Ed}$$

When these parameters are calculated, necessary reinforcement amount according to yield line theory may be determined. Since a single negative moment is defined for the entire slab segment, and one positive moment is defined for each edge, it can clearly be seen that yield line theory provides simple reinforcement layouts.

3.3.5 Punching shear

Two piles, one edge pile and one internal pile, are selected for punching shear capacity control. The two piles' placements within slab D3-2 are illustrated in Figure 39.

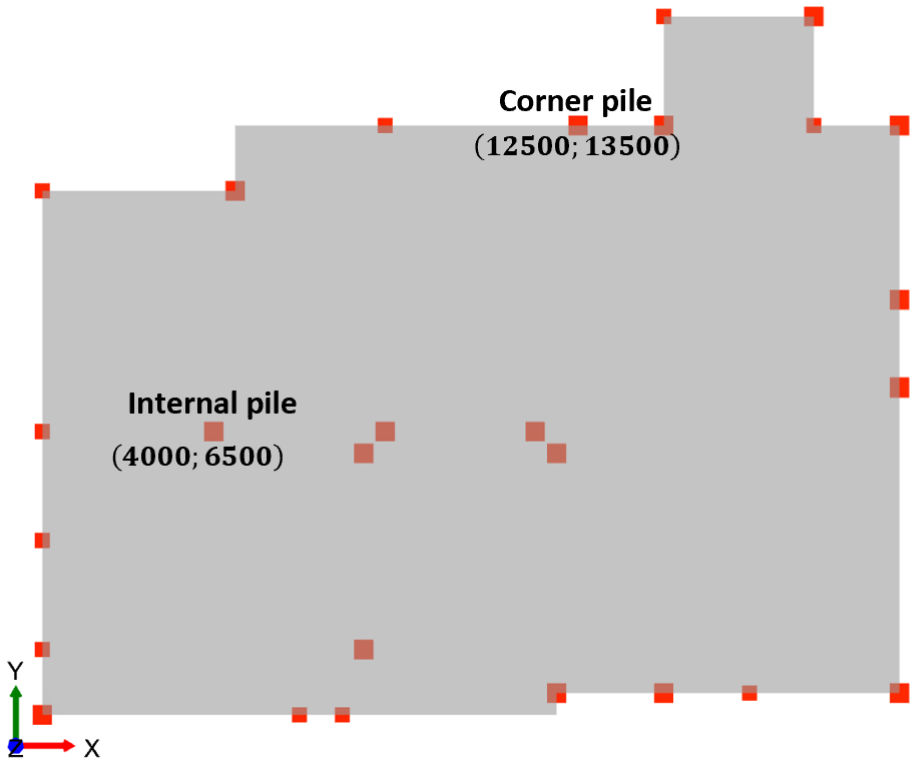

Figure 39: The placement of the piles chosen for punching shear calculations.

These two piles are chosen because they have large shear loads acting on them, and in order to highlight the differences in how internal piles and edge piles are handled in both the current Eurocode 2 and the proposed new EC2. Since this thesis mainly investigates how capacity calculations are affected by different reinforcement solutions and not how to detail reinforcement placement and layout, the piles with the largest shear forces acting on them are deemed not to be the most interesting to investigate. The pile heads are $450x450\ mm$ for both the internal and the edge pile. Figure 40 illustrates the basic control perimeters around an internal and edge-adjacent load area, adapted from EC2.6.4.2.

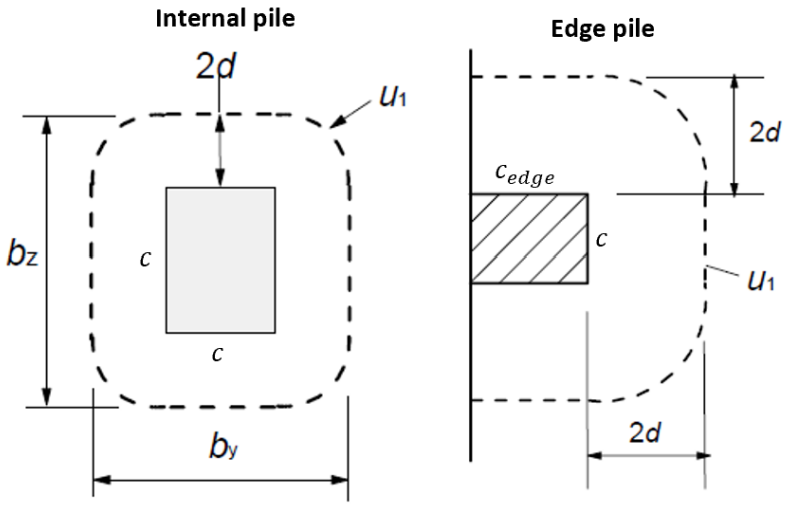

Figure 40: Illustration of basic control perimeters around the two pile types investigated in this thesis (CEN, 2004).

The formulae for the two basic control perimeters, set at a distance equal to $2d$ from the pile face, according to the current Eurocode are:

$$u_{1internal} = 4\pi d + 4c; u_{1edge} = 2\pi d + 2c_{edge} + c$$

For calculations according to the proposed new Eurocode, the perimeter is set at $\frac{d}{2}$. This gives:

$$b_{0.5internal} = \pi d + 4c; b_{0.5edge} = \frac{\pi d}{2} + 2c_{edge} + c$$

The lowered area added underneath the slab under walls and where there are piles fixed to the slab, are intended to ensure sufficient shear capacity. In addition, they make placement of shear reinforcement, as well as fastening of reinforcement from adjacent structures, easier to perform. An illustration of how the pile is fixed to the slab via the lowered area, and how this affects the control perimeter, is shown in Figure 41. The load area is considered as containing the pile head through which the shear forces are transferred to the pile and into the ground, in addition to the extra width provided by the lowered area at the height where the pile head is located. For the edge pile, only one of the sides of the lowered area is slanted. Thus, the internal load area has an area of $A_{internal} = 700x700\ mm$, while for the edge pile it is $A_{edge} = 700x600\ mm$.

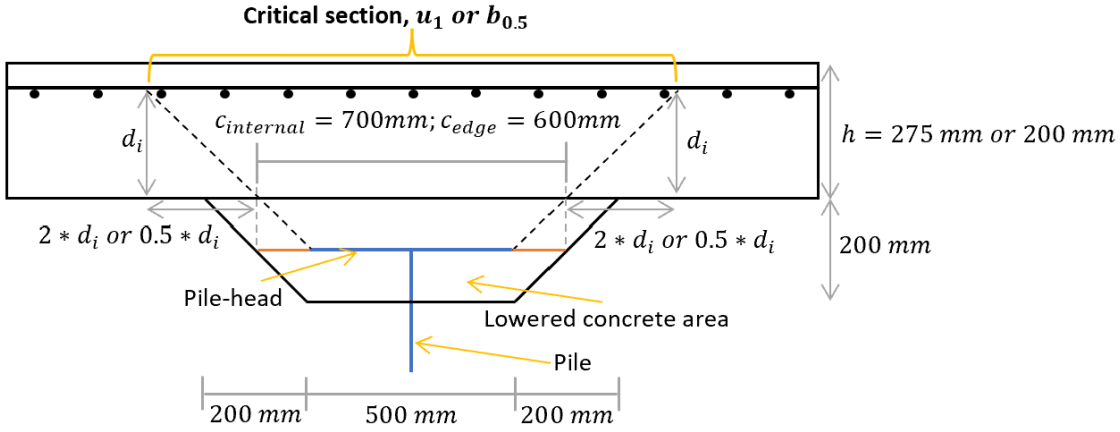

Figure 41: An illustration of the cross-section near the internal pile controlled for punching shear.

The comparison of how the reinforcement solutions affect the outcome of the calculations, as well as how the revised calculations in the new EC2 impact the results, are the main objectives of the punching shear calculations. Therefore, the calculations for all solutions include capacity calculations of a concrete cross-section without shear reinforcement, whether this check is required or not by the procedure in either edition of the Eurocode for any given reinforcement solution.

The current EC2 does not provide formulae for handling concrete structures with fiber reinforcement. Thus, only the solutions without fibers are checked according to these rules. For these solutions, v_{Ed1}, v_{Rdmin} and v_{Rdc} are calculated and compared. Following the new EC2, the equivalent calculations of τ_{Ed}, τ_{Rdcmin} and τ_{Rdc} are made. This makes a comparison of both how the reinforcement solutions affect the results within a given calculation methodology, and how the different methodologies affect the results of a given reinforcement solution.

The solutions containing fibers are only checked according to the proposed new Eurocode. The same calculations are made for all solutions, as far as this is possible. The proposed new EC2, like the current, is not always applicable to concrete structures without conventional reinforcement. For example, the formula for τ_{Ed} contains the mean reinforcement depth of the cross-section, which is unapplicable to a fiber reinforced concrete that has no other form of reinforcement. This enables, for the most part, a comprehensive comparison between several reinforcement solutions to be made.

3.3.6 Reinforcement solutions

Although the methods of analysis and the base assumptions are the same for all reinforcement solutions, they have several differences which make the design processes different. Therefore, a short summary of how each reinforcement solution is designed is presented. These summaries emphasize each solution's unique features and how they affect the calculations and design. Every slab design which is evaluated in this thesis is analyzed and discussed with cast-in-situ concrete in mind.

A. The conventionally reinforced solution is the reference case when analyzing slab D3-2. This is because conventional reinforcement is a well-tried method for reinforcing a slab. Furthermore, the authors of this thesis has access to proposed real-life reinforcement solutions for slab D3-2, which makes early-stage comparisons and quality checks a possibility. Based on the adjusted bending

moment distribution obtained from the LFEA, the design bending moments in the critical sections are acquired. Then, using the equilibrium equations presented in Section 2.7, necessary and chosen reinforcement amounts are calculated for each critical section according to EFM. Section NA.9.3.1.1(3) in EC2 defines $s = 400mm$ as the largest bar spacing which should be used in slabs. Thus, all chosen reinforcement amounts have a lower bar spacing than this. Lastly, using the equations and yield line pattern presented in Section 3.3.4, necessary and chosen reinforcement amounts are calculated using yield line theory. Then, the punching shear procedures in both versions of EC2 are followed.

B. The second solution to be investigated is the combination of PT reinforcement and conventional reinforcement. Since Eurocode 2 does not allow prestressed tendons to be considered as minimum reinforcement, a K257 reinforcement net is combined with $\phi 12 s 900$ rebars to fulfill the requirements. The minimum reinforcement requirement for this slab is $361 mm^2/m$, and the choice of conventional reinforcement provides a steel area of $383\ mm^2/m$. Even though the Eurocode does not demand minimum reinforcement in the top of the slab, a K257 net is provided here as well. This evenly distributed conventional reinforcement contributes to crack limitation, which gives better results in SLS and a tighter slab. Furthermore, it provides a rigid support upon which the post-tensioned tendons may be placed and fastened. Then, concentrated tendon strips are placed in x-direction and distributed tendons in y-direction. With these assumptions made, an estimated design prestressing force is calculated according to Eurocode 2 and applied to all tendons. Then, using the moment equilibrium equations described in Section 2.10.1, a necessary number of tendons is calculated in each critical section. Based on this number and the widths of each strip, a number of tendons is chosen for each concentrated tendon strip. This is done in all critical sections according to EFM. For yield line theory analysis, the equations for moment equilibrium are used to find the necessary moment capacity of the tendons. This is, in turn, utilized to calculate the necessary tendon number in concentrated tendon strips as well as the necessary number of distributed tendons. Punching shear calculations are made identically as for solution A, but with the contribution of the prestressing tendons taken into account.

C. Since using PT reinforcement is an effective way of reducing deflections, either larger spans or leaner structures may be constructed. Thus, an alternative design with the same reinforcement as solution B, but with a smaller cross-section height is investigated. The reduced slab height ensures that a single K257 net is sufficient as minimum reinforcement. Furthermore, the leaner slab has a reduced load acting on it, with an evenly distributed load of $q_C = 15\ kN/m^2$. This reduces the design bending moments in the critical sections. The reduced load and different cross-section data are used in the same calculation procedure as for reinforcement solution B.

D. For the solution with conventional, post-tensioned and fiber reinforcement, the amounts of conventional and fiber reinforcement are chosen beforehand. This makes the calculation of necessary reinforcement easier. The amount of conventional reinforcement is based on minimum reinforcement and practical reasons, like for solution B and C. For fiber reinforcement, an assumed $f_{Ftud} = 1.2\ MPa$ is used. This corresponds to $f_{Ftuk} = 1.8\ MPa$, and a proportion of fiber

reinforcement of approximately $45\ kg/m^3$. This is based on tests according to NS-EN 14651. It is possible to design slabs with both larger and smaller fiber dosages. This amount is chosen because the chance of obtaining a sufficient residual flexural strength is greater than for smaller proportions, while making it easier to obtain the desired fresh concrete properties than for higher dosages. In addition, it is convenient to investigate the capacity of a slab with a medium amount of fiber reinforcement, because the slab is investigated for different combinations of reinforcement. This way, the fiber amount might be sufficient to fulfill demands for yield line theory, but still small enough to require supplementary contributions from other reinforcement types when using EFM.

E. The post-tensioned and fiber solution is investigated the same way as solution D. The fiber dosage is the same, which makes a comparison easier, but there is no conventional reinforcement. This makes the provisions given in Eurocode 2 challenging to follow, because they assume conventional reinforcement.

F. The amount of fibers is the same as for previous solutions. This solution is not accepted by Eurocode 2 but is still investigated to show the effect of fibers. EFM is not applicable for this solution and is therefore not used here. For punching shear capacity, the value used in capacity calculations is f_{Ftud}.

In every solution containing post-tensioned reinforcement, the number of tendons chosen is based on the need for additional moment capacity beyond what the minimum conventional reinforcement and the fibers provide. For EFM, this additional capacity is checked for each strip individually, but an assessment is also made for the entire sections. This way, it is possible to get an overview over the necessary post-tensioned reinforcement in each strip, as well as the whole section. To take plastic-like behavior into account, the solutions are mainly based on the total moment capacity for the whole section. The exception is when the moments are densely concentrated, like adjacent strips with especially high design moments. In these cases, it is considered necessary with an extra tendon for such strips, even if the total capacity in the section is already sufficient.

A detailed calculation of the tendon prestressing losses is not made, as it is beyond the scope of this thesis. However, an estimation of a tendon loss is calculated according to Eurocode 2 and applied equally to all tendons in the ULS-calculation. Losses due to the instantaneous deformation of the concrete structure is neglected, as it is demanding to calculate and depends on the order in which the tendons are stressed. Furthermore, an anchorage loss of 6 *mm* is assumed. This number is based on previous tests in which the authors of this thesis were involved. Thus, the equations in EC2 are followed to produce a conservative estimate, and this estimate provides the design prestressing force for all tendons.

4 Results

In this chapter, the results produced using the methodology described in the previous chapter are presented. First, the relevant load actions obtained from Focus Konstruksjon (FK) are shown. These include the adjusted bending moment distributions that are adjusted according to NB 33, the design load actions obtained through yield line theory analysis, and the design shear forces used in punching shear calculations. The results are presented for the slab with full height and the slab with reduced height. Then, each reinforcement solution's results are introduced and listed for EFM, yield line theory and punching shear respectively. These results are presented for the different reinforcement solutions in turn. The reinforcement designs are A (conventional reinforcement), B (conventional and post-tensioned (PT) reinforcement), C (conventional and PT reinforcement with reduced slab thickness), D (fiber, PT and conventional reinforcement), E (fiber and PT reinforcement), and F (fiber reinforcement). Lastly, a summary which compares some of the most central results is given. This includes a comparison of total calculated reinforcement amounts for each reinforcement solution obtained from analysis with EFM and yield line theory separately, and comparisons of the two methods.

4.1 Load actions

This section presents the load actions that are used in the different analyses. These are the adjusted bending moments calculated through an LFEA and used in calculations according to EFM, the design moments for the critical yield line pattern obtained by standard formulae, and the design shear forces used in the punching shear calculations.

4.1.1 Adjusted bending moments

The distributions of the adjusted bending moments from the elastic analysis done in FK, for each strip in every chosen section, are shown in Table 2 and Table 3.

Table 2: Adjusted bending moments in critical sections over columns.

	m_{SFL}	m^2_{SSL}	m^1_{SS}	m^2_{SSR}	m_{SFR}	
Section 1	42,00	89,00	170,00	84,00	44,00	Mx [kNm/m]
Section 3	36,00	48,00	109,00	52,00	20,00	Mx [kNm/m]
Section 4	31,00	93,00	160,00	54,00	31,00	My [kNm/m]
Section 6	40,00	47,00	110,00	66,00	32,00	My [kNm/m]
Section 7	1,00	17,00	81,00	25,00	7,00	My [kNm/m]
Section 9	35,00	47,00	87,00	35,00	27,00	My [kNm/m]

Table 3: Adjusted bending moments in critical sections in fields.

	m_{FFL}	m_{FS}	m_{FFR}	
Section 2	-43,00	-51,00	-40,00	Mx [kNm/m]
Section 5	-43,00	-47,00	-44,00	My [kNm/m]
Section 8	-28,00	-33,00	-30,00	My [kNm/m]

The reduced moments that are applicable for reinforcement solution C, with lower slab height, is shown in Table 4 and Table 5.

Table 4: Reduced bending moments over columns.

	m_{SFL}	m^2_{SSL}	m^1_{SS}	m^2_{SSR}	m_{SFR}	
Section 1	36,52	77,39	147,83	73,04	38,26	Mx [kNm/m]
Section 3	31,30	41,74	94,78	45,22	17,39	Mx [kNm/m]
Section 4	26,96	80,87	139,13	46,96	26,96	My [kNm/m]
Section 6	34,78	40,87	95,65	57,39	27,83	My [kNm/m]
Section 7	0,87	14,78	70,43	21,74	6,09	My [kNm/m]
Section 9	30,43	40,87	75,65	30,43	23,48	My [kNm/m]

Table 5: Reduced bending moments in fields.

	m_{FFL}	m_{FS}	m_{FFR}	
Section 2	-37,39	-44,35	-34,78	Mx [kNm/m]
Section 5	-37,39	-40,87	-38,26	My [kNm/m]
Section 8	-24,35	-28,70	-26,09	My [kNm/m]

4.1.2 Yield line theory

Only one yield line pattern is investigated as it is assumed to be critical. Through standard formulae in Kennedy & Goodchild, the following design moments are calculated, and the results are presented in Table 6.

Table 6: Bending moments found with yield line theory.

Yield line theory - bending moments			
Evenly distributed load	q	17,3	kN/m^2
From formulae	m	37,8	kNm/m
Field moment	m_{field}	43,5	kNm/m
Moment edge 1 $(i=1)$	m'_1	43,5	kNm/m
Moment edge 2	m'_2	21,8	kNm/m
Moment edge 3 $(i=1)$	m'_3	43,5	kNm/m
Moment edge 4 $(i=1)$	m'_4	43,5	kNm/m

The equivalent moments for reinforcement solution C, with reduced slab thickness, are given in Table 7.

Table 7: Bending moments for solution C found with yield line theory.

Yield line theory - bending moments solution C			
Evenly distributed load	q	15,0	kN/m^2
From formulae	m	32,9	kNm/m
Field moment	m_{field}	37,8	kNm/m
Moment edge 1 $(i=1)$	m'_1	37,8	kNm/m
Moment edge 2	m'_2	18,9	kNm/m
Moment edge 3 $(i=1)$	m'_3	37,8	kNm/m
Moment edge 4 $(i=1)$	m'_4	37,8	kNm/m

4.1.3 Shear

In order to conduct the punching shear calculations according to both the current Eurocode 2 and the proposed new Eurocode 2, the design shear forces acting on the chosen piles are needed. These are calculated through the same elastic analysis with

which the design bending moments were obtained. Table 8 presents the design shear forces on the two selected piles for punching shear calculations.

Table 8: Design shear forces acting on the chosen piles.

Pile type	V_{Ed}	
Edge	203	kN
Internal	387	kN

4.2 EFM

This section presents the calculated necessary reinforcement amounts for each reinforcement solution. These are found by using moment equilibrium formulae, where the formulae that are used depends on the reinforcement solution under investigation. Furthermore, a chosen reinforcement area is given, in addition to an illustrated proposed layout of this chosen reinforcement area. A total of nine sections are chosen for analysis, based on the moment distribution and span lengths.

4.2.1 Conventional reinforcement

Table 9 provides an overview of the calculated necessary reinforcement area for each strip in every chosen section over piles in slab D3-2, in addition to the reinforcement amount that is chosen. Table 10 presents necessary and chosen reinforcement areas for sections in fields. Since $s = 400mm$ is the largest allowable bar spacing according to the Eurocode, some strips exhibit big differences between the chosen and necessary reinforcement amounts. Furthermore, the bar spacings are rounded down so that there are fewer different spacings altogether.

Table 9: Necessary and chosen reinforcement amounts over columns for solution A.

		m_{SFL}	m^2_{SSL}	m^1_{SS}	m^2_{SSR}	m_{SFR}	
$A_{snecessary}$	Section 1	438	930	1869	877	459	mm^2
$A_{schosen}$		603	1005	2011	1005	603	mm^2
$A_{snecessary}$	Section 3	376	501	1153	543	209	mm^2
$A_{schosen}$		804	603	1206	603	804	mm^2
$A_{snecessary}$	Section 4	324	1038	1785	602	346	mm^2
$A_{schosen}$		402	1005	2011	1005	402	mm^2
$A_{snecessary}$	Section 6	417	490	1165	689	334	mm^2
$A_{schosen}$		603	603	1608	804	603	mm^2
$A_{snecessary}$	Section 7	10	177	845	261	73	mm^2
$A_{schosen}$		603	402	1005	402	603	mm^2
$A_{snecessary}$	Section 9	365	490	908	365	282	mm^2
$A_{schosen}$		603	603	1005	402	603	mm^2

Table 10: Necessary and chosen reinforcement amounts in fields for solution A.

		m_{FFL}	m_{FS}	m_{FFR}	
$A_{snecessary}$	Section 2	480	569	446	mm^2
$A_{schosen}$		804	1608	804	mm^2
$A_{snecessary}$	Section 5	480	524	491	mm^2
$A_{schosen}$		603	1005	603	mm^2
$A_{snecessary}$	Section 8	312	368	335	mm^2
$A_{schosen}$		603	1005	603	mm^2

The chosen reinforcement amounts, and their placement within the critical sections, are illustrated in Figure 42 and Figure 43.

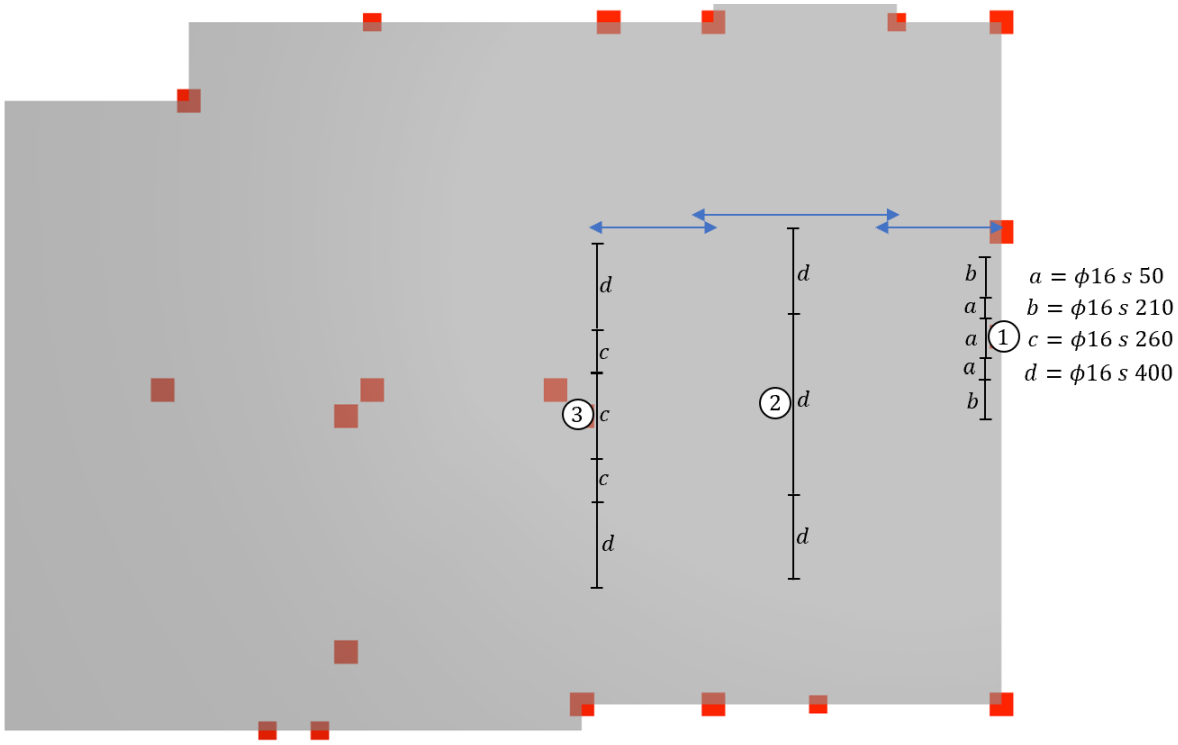

Figure 42: Illustration of chosen reinforcement amounts in x-direction for solution A.

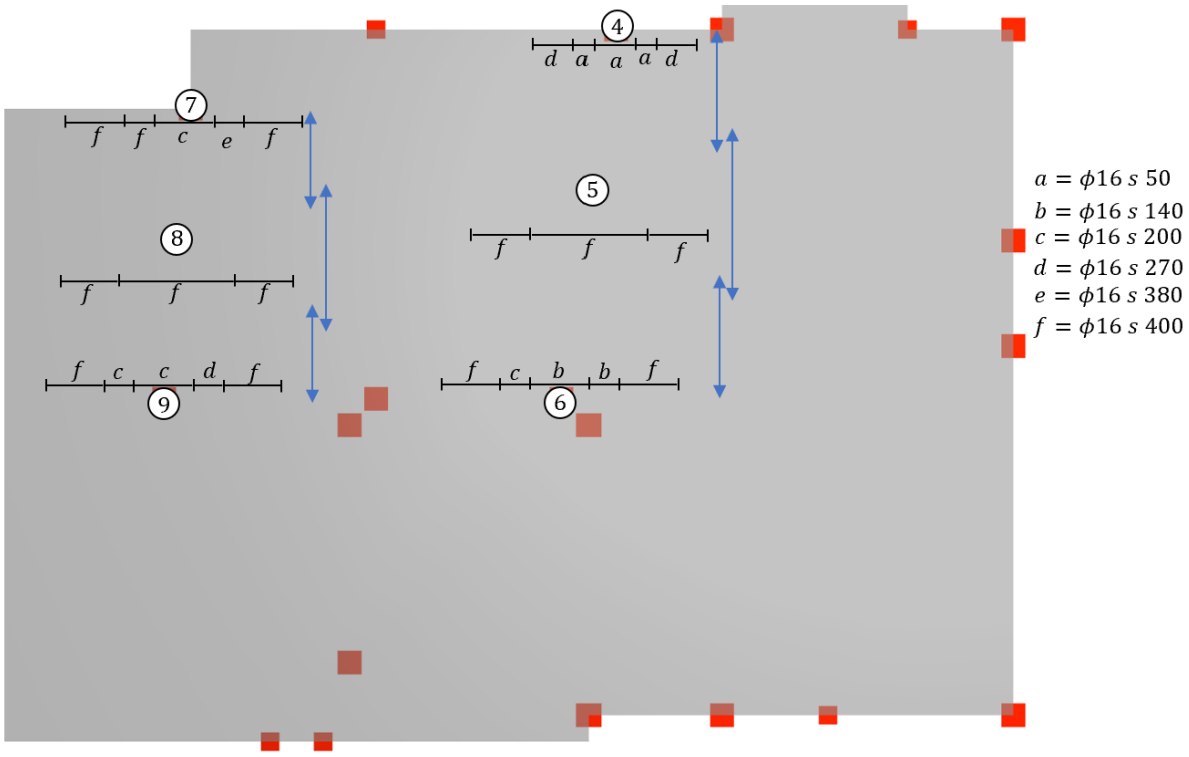

Figure 43: Illustration of chosen reinforcement amounts in y-direction for solution A.

4.2.2 Conventional and post-tensioned reinforcement

For this solution the necessary number of tendons in each strip of the chosen sections are presented. Table 11 and Table 12 present the calculated number of necessary tendons in each strip, where negative numbers indicate that the uniform conventional reinforcement in that strip is sufficient. The necessary number of tendons guides the choice of tendon number in each tendon strip, which is presented in Table 13 for sections 1-3, sections 4-6, and sections 7-9 respectively.

Table 11: Necessary number of tendons over columns for solution B.

	n_{SFL}	n^2_{SSL}	n^1_{SS}	n^2_{SSR}	n_{SFR}
Section 1	0,45	1,65	3,91	1,52	0,50
Section 3	0,30	0,60	2,18	0,70	-0,09
Section 4	0,18	1,75	3,62	0,75	0,18
Section 6	0,40	0,57	2,21	1,05	0,20
Section 7	-0,55	-0,17	1,44	0,03	-0,40
Section 9	0,27	0,57	1,59	0,27	0,08

Table 12: Necessary number of tendons in fields for solution B.

	n_{FFL}	n_{FS}	n_{FFR}
Section 2	0,44	0,69	0,34
Section 5	0,44	0,56	0,47
Section 8	-0,02	0,13	0,04

Table 13: The chosen number of tendons for solution B.

	n_{SFL}	n^2_{SSL}	n^1_{SS}	n^2_{SSR}	n_{SFR}	SUM
Section 1-3	1	1	4	1	1	8
Section 4-6	0	2	3	1	0	6
Section 7-9	0	1	1	1	0	3

As some of the wider strips require less than one tendon, a choice is made to concentrate the tendons in the center of the sections. Thus, some extra conventional reinforcement is necessary. The required area of extra conventional reinforcement, made necessary by the choice of tendon strip layout, is presented in Table 14 for strips over columns and Table 15 for strips in fields.

Table 14: Necessary extra conventional reinforcement over columns for solution B.

		m_{SFL}	m^2_{SSL}	m^1_{SS}	m^2_{SSR}	m_{SFR}	SUM	
A_{sextra}	**Section 1**	0	291	0	232	0	523	mm^2
A_{sextra}	**Section 3**	134	0	0	0	0	134	mm^2
A_{sextra}	**Section 4**	79	0	277	0	79	434	mm^2
A_{sextra}	**Section 6**	179	257	0	473	90	998	mm^2
A_{sextra}	**Section 7**	0	0	197	0	0	197	mm^2
A_{sextra}	**Section 9**	123	0	268	0	35	425	mm^2

Table 15: Necessary extra conventional reinforcement in fields for solution B.

		m_{FFL}	m_{FS}	m_{FFR}	SUM	
A_{sextra}	**Section 2**	450	0	399	849	mm^2
A_{sextra}	**Section 5**	450	0	467	918	mm^2
A_{sextra}	**Section 8**	197	0	231	428	mm^2

Based on the chosen number of tendons, an illustration of the proposed tendon layout is made and Figure 44 shows this layout.

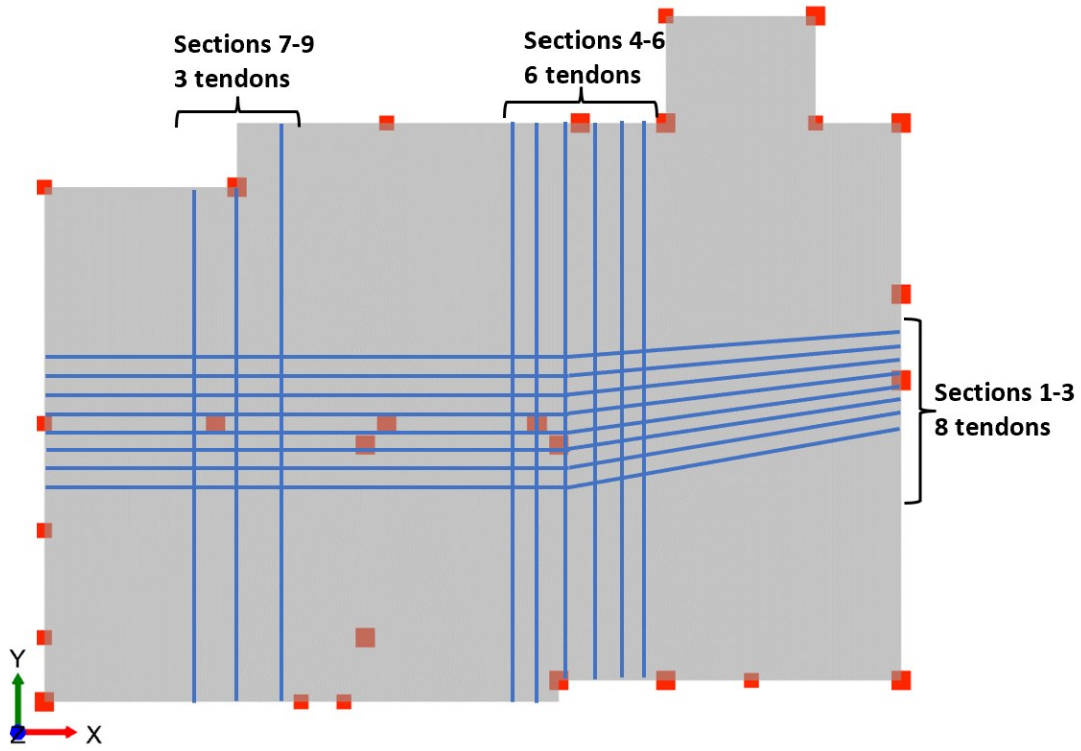

Figure 44: Illustration of proposed tendon layout for solution B.

4.2.3 Conventional and post-tensioned reinforcement, reduced slab height

This solution is analyzed in a manner which is identical to solution B, but with the reduced moments. Table 16 and Table 17 present the calculated number of necessary tendons in each strip, where negative numbers indicate that the uniform reinforcement in that area is sufficient. Table 18 presents the chosen number of tendons in each tendon strip.

Table 16: Necessary number of tendons over columns for solution C.

	n_{SFL}	n^2_{SSL}	n^1_{SS}	n^2_{SSR}	n_{SFR}
Section 1	0,75	2,39	5,95	2,21	0,81
Section 3	0,55	0,95	3,17	1,08	0,04
Section 4	0,39	2,55	5,44	1,15	0,39
Section 6	0,68	0,91	3,21	1,56	0,42
Section 7	-0,54	-0,05	2,10	0,20	-0,36
Section 9	0,52	0,91	2,32	0,52	0,26

Table 17: Necessary number of tendons in fields for solution C.

	n_{FFL}	n_{FS}	n_{FFR}
Section 2	0,95	1,26	0,84
Section 5	0,95	1,10	0,99
Section 8	0,40	0,58	0,47

Table 18: The chosen number of tendons for solution C.

	n_{SFL}	n^2_{SSL}	n^1_{SS}	n^2_{SSR}	n_{SFR}	SUM
Section 1-3	1	2	6	2	1	12
Section 4-6	1	2	5	1	1	10
Section 7-9	0	1	2	1	0	4

Table 19 and Table 20 present the necessary extra amounts of conventional reinforcement for reinforcement solution C.

Table 19: Necessary extra conventional reinforcement over columns for solution C.

		m_{SFL}	m^2_{SSL}	m^1_{SS}	m^2_{SSR}	m_{SFR}	SUM	
A_{sextra}	**Section 1**	0	178	0	94	0	272	mm^2
A_{sextra}	**Section 3**	248	0	0	37	0	285	mm^2
A_{sextra}	**Section 4**	0	245	196	67	0	509	mm^2
A_{sextra}	**Section 6**	307	0	0	253	190	751	mm^2
A_{sextra}	**Section 7**	0	0	45	0	0	45	mm^2
A_{sextra}	**Section 9**	234	0	144	0	118	496	mm^2

Table 20: Necessary extra conventional reinforcement in fields for solution C.

		m_{FFL}	m_{FS}	m_{FFR}	SUM	
A_{sextra}	**Section 2**	428	0	378	806	mm^2
A_{sextra}	**Section 5**	428	0	445	874	mm^2
A_{sextra}	**Section 8**	180	0	212	392	mm^2

Based on the chosen number of tendons, an illustration of the proposed tendon layout is made and is presented in Figure 45.

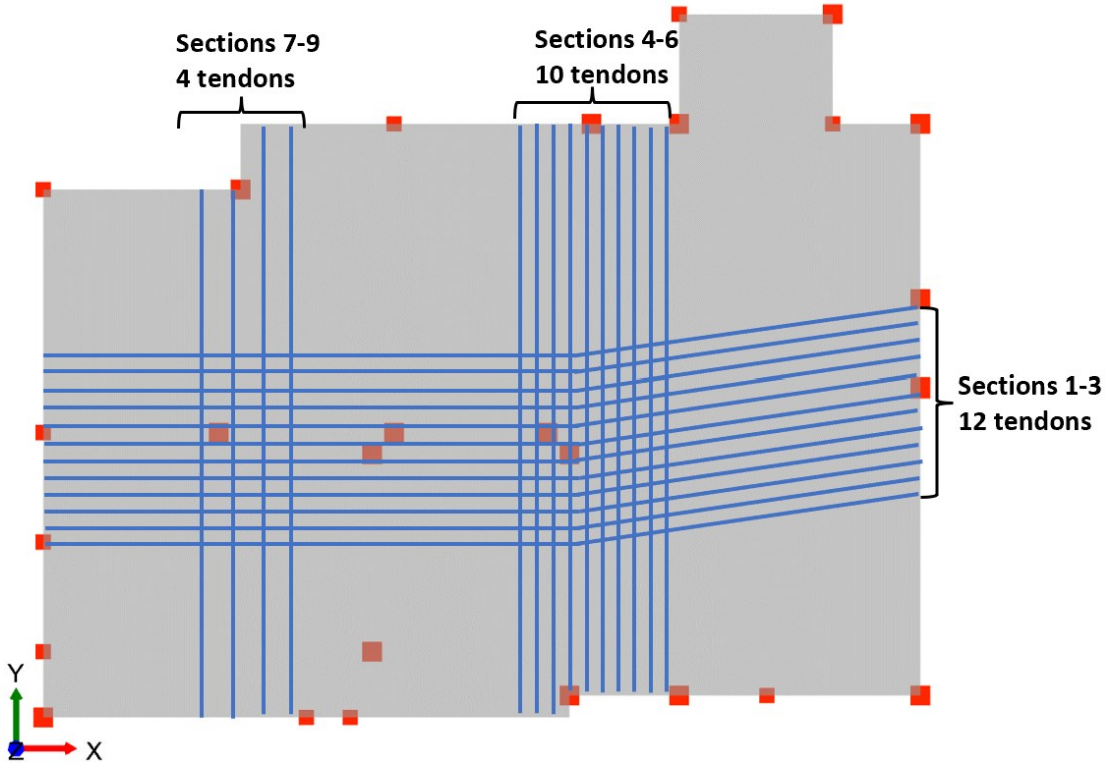

Figure 45: Illustration of proposed tendon layout for solution C.

4.2.4 Conventional, post-tensioned and fiber reinforcement

To choose a sufficient and appropriate reinforcement solution, the design moments for each strip are compared to the moment capacities. These are calculated with moment equilibrium formulae which includes the contribution of all three reinforcement types, provided in NB 38. Table 21 is used to choose an appropriate number of tendons to achieve sufficient capacity. Table 22 and Table 23 show the necessary number of tendons for each section, and Table 24 shows the chosen number of tendons. Figure 46 illustrates the proposed reinforcement solution.

Table 21: Moment capacities for different number of tendons.

	Fiber		Fiber and conventional	
	Asc=0	Asf=0	Asc=257	Asf=383
n=0	42783	42783	70295	78328
n=1	76196	69553	102658	103565
n=2	108222	94938	133667	127393
n=3	138862	118935	163264	149835
n=4	168115	141547	191475	170890
n=5	196031	162820		

Table 22: The necessary number of tendons for each section over columns for solution D.

	n_{SFL}	n^2_{SSL}	n^1_{SS}	n^2_{SSR}	n_{SFR}
Section 1	0,00	0,00	3,00	0,00	0,00
Section 3	0,00	0,00	1,00	0,00	0,00
Section 4	0,00	0,00	2,00	0,00	0,00
Section 6	0,00	0,00	1,00	0,00	0,00
Section 7	0,00	0,00	0,00	0,00	0,00
Section 9	0,00	0,00	0,00	0,00	0,00

Table 23: The necessary number of tendons for each section in fields for solution D.

	n_{FFL}	n_{FS}	n_{FFR}
Section 2	0,00	0,00	0,00
Section 5	0,00	0,00	0,00
Section 8	0,00	0,00	0,00

Table 24: The chosen number of tendons for solution D.

	n_{SFL}	n^2_{SSL}	n^1_{SS}	n^2_{SSR}	n_{SFR}	Sum
Section 1-3	0,00	0,00	3,00	0,00	0,00	3
Section 4-6	0,00	0,00	2,00	0,00	0,00	2
Section 7-9	0,00	0,00	0,00	0,00	0,00	0

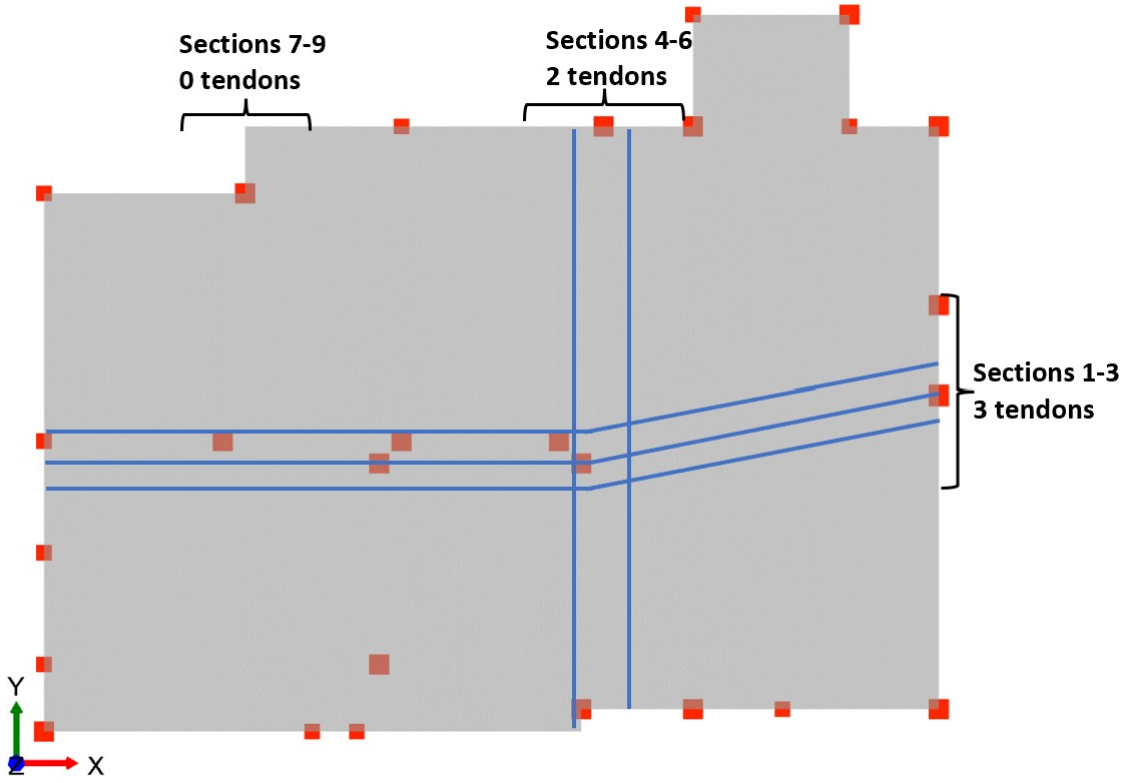

Figure 46: Illustration of proposed tendon layout for solution D.

4.2.5 Post-tensioned and fiber reinforcement

Table 21, with the calculated moment capacity for a given number of tendons, provides the basis for design in this solution as well. The necessary number of tendons in each section are shown in Table 25 and Table 26. The chosen number of tendons are shown in Table 27, and Figure 47 illustrates the proposed reinforcement solution.

Table 25: The necessary number of tendons for each section over columns for solution E.

	n_{SFL}	n^2_{SSL}	n^1_{SS}	n^2_{SSR}	n_{SFR}
Section 1	0,00	1,00	5,00	1,00	0,00
Section 3	0,00	1,00	2,00	1,00	0,00
Section 4	0,00	1,00	4,00	1,00	0,00
Section 6	0,00	0,00	2,00	1,00	0,00
Section 7	0,00	0,00	1,00	0,00	0,00
Section 9	0,00	0,00	1,00	0,00	0,00

Table 26: The necessary number of tendons for each section in fields for solution E.

	n_{FFL}	n_{FS}	n_{FFR}
Section 2	0,00	1,00	0,00
Section 5	0,00	1,00	1,00
Section 8	0,00	0,00	0,00

Table 27: The chosen number of tendons for solution E.

	n_{SFL}	n^2_{SSL}	n^1_{SS}	n^2_{SSR}	n_{SFR}	Sum
Section 1-3	0,00	1,00	5,00	1,00	0,00	7
Section 4-6	0,00	1,00	4,00	1,00	0,00	6
Section 7-9	0,00	0,00	1,00	0,00	0,00	1

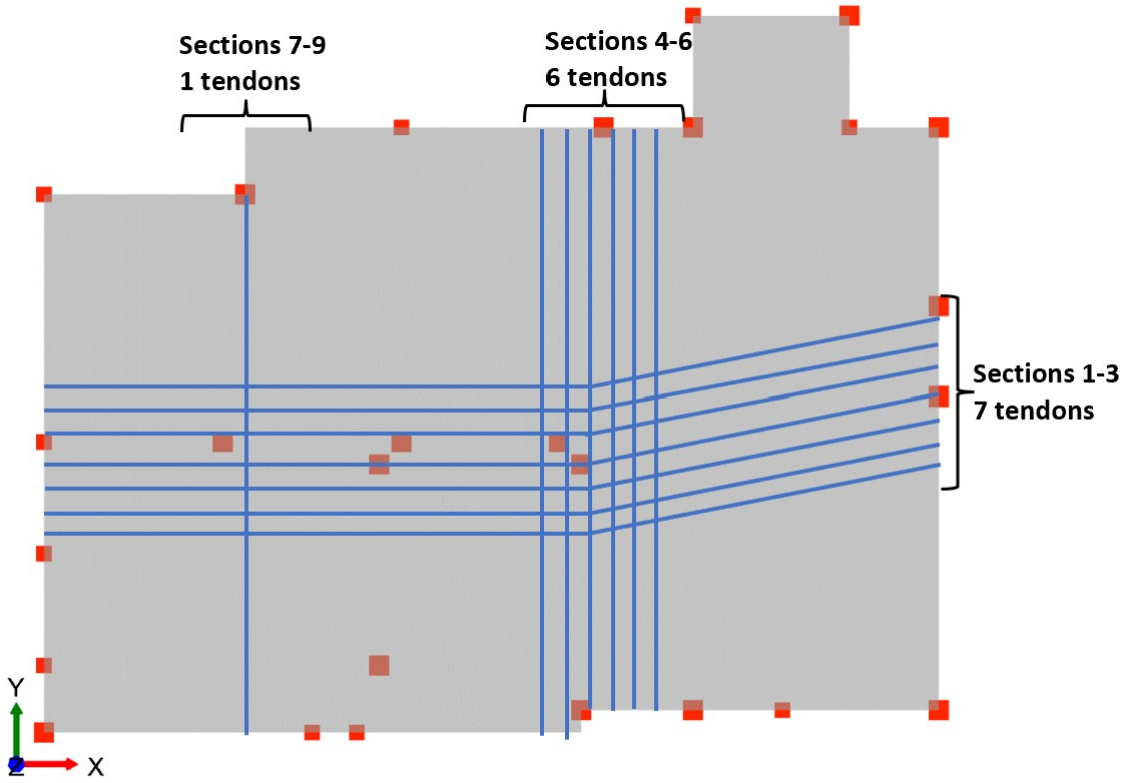

Figure 47: Illustration of proposed tendon layout for solution E.

4.3 Yield line

This section presents the reinforcement amounts that are sufficient after analysis with yield line theory. These are calculated by finding the necessary distributed reinforcement to handle the distributed moment calculated with standard formulae. Also, a proposed reinforcement layout based on the distributed reinforcement amounts and the yield line pattern's geometry is illustrated.

4.3.1 Conventional reinforcement

Table 28 presents the calculated reinforcement amount and the chosen bar spacing for each area, namely the field and the four edges, of the yield line pattern.

Table 28: Necessary reinforcement amount per meter and bar spacing for solution A.

Reinforcement area and bar spacing		
Field	486 410	$A_{sfield}\ [mm^2/m]$ $s_{field}\ [mm]$
Edge 1	454 440	$A_{s1}\ [mm^2/m]$ $s_1\ [mm]$
Edge 2	227 550	$A_{s2}\ [mm^2/m]$ $s_2\ [mm]$
Edge 3	454 440	$A_{s3}\ [mm^2/m]$ $s_3\ [mm]$
Edge 4	454 440	$A_{s4}\ [mm^2/m]$ $s_4\ [mm]$

These calculation results provide a simple reinforcement solution, with orthotropic bar layout in the field. An illustration of this proposed reinforcement layout is presented in Figure 48.

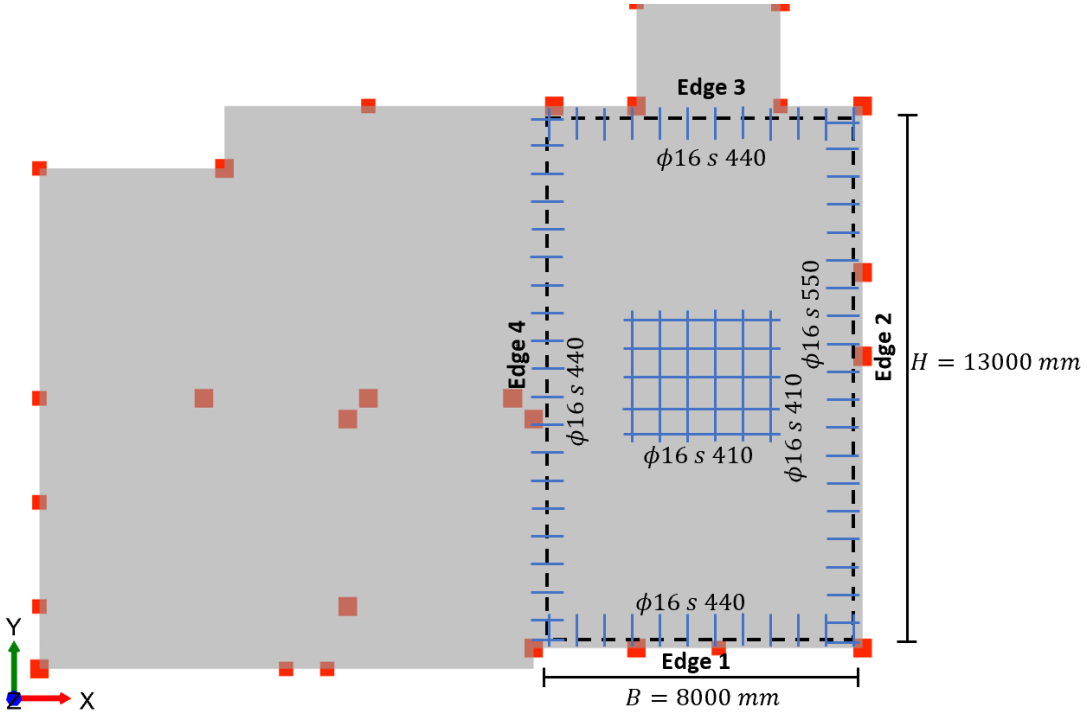

Figure 48: Illustration of proposed reinforcement layout for solution A.

4.3.2 Conventional and post-tensioned reinforcement

The design moment from yield line theory is resisted by tendon strips in x- and y-direction. Table 29 presents the chosen number of tendons per meter, and in total for each area in the yield line pattern. The tendon strip layout follows the illustration given in Figure 49.

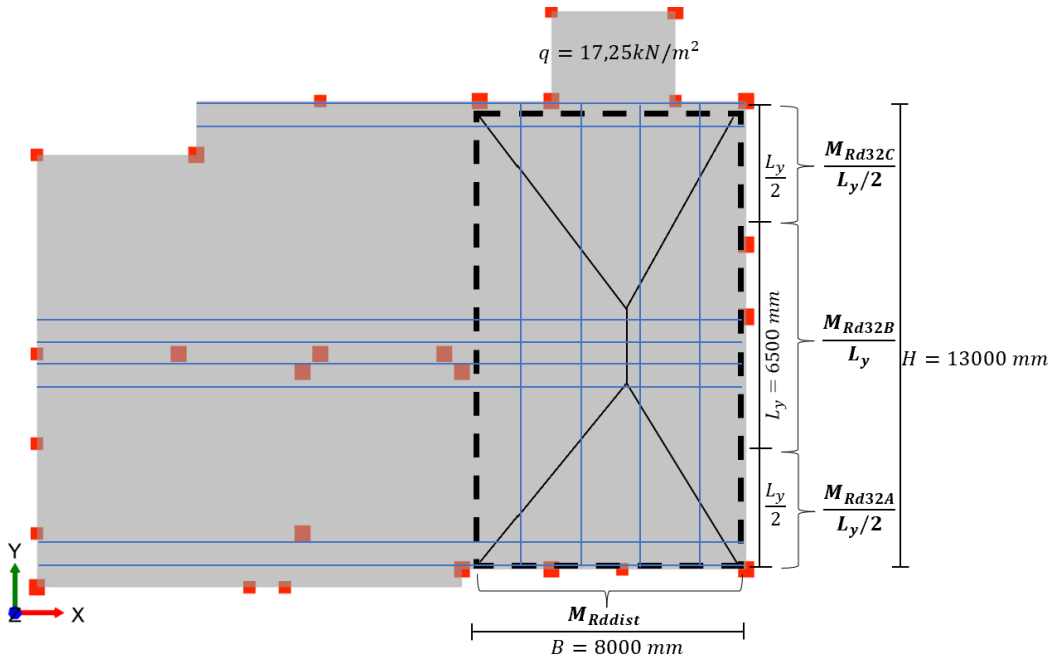

Figure 49: Tendon layout in design yield line pattern.

Table 29: Chosen number of tendons per meter and total number of tendons for each area in solution B.

Tendon strip	Chosen amount	Strip width [m]	Total area
Distributed	0,5	8	600
32A	2	3,25	900
32B	3	6,5	2850
32C	2	3,25	900

4.3.3 Conventional and post-tensioned reinforcement, reduced slab height

Solutions B and C are handled identically, the only difference being the reduction in load and moments in solution C. Table 30 presents the necessary and chosen tendon number in each area. For this reinforcement solution as well, the tendon layout is principally the same as in Figure 49.

Table 30: Chosen number of tendons per meter, and total number of tendons for each area in solution C.

Tendon strip	Chosen amount	Strip width [m]	Total area
Distributed	1	8	1200
32A	3	3,25	1350
32B	6	6,5	5850
32C	3	3,25	1350

4.3.4 Fiber reinforced concrete solutions

For all reinforcement solutions containing steel fibers, the moment capacity contribution from the fibers is calculated separately. As the steel fibers are assumed to be evenly distributed throughout the concrete slab, like the design moment from the yield line analysis is, this contribution is checked against the design moment. It is found that the steel fibers give the slab a moment capacity that is very close to the design moment. Thus, no additional reinforcement, neither post-tensioned nor conventional, is necessary. Consequently, no reinforcement solutions for the yield line analyses of reinforcement solutions D-F are made.

4.4 Punching shear

The results for punching shear capacities according to both Eurocodes and solution A-F are presented in this section. The current Eurocode does not take fibers into account. Hence, this Eurocode does not provide any punching shear values for the reinforcement solutions containing fibers. The new Eurocode does consider fibers, but not solutions without longitudinal reinforcement. Table 31 presents the design shear stresses for each solution and for both Eurocodes. Table 32 and Table 33 presents the punching shear capacities, without and with consideration of $\tau_{Rdc,min}$, respectively. To make it easy to evaluate how much of the capacity is necessary, the utilization ratios for punching shear capacity are presented in Table 34.

Table 31: Design shear stress for punching.

	EC2:2004 - v_{Ed1}		EC2:2021 - τ_{Ed}	
	Internal	Edge	Internal	Edge
A	0,34	0,37	0,54	0,54
B	0,37	0,40	0,59	0,59
C	0,51	0,54	0,74	0,73
D	-	-	0,57	0,56
E	-	-	0,59	0,59
F	-	-	-	-

Table 32: Punching shear capacity, without minimum capacity.

	EC2:2004 - v_{Rdc}		EC2:2021 - τ_{Rdc}		τ_{RdcF}	
	Internal	Edge	Internal	Edge	Internal	Edge
A	0,62	0,55	0,76	0,39	-	-
B	0,69	0,63	0,56	0,40	-	-
C	0,87	0,69	0,53	0,44	-	-
D	-	-	0,61	0,54	1,81	1,74
E	-	-	0	0	1,2	1,2
F	-	-	0	0	1,2	1,2

Table 33: Punching shear capacity.

	EC2:2004 - v_{Rdc}		EC2:2021 - τ_{Rdc}		τ_{RdcF}	
	Internal	Edge	Internal	Edge	Internal	Edge
A	0,62	0,55	0,90	0,90	-	-
B	0,69	0,63	0,94	0,94	-	-
C	0,87	0,69	1,09	1,09	-	-
D	-	-	0,92	0,92	2,12	2,12
E	-	-	0,94	0,94	2,14	2,14
F	-	-	0	0	1,2	1,2

Table 34: Utilization ratios for punching shear.

	EC2:2004 - v_{Ed1}/v_{Rdc}		EC2:2021 - τ_{Ed}/τ_{Rdc}		τ_{Ed}/τ_{RdcF}	
	Internal	Edge	Internal	Edge	Internal	Edge
A	0,54	0,66	0,60	0,60	-	-
B	0,54	0,64	0,63	0,63	-	-
C	0,59	0,79	0,68	0,67	-	-
D	-	-	0,62	0,61	0,27	0,27
E	-	-	0,63	0,63	0,28	0,28
F	-	-	-	-	-	-

4.5 Total reinforcement amount / summary

The total area and weight of reinforcement per meter is summed up for each solution and for both methods. This is shown in Table 35 and Table 36, and makes it possible to compare how much steel is needed for each solution. In addition, Table 37 visualizes the average use of steel per meter width and length. This provides an easier and more accurate comparison of steel consumption between EFM and yield line theory. However, it is important to be aware of the direction of the reinforcement. The tables are based on reinforcement bars in only one direction, but the fibers are distributed in all directions. For a better comparison, the mass of steel should be multiplied with a factor of two for conventional and PT reinforcement, as a simplified assumption of orthotropic reinforcement. For EFM, this factor should be somewhat smaller than two, since the most

critical directions are investigated. This results in a principal reinforcement direction, and a slightly smaller reinforcement amount in the other direction. As a simplification, all conventional and PT reinforcement is multiplied with two for both EFM and yield line theory and these results are shown in Table 38.

Table 35: Total reinforcement area and weight for all sections, using EFM.

EFM		A	B	C	D	E	F	
A_{stot}	SUM	32170	15924	13681	11016	0	-	mm^2
A_{ptot}		0	7650	11700	2250	6300	-	mm^2
M_{A_s}		253	125	108	86	0	-	kg/m
M_{A_p}		0	60	92	18	49	-	kg/m
M_{A_F}		0	0	0	446	446	-	kg/m
M_{Steel}		253	185	199	550	495	-	kg/m

Table 36: Total reinforcement area and weight, using yield line theory.

Yield line		A	B	C	D	E	F	
A_{stot}	SUM	18004	10794	10794	0	0	0	mm^2
A_{ptot}		0	3300	6000	0	0	0	mm^2
M_{A_s}		141	85	85	0	0	0	kg/m
M_{A_p}		0	26	47	0	0	0	kg/m
M_{A_F}		0	0	0	520	520	520	kg/m
M_{Steel}		141	111	132	520	520	520	kg/m

Table 37: Average mass of steel per meter width for the two methods. Reinforcement bars are in only one direction.

Average mass of steel per meter width		A	B	C	D	E	F	
M_{Steel}	EFM	7,0	5,1	5,5	15,3	13,7	-	kg/m^2
M_{Steel}	Yield line	3,4	2,6	3,1	-	-	12,4	kg/m^2

Table 38: Average mass of steel, assumed equal reinforcement in both directions.

Adjusted average mass of steel		A	B	C	D	E	F	
M_{Steel}	EFM	14,0	10,3	11,1	18,2	15,1	-	kg/m^2
M_{Steel}	Yield line	6,7	5,3	6,3	-	-	12,4	kg/m^2

5 Discussion

This section discusses the results of the work that has been done in this thesis. First, some of the peculiarities of a pile supported ground slab as opposed to flat slabs are presented. Then, the methods of analysis that are utilized are discussed, both separately and weighed against each other. In Section 5.5, some general points on what may be expected to apply to the parts of slab D3-2 which are not investigated directly are raised. At that point, the calculation results are applied to weigh each reinforcement solution against the others. This is done for the moment calculations and then for the punching shear procedures. Finally, a discussion on the aspects of each reinforcement solution which goes beyond the results obtained in this thesis is presented.

5.1 Differences between flat slabs and ground slabs

Flat slabs supported by columns and ground slabs supported by piles are, in many regards, akin to each other. They behave similarly under heavy loads, and for ULS analysis the same checks need to be made. In SLS however, the differences are bigger. Deflections are important to investigate, and deflection requirements often become critical for flat slabs. This problem is, for the most part, not critical for ground slabs, though, as they are not suspended on columns. However, ground slabs are more exposed to the environment through the surrounding soil, which may cause aggressive substances to seep into cracks and accelerate the deterioration process. This also makes water-tightness relevant, as a water-tight ground slab will be durable and experience limited cracking. Also, industrial floor slabs in particular have a high degree of wear and tear during their service life, which may exacerbate crack propagation. Ground slabs are also susceptible to shrinkage cracks, because the slabs are often cast in large stages, which makes the tensile stresses due to shrinkage larger. Thus, pile supported ground slabs need high crack resistance to function well. Furthermore, extensive cracking may be visible on ground slabs, as opposed to on flat slabs which are usually covered by raised floors and/or ceilings. Thus, aesthetic demands, as well as durability demands, may contribute to making crack control critical in the design process for ground slabs. For SLS analysis of ground slabs, it is therefore important to consider crack width and crack propagation. This can be handled during the design process with measures regarding pile-slab connections, concrete mix, casting method and reinforcement solution. SLS is however not considered in the calculations in this thesis but should be taken into account when the reinforcement solutions are compared, with emphasis on crack width. It is expected that both post-tensioned and fiber reinforcement will perform well, as they reduce the crack width.

Due to limited time the calculations in this thesis are only done for ULS design. Furthermore, the ground slabs may be a lowly prioritized construction part in many projects. This is because of the entire structure, especially in high-rise office- or apartment buildings, the ground slab comprises a small part. Thus, conservative ULS design solutions may be assumed to provide satisfactory SLS behavior as well. Whilst the design process of, for example, the flat slabs in the floor system is more carefully analyzed. Thus, the resources which are applied to optimization ensure a higher reward.

This does not necessarily apply to industrial ground floors, which are more heavily loaded and where the cost of repairs is higher.

5.2 Elastic bending moments (EFM and focus adjusted)

The elastic analysis executed by FK causes the peaks in the moment distributions to be very large. If the design process required that the local reinforcement could handle these maximum moments, it would make for unreasonably large reinforcement amounts. This is handled by spreading the reinforcement over a larger area, which assumes a more plastic-like behavior during the highest loading, which is a realistic assumption for concrete after cracking occurs. These areas are based on the distribution into strips which is given in NB 33 and illustrated in Figure 13. A comparison between two methods of producing the moment distribution in accordance with NB 33 is presented in Section 2.7. One is obtained through a two-dimensional analysis of the slab, calculating the bending moments in each direction. The other uses an elastic analysis in 3D from FK, which is suitable for complicated slabs, and adjusts the moments obtained to fit NB 33.

This example shows that the focus adjusted solution results in somewhat lower values for bending moments than NB 33. The differences are, for the most part, relatively small and not more than about 20 *kNm/m*. This is the case for both columns and fields, but the relative difference is higher in the fields, since the moments are smaller here. Since the loads, materials and cross-section in the example are comparable with slab D3-2, it may be assumed that the difference between a 2D frame analysis and the adjusted elastic analysis moments are similar in size. Thus, some additional reinforcement would have been required by executing simpler moment calculations, but this result would have been more conservative. This is because a simple 2D analysis of a slab assumes that all loads are handled as bending moments in x- and y-direction. This neglects, among other load actions, torsion. There are some important differences between slab D3-2 and the example slab which must be considered. The example consists of a doubly symmetrical slab to which the partitioning into column- and field strips according to EFM is well adapted. Furthermore, the load actions are symmetrical and, consequently, more manageable to obtain. Slab D3-2, however, is more complicated to fit to EFM analysis. Analyzing this slab as 2D frames is very complicated due to its irregular geometry, and the most practical way to obtain the load actions is to conduct a full elastic analysis with a computer program. These bending moments are less conservative, as the analysis includes all load actions.

To account for some load redistribution and the size of the pile heads through which the forces are led, the peaks in the moment distributions are adjusted. Thus, a slightly lower bending moment is allowed to be resisted in a larger area of the slab. This is based on well-documented knowledge of how concrete structures act in ULS and gives a more economical reinforcement layout. There are also other effects than the aforementioned which may contribute to give a slab higher capacity than what is calculated. Membrane action is one such effect and acts as internal compressive forces stiffening up the slab as it deflects. The impact of this effect is larger over the internal piles in slab D3-2, meaning that sections 3, 6 and 9 are affected the most. Thus, the capacity of these areas in particular may be expected to exceed the calculated moment resistance. It is however difficult to estimate the exact increase.

5.3 Yield line theory

As mentioned in Section 2.6.3, yield line theory is an upper bound method. Consequently, awareness of all parameters affecting the outcome of a yield line theory analysis is required in order to ensure safely designed structures. A large portion of the factors pushing the design moments to the unsafe side are taken care of through the 10%-rule, or 15% rule for slabs with an irregular geometry, in which an additional 10% (or 15%) is added to the calculated design moment. For a precise and economical design however, great care should be taken in choosing both type of yield line mechanism and the location of the yield line pattern. How the yield lines are placed in relation to piles and edges should also be considered, in order to ensure that the critical scenario is analyzed. Furthermore, the assumption of how large the negative bending moments are in relation to the positive bending moments, through the factor $i = \frac{m'}{m}$, also impact how the slab is designed.

Since the LFEA from FK provides a simple overview of the largest moments in the slab, the area with the largest moments and the largest spans is a logical location in which to analyze a yield line pattern. Slab D3-2 is exposed to moments in both directions, and a two-way slab yield line pattern is, therefore, an obvious choice. Furthermore, the boundary conditions, which are fixed for this case, make an envelope-like yield line pattern likely to occur. This kind of mechanism is illustrated in Figure 27. A folding plate failure mechanism is usually critical, but this requires other boundary conditions, like free edges on two opposing sides. This is illustrated well by the example presented in Section 3.2. The slab presented there is a flat slab with regular geometry and column layout, and boundary conditions consisting of three free edges and one fixed edge. This makes a folding plate failure mechanism critical. Thus, it becomes apparent how different boundary conditions may alter which yield line pattern a structure must be designed for. The moment distributions and the geometry of slab D3-2 makes one area stand out as the most interesting one. Thus, no other yield line patterns or areas are checked. Also, using the standard formulae ensures that the critical geometry for the chosen yield line mechanism may be calculated definitively, given the assumptions that are made. This gives further confidence to the fact that the design moment calculated with the formulae, especially after adding 15%, is a safe moment to design the slab for. Furthermore, extensive iterative calculations to ensure that the critical yield line pattern is chosen is beyond the scope of this thesis. Also, it is not necessary in order to provide results on which a comparison of reinforcement solutions and analysis methods could be based. Ultimately, a more detailed process to find another yield line pattern would probably not produce better results in this thesis.

As Section 2.6.4 presents, there are differing views on precisely where yield lines should be placed in relation to columns in flat slabs, or piles in pile supported slabs. As can be seen in the standard formulae from Kennedy & Goodchild, placing the yield lines at the face of the pile heads, as opposed to at a distance on the inside, affects the span of the rotating slab segments. Thus, assuming yield lines along the pile head faces is a more conservative assumption than placing them inside of them. Since tests have previously shown that slabs exhibit yield lines through the centerline of the columns, a yield line pattern with yield lines directly over the pile heads is assumed. The choice of the bending stiffnesses of each edge in relation to the field is one which the designer may choose relatively freely. A rule of thumb, provided in Goodchild & Kennedy, is to choose a value between 0.5 and 2. As the authors of this thesis has access to information about, and drawings of, slab D3-2 as it is designed in real-life, it is found that three of the four

edges in the chosen yield line pattern has slabs adjacent to them. These edges are chosen to have a rotation resistance like the resistance in the field, as recommended by Goodchild & Kennedy. This implies a choice of $i = 1$. The edge on the right of the yield line pattern, as it is shown in Figure 38, is free. This implies zero bending stiffness. In this case, however, there is a wall fixed to the slab along this edge. The reinforcement in this area, as obtained from reinforcement detailing drawings which the authors have available, ensures some flexural resistance. This leads to the choice of $i = 0.5$ for this edge. Preliminary tests of how the chosen i-values impacts the reinforcement amounts show that the slab has sufficient capacity without requiring large amounts of reinforcement independently of what is chosen.

5.4 Comparison between EFM and yield line theory

Both methods of analysis that are used in this thesis have been developed in order to simplify otherwise complicated calculations of load actions and moment equilibrium in slabs. This, in turn, simplifies the calculations of necessary reinforcement amounts and the reinforcement detailing. Yield line theory assumes an evenly distributed bending moment which is equal in both directions. Thus, the reinforcement solution also becomes evenly distributed and orthogonal. Analysis according to EFM however, estimates a peak moment at a certain point, and assumes a distribution of this moment over the slab's span in the transverse direction. Thus, the two methods each provide an efficient way of designing slabs for moment resistance, without needing to carefully consider every load action. This efficiency in the design procedure is obtained on the expense of slab designs that are optimal and they may therefore be most suitable for preliminary design or in combination with other, more refined, design methods.

Since yield line theory spreads the moment over the entire area under consideration, the necessary reinforcement amounts become smaller than for EFM. Thus, provided the assumption of sufficient cross-section ductility is fulfilled, the relatively low reinforcement amount distributed over a large area gives an economical slab design. EFM, on the other hand, facilitates local adaptation of reinforcement in order to handle peak moments. This allows the designer to obtain a more finely detailed reinforcement layout, especially by following the partitioning of a slab into strips as given in NB 33. This latter quality of the EFM makes it suitable for analysis of PT concrete. This is because prestressing tendons are usually placed in a manner emulating strips, especially when concentrated. Accordingly, the tendon layout in a slab may be fitted to the strip partitioning used in EFM design. Fiber reinforcement, on the other hand, is not compatible with EFM analysis. This is because the fibers are mixed into the fresh concrete before it is cast and, consequently, are distributed throughout the concrete structure. Consequently, the moment capacity cannot be concentrated in the strips which experience the largest bending moments.

For such situations, the yield line theory is applicable. The evenly distributed moment that is assumed in a yield line analysis, may be resisted by the evenly distributed moment capacity of the fiber reinforcement. A challenge that the designer must be aware of however, is that the fibers are short, at least when compared to other reinforcement types. This causes the fibers to be pulled out, or to be torn off, as the crack widths increase. Since yield line failure mechanisms assume that the structure rotates along the yield lines, which are ultimately long and wide cracks, the fibers may end up offering little resistance as the structure approaches failure. If this is the case, the failure may be more brittle than what is acceptable. This is possible to handle by combining fiber

reinforcement with bars or prestressed tendons. However, the fibers may be assumed to provide enough flexural resistance that the structure under consideration will have experienced large deformations before failure.

As this thesis is limited to ULS analysis, the yield line theory is suitable. The rotation of stiff slab elements in between the yield lines requires large deformations in order to occur. Thus, the yield line theory provides no information about the structural behavior at SLS loading. It only describes the mode of failure for a ductile cross-section, with no results obtained on deformations or crack development. It does, on the other hand, provide a simple and efficient method of designing concrete structures. Safe designs using this method requires a good understanding of how the structure under consideration behaves under large loads. This is because such understanding guides the choice of which yield line patterns are considered and ensures that the critical one is investigated. It also makes the choice of boundary conditions easier to make correctly. Another requirement is for the cross-section to have sufficient ductility. This criterion may be assumed to be fulfilled when designing an under-reinforced cross-section, which is what this thesis bases its moment equilibrium equations upon. Lastly, as already mentioned, an extra margin of safety must be added to the solution in order to account for the fact that the yield line theory is an upper bound method. As the EFM allows for local adaptation of reinforcement, it may be combined with SLS analysis. Thus, calculations of deformations and crack development before ultimate loading may guide placement of additional reinforcement in the strips at which these problems are the most prevalent.

The modelling in FK of slab D3-2 is based on the documentation of its real-life design. Thus, the model includes features such as the expected loading on the slab, the walls upon the slab, and the lowered areas on the slab. The two latter features, also being made of concrete, add to the other loads on the slab. This makes the moments obtained from FK and adjusted into the moment distributions for each critical section in the EFM analysis, higher than what the load used in the yield line theory analysis accounts for. This is considered not to lessen the utility of the yield line theory analysis' results, as the key differences between EFM and yield line theory are effectively highlighted either way. The comparison of different reinforcement solutions is also considered not to be substantially affected by this fact, as all results for the different solutions are produced with the same assumptions in place. Furthermore, the additional stiffness provided by these adjacent structures, and their location, contribute to making the moments obtained from FK larger over piles and smaller in fields than if calculated with another method. With all things considered however, it is likely that implementing as much information as is available into the LFEA produces the most realistic elastic moments that may be acquired.

The elastic moment values from the LFEA are adjusted in order to account for, among other things, load redistribution. They are also, in this process, fitted to the strips according to NB 33. In doing this, assumed values based on a combination of subjective considerations and mean values from FK is used. Furthermore, the strips that NB 33 provides are based on slabs with regular geometry. The pile layout of slab D3-2 means that the symmetrical moment distributions seen in Figure 26 are sometimes disrupted by nearby piles, complicating the adjustment procedure. Thus, even though adjusting the elastic moments and placing the reinforcement according to each strip's calculated requirements gives a comprehensive and adaptive solution for the critical sections, many sections would need to be investigated in order to design for the largest moments. As the

yield line theory solution also requires several assumptions to be made, it is clear that both methods of analysis demand subjective judgements from the designer. These are, fortunately, possible to make soundly for an experienced designer.

The calculated design moment from yield line theory is, as presented in Table 6 and Table 7, $43.5\ kNm/m$ for most solutions. As Table 2 and Table 3 show, this is a comparably low design moment. Only the moments in the outer column strips in sections 7 and 9 are lower, in addition to the moments in the field column strips. Inversely, only a few field moments are higher than the design yield line moment. Of the 39 bending moments that are calculated in the EFM analysis, 18 are smaller than the yield line design moments. These moments are chiefly located in the widest strips into which the slab is partitioned, making them account for the largest part of the area under investigation. The strips requiring the largest reinforcement amounts account for a comparably small fraction of the critical section's area. This is illustrated in Figure 37. Consequently, the EFM provides designs with lower total reinforcement amounts than what is apparent at first glance. Table 37 shows that despite this, the average reinforcement amount is considerably larger for the EFM designs than for the designs according to yield line theory. An effect which may contribute to this result is the requirement for minimum reinforcement. It is estimated that the minimum reinforcement amount, depending on whether it is located in the top or bottom of the cross-section, provides between $30 - 35\ kNm/m$ of moment resistance. Approximately seven of the 18 smallest EFM moments are lower than what the minimum reinforcement requires. It may be expected that for a slab with larger loads and larger required reinforcement amounts, the EFM solution would be closer to the yield line solution. Also, more emphasis on material usage and less on a tidy reinforcement layout would reduce the difference. The fact that yield line theory is an upper bound method also increases the differences, as the EFM solutions are more conservative than the yield line solutions. For the solutions with fiber, the relative differences in material usage for the two methods are significantly smaller than for solutions A-C. The difference in $\frac{kg}{m^2}$, however, are of a similar order of magnitude.

Yield line theory is a quick and simple method to use. The calculations are easily completed and produce results that need minimal processing by the designer. Especially when using standard formulae, these advantages become apparent. The challenge when analyzing a structure with yield line theory is to choose the correct failure pattern, in addition to the different assumptions which affect the results. The 10%-rule offsets some of the uncertainty associated with making these choices. Furthermore, an investigation of different yield line patterns and the parameters' impact on the result may reduce the uncertainty of the initial analysis, as more precise calculation results will be produced. This complicates the design process and negates one of the main benefits of yield line theory analysis. Design with EFM based upon an elastic analysis, on the other hand, demands more numerous calculation operations and a more complicated process altogether. The elastic analysis, though it may add more work than simple frame analyses, adds the benefit of providing more accurate moment distributions. Furthermore, the designs produced in this manner are more conservative than yield line theory solutions. This implies that errors in the design process could have larger consequences for the structure's performance when using yield line theory.

5.5 Reinforcement distribution

The calculations done for slab D3-2 do not apply for all sections of the slab, as only a selected and assumed critical few sections were picked for analysis. The main purpose of this thesis is to assess different calculation methods and reinforcement solutions in general, with a real slab as a basis. Therefore, the other sections of the slab are not prioritized. It is, however, possible to do an assessment of how the rest of the slab would be designed, using the calculated sections as basis. The color maps of the moment distributions in Figure 33 and Figure 34 give a quick overview of how much moment affects different sections of the slab. Looking at these moment distributions, in both directions, section 8 seems to be similar to the parts of the slab which are not investigated. As can be seen from the moments presented in Table 3, this section only requires minimum reinforcement. Thus, it may be assumed that for most areas of the slab which are not reinforced according to EFM, minimum reinforcement is sufficient. Consequently, the reinforcement solution produced with yield line theory analysis is also applicable to larger portions of the slab.

The basis for yield line theory analysis is the same as for EFM analysis. Thus, the assumed critical area of the slab is investigated. A general feature of yield line theory is that the same amount of reinforcement is used in large areas of the structure which is designed. Slab D3-2 is varied when it comes to geometry in different sections, making a large variety of yield line patterns possible in different areas of the slab. Thus, each area of the slab would require a different reinforcement amount, providing a more comprehensive reinforcement solution. As the boundary conditions are similar throughout most of the slab, the expected difference in design moments is expected to be low, mostly affected by span lengths. As such, though such a design process may lead to a somewhat smaller reinforcement amount in the slab, the benefits are limited.

In the punching shear analysis, there is no need for shear reinforcement. The piles that are chosen are moderately loaded, since the main objective of the calculations is to produce results with which to compare the different solutions and Eurocodes. Consequently, detailing of shear reinforcement is not investigated. The results then imply that most of the piles in slab D3-2 have sufficient punching shear capacity without requiring shear reinforcement. There are several piles, however, which are expected to have insufficient punching shear capacity. Among these are the pile in section 1.

5.6 Comparison of reinforcement solutions based on results

As explained in Section 3.3.3, a certain amount of conventional reinforcement and fibers are determined before calculations are completed. These quantities are based on minimum reinforcement requirements, practical reasons, and previous experimental experiences. There are, however, no requirements for minimum reinforcement amount in the top of the cross-section. Thus, the predetermined reinforcement in the top is chosen mainly in order to supply the slab with some moment capacity throughout its entire area. As the moments over the piles are the largest, a possibility is to have a larger distributed top reinforcement amount. This will decrease the need for additional reinforcement in the strips which are analyzed and may also simplify the reinforcement solutions. A higher proportion of conventional reinforcement, assuming the fiber content to be unchanged, would lead to less need for PT reinforcement. This would again lead to higher steel consumption. This would, also, make the design conservative and uneconomical for large swathes of the slab.

A fiber dosage of 45 $\frac{kg}{m^3}$ is assumed in the fiber reinforced solutions, as the authors of this thesis have previous experience with this dosage. With this proportion of fiber reinforcement, the slab achieves a bending moment capacity with is barely insufficient according to yield line analysis. A slightly higher fiber dosage would have increased the residual flexural tensile strength and provided sufficient capacity. Alternatively, a small amount of conventional reinforcement would be sufficient. Great care must be taken when increasing the fiber dosage, however, as it affects the fresh concrete's workability. As the punching shear capacity is already sufficient, an increase in fiber content will only benefit the moment capacity. However, as the moment resistance provided by the fiber reinforcement is sufficient for several of the strips that are analyzed with EFM, much of the increased steel area would be unnecessary. This illustrates the point that fiber reinforcement cannot be placed according to where it is needed, which in some cases makes a combination with other reinforcement types more efficient. Such combinations help limiting the steel consumption, which Table 37 shows is the highest for the fiber reinforced solutions with the current dosage. The same table shows that including prestressed tendons may decrease the steel consumption, implying that post-tensioned designs are efficient. If, however, savings in labor and time consumption is more important than limiting overall steel amount, Table 2 and Table 3 shows that if the moment capacity due to fiber reinforcement were to increase from 43 kNm/m to 54 kNm/m, several extra sections would achieve sufficient capacity. This is possible to achieve by increasing the fiber content. Assuming a linear relation between fiber content and moment capacity, the required fiber content for achieving a moment capacity of 54 kNm/m is approximately 60 $\frac{kg}{m^3}$. This linear relation is, by the authors, assumed valid for such fiber contents, after consultation with the project's supervisor. This fiber content is also within the normal range of fiber contents. This will lead to fewer sections where additional reinforcement is needed, producing a simpler reinforcement layout which will be quicker to execute.

Solution A, B, C and D all include conventional reinforcement. Reinforcement bars provide the possibility of providing extra reinforcement area at the locations where this is needed. This is beneficial in ULS design, as the conventional reinforcement may be placed according to the top moments as well as over piles to handle shear stresses. Furthermore, crack control and deflections may be handled with additional reinforcement bars in SLS design. For structures where the need for extra capacity is concentrated in a small area, this may lead to the most efficient reinforcement designs. For example, as Table 11 and Table 12 show, several strips have the need for only half the capacity which is provided by a prestressed tendon. If such areas are few and far in between, adding an entire tendon for each such area may be less efficient than providing extra reinforcement bars. This is utilized for solutions B and C, where Table 14, Table 15, Table 19 and Table 20 show the extra conventional reinforcement amounts. In solution D, which includes fiber, no extra conventional reinforcement is added. This is a consequence of the moment resistance provided by the fiber reinforcement, causing few tendons to be necessary and little to be gained by adding reinforcement bars. Another argument against adding conventional reinforcement to this solution is the practicality and time-efficient nature of using fibers as opposed to reinforcement bars. Furthermore, solution E has no conventional reinforcement and, consequently, tendons are necessary where the moments exceed the moment capacity of the fiber reinforcement. Lastly, solution F is only designed according to yield line theory as the fiber reinforcement cannot be placed

according to the largest moments. The yield line calculations, as already mentioned, result in fiber reinforcement only being nearly sufficient.

The calculated necessary bar spacing of conventional reinforcement that is produced for solution A provides a unique number for every strip which is analyzed. As such a solution would be highly impractical, a rounded number is chosen. The maximum spacing of 400 mm provided by EC2.9.3.1.1(3) simplifies the process, but a choice must be made by the designer for the spacings which are lower than this threshold. Since a tidy reinforcement layout is paramount for the execution process to go smoothly, relatively few different spacings have been chosen in solution A. Figure 42 and Figure 43 illustrate this. As this process of selecting the bar spacings require a majority of the required spacings to be rounded down, solution A is among the solutions requiring most steel according to Table 37. This effect is exacerbated by the relatively low strength of conventional reinforcement as opposed to prestressed tendons. In order to reduce the steel consumption of reinforcement solution A, a more optimized bar spacing layout must be chosen. This will result in a more material-effective, but also more complicated design.

For a comparison of Table 35 to be made, it is necessary to note that fiber reinforcement is distributed. Thus, the amount of steel which is included in this table includes those parts of the cross-section where the design moment is not acting. Thus, this steel mass also contains the fiber reinforcement acting in all directions and in the entire cross-section. The mass of other reinforcement types, however, only incorporates that which is placed in one direction and at a certain place in the cross-section. To ensure that the reinforcement in both directions is included, multiplying the amounts of conventional and prestressed reinforcement with two is feasible. This will give an approximate value of total steel amount of that reinforcement type in the area under investigation for most areas of slab D3-2. This is because the minimum reinforcement amount that is placed in the slab is orthotropic. Furthermore, an area with a large moment in one direction, usually also has a large moment in the other direction, especially over piles. This can be seen from the Figure 33 and Figure 34. Doing this multiplication for the yield line theory numbers gives a more accurate result than for the EFM numbers. This is because of the distributed and orthotropic reinforcement solution which the yield line theory produces. These multiplied values are shown in Table 38, and the results become more comparable. Still, the solutions including fiber require the most steel. The solutions with no fiber reinforcement, and especially solution A, receive the largest increase in steel amount. Thus, for the EFM results in particular, it can be observed that the fiber solutions are nearer the non-fiber solutions than at first appearance. Also, the effect of including PT reinforcement remains, with solution B resulting in the lowest usage of steel according to both calculation methods.

This effectiveness of PT reinforcement might also be used to achieve leaner constructions. Solutions B and C have the same reinforcement combination, but with different slab thickness. Based on Table 38, the difference in necessary reinforcement amount is small, considering how much concrete is saved in solution C. To compare, for one meter in x- and y-direction, and with a 75 mm reduction in thickness, approximately 180 kg concrete is saved. This strengthens the assertion that post-tensioned concrete is suitable when designing leaner constructions. Thus, solution C is best if material savings is the only requirement. Based on the same requirement, PT reinforcement is the most efficient, followed by conventional reinforcement and then fiber, which is the least efficient.

As previously mentioned, membrane action is an effect that increases the capacity of the slab as it deflects. The effect of CMA is also larger in some parts of the slab than others, as internal bays receive the largest capacity increase. This means that this effect may not be utilized when designing fiber reinforcement amounts in slabs, as it is impractical to cast concrete with a smaller fiber dosage in the areas where the CMA is most beneficial. It is also difficult to take advantage of for post-tensioned solutions, since the other sections in the same tendon strip may be critical for the reinforcement amount. The exception for slab D3-2 is sections 7-9, where section 9 has the highest moments as well as the largest membrane action effect. For conventional reinforcement, however, it is possible to decrease the quantity of reinforcement for the areas with lower requirements. Estimating the added load capacity due to membrane action is complicated and requires a cumbersome calculation process. Furthermore, much care is needed in order to satisfactorily document sufficient safety of designs which reduce the reinforcement due to the CMA contribution. Thus, spending the resources that are required in order to design a slab with the CMA effect included may be an impractical way in which to reduce reinforcement amounts.

5.7 Punching shear

Punching shear is often the critical mode of failure in concrete slabs. This is especially true when slabs are designed as increasingly slender structures, because sufficient slab thickness is one of the most effective measures to increase a slab's shear capacity. Pile supported ground slabs transfer the combined loads from the building above it into the ground through the piles. Thus, transfers of large shear forces from the slab into the piles may occur, which makes shear capacity checks an important part of the design process. An important feature of slab D3-2 which improves shear capacity in critical areas are the lowered areas. These are located underneath walls and where columns are led into the slab, as well as over the piles. The pile heads are placed in the center of these areas, and this detail increases the concrete area through which shear stresses may be transferred. In addition, they provide sufficient space for the shear reinforcement which may be necessary around the pile heads. As the transfer of both large shear forces and bending moments often require slab-column, or slab-pile, connections to be improved, similar measures are often necessary.

Both the current and the proposed new Eurocode 2 assume concrete structures with conventional reinforcement. This makes slab designs with little or no conventional reinforcement more challenging. Thus, making such solutions competitive becomes difficult. For concrete slabs with post-tensioned reinforcement, this problem is surmountable. Extra reinforcement will often be necessary near columns or piles, and this is practical to add by placing additional reinforcement bars. Another benefit with using post-tensioned tendons in slabs, is that punching shear capacity calculations in both Eurocodes include coefficients which account for the axial stresses imposed by the tendons. As can be seen in Table 32, however, these coefficients have a limited impact on the punching shear capacity. Consequently, the added shear resistance provided by both the axial stresses introduced by the tendons, and their inclination near piles and columns, contribute more to a structure's punching shear capacity than what seems to be included in the current formulae. The low impact of adding prestressed reinforcement may also be partly explained by the fact that a solution with post-tensioned tendons will have a smaller area of bonded reinforcement bars. This, in turn, decreases the calculated punching shear capacity. Underlining this point, studies have shown that the current

capacity calculations in EC2 produce more conservative values for slabs with post-tensioned reinforcement than for conventionally reinforced solutions.

Fiber reinforced concrete is even more difficult to design for punching shear according to Eurocode 2. The current Eurocode does not allow for analysis of fiber reinforced concrete structures. This is despite the fact that several tests have shown concrete slabs with fiber reinforcement to achieve a significant increase in punching shear capacity. This capacity increase is mainly attributed to the fiber reinforcement's orientation and distribution, making it efficient at bridging shear cracks before they propagate. The proposed new EC2, however, allows for the contribution of steel fiber reinforcement to be included through the formulae in Annex L. These formulae assume the concrete structure to contain some bonded flexural reinforcement. If this is not the case, the shear capacity of the concrete cross-section is limited to the design residual flexural tensile strength of the steel fibers. This is because most formulae contain either the reinforcement depth or design yield strength of the conventional reinforcement, which become zero when the structure is reinforced with fibers only. This also applies to the calculated design shear stress. Furthermore, clause L.8.4.1(2) in EC2:2021 gives that the punching shear capacity formula for steel fiber reinforced concrete is not valid where axial stresses are present. This makes the structures with prestressed reinforcement in combination with steel fibers difficult to design. Consequently, the proposed new shear procedure in EC2 may also give conservative or insufficient results for concrete structures without conventional reinforcement. This is unfortunate as steel fiber reinforcement and prestressed reinforcement both contribute to a slab's punching shear capacity, both separately and when combined. The steel fibers are effective at bridging small cracks near columns or piles due to their orientation and distribution. Prestressed tendons provide axial stresses which negate the shear stresses and additional inclined reinforcement area over columns. Thus, a combination of the two reinforcement types is beneficial for punching shear capacity, especially in slender slabs with limited area for additional reinforcement bars near columns or piles.

The choice of critical section for punching shear control is different between the current and the proposed new Eurocodes. Since the distance from the column or pile head face is larger in the current version, the shear stresses become smaller. This can be seen in Table 31. Despite this, Table 32 shows that the calculated punching shear capacities are higher with the current calculation method. This may be attributed mainly to the inclusion of the failure zone roughness and reinforcement depth in the new EC2. When the minimum punching shear capacity is considered, however, the capacities calculated according to EC2:2021 become the largest. This is shown in Table 33. These differences in capacity and design shear stresses seem to negate each other to a large extent, however. As Table 34 shows, the utilization ratios of the six solutions which were analyzed according to both procedures are comparable. The mean degree of utilization for the six results after EC2:2004 is 62.7%, while it is 63.5% according to EC2:2021. Thus, the punching shear analysis shows that all reinforcement solutions have sufficient punching shear capacity, without needing shear reinforcement. Especially the proposed new Eurocode give a simple procedure for this slab, since the minimum shear resistance is large enough to eliminate the need for further checks.

The design shear force is the same for all reinforcement solutions, and for calculations according to both Eurocodes. As expected, this gives similar shear stresses for the same control sections. The difference between solutions A and B, as well as D and E, are because of the changes in reinforcement depth as a result of differences in the

reinforcement solutions. Naturally, the stresses are largest for solution C, since the slab is thinner. Coincidentally, the stresses are almost identical for edge piles and internal piles. This is because the difference in shear force is negated by the difference in control perimeter length. Since the formulae for calculating shear stresses include reinforcement depth, no shear stress could be calculated for solution F. This illustrates the challenging nature of analyzing structures with fiber reinforcement. The shear forces were obtained from the LFEA conducted in FK, and, consequently, they are elastic shear forces. A more extensive punching shear check could have included calculations with plastic as well as elastic shear forces. As the elastic shear forces are considered to be critical due to the redistribution of load actions during plastic deformations, these were deemed to be sufficient for the scope of this thesis.

When the minimum shear capacity of the concrete cross-section is neglected, as presented in Table 32, the differences between the reinforcement solutions calculated according to EC2:2021 become apparent. It seems that using prestressed reinforcement is not awarded when using the proposed new procedure. This is because in many formulae, the reinforcement is required to be bonded for its capacity to be included. However, including more conventional reinforcement achieves higher punching shear resistance. As the internal pile in solution A according to EC2:2021 has considerably more conventional reinforcement than the other piles, it achieves the highest punching shear capacity of the solutions without fiber. Reducing the cross-section height and adding more reinforcement enables the calculated resistance of the slab to remain similar according to the work in this thesis. Adding steel fibers, especially when combined with conventional reinforcement as in solution D, significantly increases the capacity. Calculations according to EC2:2004 shows that in the current Eurocode, an increase in punching shear resistance is achieved when adding prestressed reinforcement. This effect is larger than the reduction in capacity from reducing the slab's thickness. Thus, the punching shear capacity of the internal pile in solution C is the largest by a significant margin. The new Eurocode considers the reinforcement depth when calculating minimum punching shear resistance, in a manner which results in a larger minimum resistance when the reinforcement depth is smaller. This is presented in Table 33. Consequently, reinforcement solution C achieves the largest minimum capacity, though this is still lower than the fiber contribution in solution D-F.

After evaluating the calculated punching shear stresses and -capacities for all solutions, the utilization ratios presented in Table 34 are as expected. Generally, the slab shows sufficient capacity, with about 60% of the capacity being expended in most cases. Solution C has a slightly larger utilization ratio, according to both Eurocodes. This is as expected since the cross-section height is significantly reduced. The edge pile in solution C, when calculated according to the current Eurocode, is better utilized than the rest. This is mainly due to the fact that the critical control section length is the smallest for this pile, resulting in a considerably higher punching shear stress. It is also possible to observe that the steel fiber reinforced solutions have very low utilization ratios. This is mainly attributable to the high punching shear capacity which the fiber reinforcement adds to the slab. Also, the difference between edge- and internal piles is more pronounced in the calculations produced by the method in EC2:2004. The edge piles are better utilized than the internal piles, which is not the case for the results obtained through the proposed new method. This can partly be explained by the fact that the minimum resistances are the design punching shear capacities according to EC2:2021. Table 32 shows that the capacities for edge piles, when neglecting the minimum resistance, are lower than for the internal piles.

5.8 Economical, practical and environmental aspects

Capacities for moment and punching shear are, in addition to necessary reinforcement amounts, central conditions when discussing the results of a design process which has evaluated several different reinforcement solutions. There are, however, other aspects of a slab design which are important to consider. These include economical parameters, time and labor expenditure during execution, and environmental aspects of the design. Often, the users and owners of concrete structures emphasize such characteristics. If the qualities of the final product are not agreeable to the users, it does not matter if the mechanical properties are sufficient. The economy of a structure is affected by the time and labor demands during execution, as well as the environmental impact of the design, and vice versa. Emphasis on environmental impact is becoming ever more prevalent in the modern construction industry. Due to the interdependency of these factors, an exact evaluation of the different reinforcement solution's effect on them is complicated to make. However, there are some clear advantages and disadvantages which may be discussed.

One of the most effective means through which a more economical and environmentally friendly concrete design may be achieved is to reduce the concrete consumption. The reduced slab height in reinforcement solution C shows that this is achievable without significantly lowering the moment or punching shear capacity. This is provided that the designer has the option of adding the right composition of reinforcement types, for example by increasing the number of prestressed tendons. Since PT reinforcement adds compressive stresses to the tensile zone of a concrete structure, it enables leaner slabs to be constructed. This quality is why a combination of prestressed and conventional reinforcement has been designed for a reduced slab thickness. Because of the qualities of fiber reinforcement regarding crack control and punching shear, a combination of prestressed reinforcement and fiber may also be effective in designing slabs with reduced height. This requires that the moment capacity of the fiber reinforcement is sufficient to handle the moments which are not taken by the tendons. Or else, a large amount of PT reinforcement will be necessary, causing poor utilization of the prestressed tendons.

Another consideration to make is the durability of the concrete structure which is being designed. A durable slab will have a longer service life, which makes it cheaper and more environmentally friendly if the whole life cycle is considered. An effective way to improve the durability of a concrete structure is to increase the concrete cover depth. The main aim of the cover depth is to prevent reinforcement corrosion. Thus, great care must be exerted when reducing a slab's height in an aggressive environment if it contains conventional reinforcement, as this will lead to poor durability. It will also cause the reinforcement depth to be so small that it reduces the additional moment resistance when adding more reinforcement. Furthermore, placing of reinforcement in-situ and proper concrete casting quickly become more challenging. These problems may be avoided to a degree by using fiber reinforcement with which corrosion is not as big of an issue. Using fibers made of other materials than steel, such as basalt or plastic, may remove the corrosion risk altogether. In theory, unbonded prestressed reinforcement is also not susceptible to corrosion, as it is placed within ducts and surrounded by grease. If these solutions were allowed to be designed with reduced cover depth according to the Eurocode, additional savings in concrete volume for constructions would be possible.

When it comes to construction time, fiber is the most efficient reinforcement type. This is because the fibers are mixed into the fresh concrete and cast with it. Thus, no time or

manpower is needed for reinforcement placing and fastening. Since adding fibers will reduce the need for other reinforcement types, the savings in time consumption may be significant even for designs with a combination of fibers and bars. Post-tensioned tendons also reduce the need for other reinforcement types. This can be seen when comparing solution A to the ones including prestressed reinforcement. However, including post-tensioned tendons in a concrete structure will not always result in a more time-efficient construction process. This is because the placing and stressing of tendons require competence and sufficient time and area, especially for cast-in-situ concrete. Prefabricated concrete is a well-established method for prestressed solutions and will be more time efficient. However, prefabrication is not considered appropriate for D3-2. For large and complicated slabs, the layout of conventional reinforcement may be exceedingly complicated, making the reinforcement laborious to place. For structures with large loads, long spans, or a combination of the two, large amounts of rebars may be necessary. In these cases, a relatively small number of tendons may replace a large reinforcement bar area. For prestressed reinforcement to work, however, both the construction site and the design process must facilitate it. The operator which stresses the tendons must be qualified and competent for the prestressed reinforcement to work as intended. Furthermore, there must be sufficient space around the formwork for the operator of the hydraulic jack to perform the stressing operation efficiently and correctly. The time schedule must also provide sufficient time for the fresh concrete to harden, and then for the tendons to be stressed, before the production moves on. Thus, for certain construction projects, prestressed reinforcement, fiber reinforcement or a combination of both may lead to leaner structures that are time-efficient to execute.

Although the on-site production with fiber reinforcement is effective, there are some conditions to be aware of. In order to achieve the intended properties of the concrete, the fibers must be oriented in every direction and evenly distributed throughout the entire slab. As the use of vibrators when compacting fresh concrete may disrupt the fiber distribution, self-compacting concrete (SCC) is the preferred choice when casting fiber reinforced concrete. This ensures that the fresh concrete, through its self-weight, fills the formwork and compacts itself without needing external compaction energy. When using self-compacting fiber reinforced concrete, great care must be taken in determining the fresh concrete properties. Furthermore, ensuring that the intended properties are achieved is monumental for achieving a good result from the casting operation. One of the main factors involved in this process is the stability of the SCC, especially if it is pumped. A sufficiently stable concrete will prevent separation of the fibers from the concrete, thus creating fiber lumps. Provided that the fresh concrete obtains the desired properties, and that the fibers are well distributed, casting a fiber reinforced concrete structure is very efficient.

Reinforcing a concrete structure with prestressed reinforcement also requires great care during the design and planning. As previously mentioned, the construction process must consider the need for sufficient time and space for the stressing process to be adequately executed. Further considerations to make are how to place and fasten the tendons with the intended profile throughout the structure, and how to handle the large forces involved in stressing the tendons. The formwork must be designed to withstand the stressing and anchoring of tendons. The tendon layout, with the correct profile and placement, is paramount for the structure to achieve its designed capacity. Thus, determining how to fasten the tendons in the correct place and with the correct profile is central in the design process. Placing nets of conventional reinforcement provides a rigid grid to which the tendons may be secured, making this work easier. Thus, including some

conventional reinforcement in prestressed concrete is desirable for both mechanical and practical reasons.

Reinforcing a concrete structure with both fibers and PT reinforcement may result in beneficial mechanical properties, as well as a smoother, more efficient construction process. As already mentioned, the fibers are very labor-effective to include as they are cast together with the fresh concrete. Including fibers in this manner ensures a minimum moment capacity throughout the entire structure, in addition to providing a significant shear resistance contribution. Furthermore, the fiber reinforcement contributes to crack control, improving the SLS performance of the structure. Combining this with prestressed tendons will then allow for high moment resistance, where the tendons are suitable for handling the largest moments that occur. The stresses which are introduced by the tendons also help reducing deflections. Furthermore, both reinforcement types are resistant to corrosion, thus facilitating the design of slender structures with sufficient durability. The benefits in crack control provided by fiber reinforcement in particular, and prestressed tendons to a degree, is especially beneficial for ground slabs. This is because the cracks which may form on the ground slab surface are more likely to be visible than for other types of slabs. Additionally, as aggressive substances may seep in through cracks adjacent to the soil, a tight ground slab is necessary for it to be durable. A possible measure that can be taken in order to increase the utilization ratio of the fiber reinforcement in such combinations, is to cast a slab in different stages. Thus, two external layers with fiber reinforcement may be cast with a pure concrete layer in between. This is however, more logistically demanding on the construction site, and the Norwegian construction industry has thus far been unwilling to test this approach. Furthermore, issues regarding bonding of fibers along the surfaces between the two types of layers may arise. Ultimately, such a reinforcement design may be expected to achieve satisfactory ULS properties, while performing well in SLS and enabling economical, efficient and durable structures to be built. It contributes with satisfactory durability without having to add large amounts of conventional reinforcement just for SLS demands.

All the reinforcement solutions which were investigated in this thesis that include both conventional and PT reinforcement facilitate a practical tendon fastening procedure. This is because they all include conventional reinforcement nets to which the tendons may be placed. Furthermore, they allow for flexibility in the reinforcement layout as the reinforcement bars can be placed locally where they are needed. An additional benefit is gained by reducing the height of the slab, as is done in solution C. The reduction which is investigated in this thesis cuts the used concrete amount significantly without reducing the capacity of the slab or necessitating an unbeneficial increase in the reinforcement amount. If the requirements for concrete cover depth were possible to disregard when using prestressed reinforcement, the thickness reduction could have been larger. This is because the internal lever arm of the reinforcement would increase. Especially for solution E, with no conventional reinforcement, this would have been beneficial.

All solutions including fiber reinforcement produce simple reinforcement layouts, because the amount of conventional reinforcement bars is lower. They also provide a benefit in construction time, and on-site labor intensity. The reinforcement layout is also simple for the prestressed designs, depending on how much extra conventional reinforcement is necessary. Thus, solution A, with only conventional reinforcement, has the layout which is the most difficult to understand and produce. One measure which alleviates this to a degree, and which is utilized in this thesis, is to choose reinforcement amounts which are

similar in strips with slightly different necessary reinforcement amounts. This does, however, involve rounding up the reinforcement areas. More rounding of reinforcement area achieves more simplicity, but at the cost of creating a more conservative reinforcement design. Another benefit which is achieved with all solutions including prestressed tendons, and especially fiber reinforcement, is that they achieve good crack resistance without needing large amounts of extra reinforcement.

6 Conclusions

Different reinforcement solutions based on combinations of conventional, post-tensioned and fiber reinforcement are examined for a pile supported ground slab in this thesis. The investigated reinforcement combinations are solution A (conventional reinforcement), B (conventional and post-tensioned), C (conventional and post-tensioned with reduced slab thickness), D (conventional, post-tensioned and fibers), E (post-tensioned and fibers) and F (fibers). The different slab designs are investigated mainly through moment calculations in ULS, with yield line theory and EFM based on adjusted linear elastic analysis as calculation methods. Punching shear according to both the current Eurocode and the proposed new draft is also investigated.

The area in which the critical yield line pattern will probably occur is clear based on the moment distributions and the spans. Hence, the accuracy obtained by only applying one yield line mechanism is sufficient. This makes yield line theory an effective method also for this slab. If the wrong yield line pattern is chosen, however, the consequences might be large for the structure's performance. For other slabs, it might therefore be wise to investigate different possible patterns. Furthermore, the 10%-rule increases the safety of yield line theory designs.

Design with EFM based upon an elastic analysis demands more numerous calculation operations and a more complicated process altogether. The elastic analysis, though it may add more work than simple frame analyses, adds the benefit of providing more accurate moment distributions. Furthermore, the designs produced in this manner may be considered as more conservative than yield line theory solutions. The reinforcement solutions tend to result in twice as much reinforcement for EFM as for yield line theory.

For punching shear calculations, the Eurocodes are not user friendly for all reinforcement solutions. The current Eurocode does not provide options for calculations to be executed on fiber reinforced concrete. The proposed new EC2, on the other hand, include provisions to include the fiber contribution. Neither version, however, addresses reinforcement designs without conventional reinforcement. Thus, making these solutions competitive in the market becomes difficult.

The punching shear analysis shows that all reinforcement solutions have sufficient punching shear capacity, without needing shear reinforcement. Especially the proposed EC2:2021 provides a simple procedure for this slab, since the minimum punching shear resistance is sufficient, thus removing the need for further checks.

Steel fiber and PT proves to contribute with great shear properties, just like the theory suggests. The solutions that include fiber reinforcement have the highest punching shear capacities, and the fibers contribute with a great proportion of this. PT achieves similar capacities as for conventional, but with less reinforcement usage. Thus, fibers seem to contribute the most, but are poorly utilized. PT results in sufficient capacity with less steel usage. A combination of fibers and PT leads to very high shear capacities which is appropriate in slender slabs with limited area for additional reinforcement bars near columns.

All the solutions containing fibers have the highest consumption of steel. This is due to the distribution in the z-direction. Additionally, solutions E and F lack the possibility of placing the reinforcement locally, causing the reinforcement in parts of the slab to be poorly utilized. This also applies for solution D, but to a lesser extent. The solutions with the lowest steel consumption are those which include post-tensioned reinforcement. Solution A, which only includes conventional reinforcement, has a moderate steel consumption compared with the other solutions. This consumption could be decreased by more variation in bar spacings, but this would lead to a more complex solution.

Solution C shows that it is possible to reduce the concrete consumption considerably, with a relatively small increase in prestressed reinforcement amount. By increasing the PT reinforcement amount by approximately 1 kg per square meter, 180 kg concrete is saved. This strengthens the assertion that post-tensioned tendons are suitable for leaner structures, which is very environmentally friendly.

For most of the investigated slab, solutions A and F are considered adequate and efficient. This is due to the low moments in most of the slab, which makes it unnecessary with PT reinforcement in these areas.

Solution A is the traditional solution, and the comparisons are based on this. The biggest advantage with conventional reinforcement, is that it is well used and that the calculation methods are well tested.

Solution B and C, with conventional and PT leads to fewer reinforcement bars, which means easier and faster construction on-site. This, in turn, may lead to more economical projects. This solution requires a low reinforcement amount. It is also possible to save concrete with this solution, by making more slender constructions. The crack widths are limited when PT is used. Reinforcement nets and PT are also a good combination because it facilitates easier placing of PT. This makes it easier to obtain the right curvature for PT. However, the use of prestressed reinforcement requires tensioning on-site, unless prefabricated elements are used. The tensioning of tendons requires competence and planning to execute effectively.

Solution D has the same properties as B and C, but with the FRC's properties as well. This mostly means that the steel consumption is higher, but the beneficial properties regarding crack widths and punching shear are improved. Less PT is required, which leads to somewhat reduced construction time. When fibers are included, there are important conditions to consider regarding the casting process. For fibers to function well, they need to be evenly distributed and oriented in all directions. This means that the concrete should not be vibrated. Hence, SCC is to prefer. The fresh concrete must also be stable enough to contain the fibers effectively when casting.

Solution E does not include conventional reinforcement. This means that corrosion is less of an issue. However, the Eurocode still requires minimum cover depth when using PT, even though it is, in principle, not necessary. Somewhat more PT are needed than for D, but steel consumption is smaller for E. It is however harder to place PT without reinforcement nets. Other properties are more or less the same.

Solution F is nearly sufficient according to yield line theory, but the fiber dosage should be increased. The solution is very time efficient, both in design and during production. This is due to yield line theory being the appropriate method, and no reinforcement bars is needed. Fiber reinforcement can be made of other materials than steel, which may reduce corrosion risk, even though the corrosion risk already is low for this solution.

Steel fibers are, however, the most ductile and the strongest fibers. The steel usage is high for this fiber solution as well. Properties, such as punching shear capacity and crack resistance is high and often sufficient, but lower than for the solutions with fibers combined with other reinforcement types.

Each solution has its own advantages and disadvantages. What is most suitable for a slab, depends on the slab and its intended use. For practical reasons, PT is desirable to combine with reinforcement nets. By adding fibers, properties regarding shear and crack width will improve. For faster production, the use of fibers is desirable.

6.1 Further work

Limitations and prioritizations are made to structure the work with this thesis, and to fulfill it within the given time and with available resources. Consequently, several interesting aspects regarding design of ground slabs with different reinforcement solutions remain either uninvestigated, or with an unexhaustive investigation having been conducted. Thus, suggestions on further work which may enlighten some additional issues regarding the themes touched upon in this thesis are provided.

- SLS analysis and design, with emphasis on crack width calculations. Crack widths are important for ground slabs due to functionality, durability and aesthetics, and the effect of post-tensioned reinforcement and fibers are beneficial and interesting to explore.
- Reinforcement solutions consisting solely of prestressed reinforcement are interesting to investigate. Assessment of ULS and SLS design criteria, and an investigation of whether this is a feasible solution at all is useful.
- Carry out a comprehensive literature study, and if possible, perform tests in order to assess the accuracy of the methods used in this thesis. Moment and punching shear capacity could be tested for several slabs with different reinforcement solutions. The results, when compared to the calculated capacities, would provide further insight into the behavior of flat slabs in both ULS and SLS. Furthermore, the impact of the different reinforcement types can be evaluated based on such results.
- Further investigation into the appropriateness of analysis using yield line theory. As this method for ULS design of concrete structures is little used in the current market, both further calculations and experimental work to examine its validity will be beneficial.
- Work to develop calculation procedures for punching shear capacity of slabs reinforced without bonded reinforcement bars.
- Parameter studies of both the calculation methods and the final reinforcement designs. Attempts to develop efficient models for doing optimizations of the calculation results may produce great benefits to future slab designs. Different fiber dosages, fiber types, post-tensioned tendon layout and yield line parameters is possible to investigate.
- Work on design of other slabs, to provide a broader understanding of which results from this thesis are project-specific, and which seem to be universal. Including comparison of current and proposed new Eurocodes.
- Investigate the possibility of casting concrete with fibers in top and bottom of the slab, to limit the steel usage.

Bibliography

Abbood, I. A., & Al-Bayati, A. F. (2021). Punching shear strength of steel fibre reinforced concrete flat slabs: A literature review and design codes evaluation. *IOP Conference Series: Materials Science and Engineering*, *1067*(1), 012061. https://doi.org/10.1088/1757-899X/1067/1/012061

Aidarov, S., Mena, F., & de la Fuente, A. (2021). Structural response of a fibre reinforced concrete pile-supported flat slab: Full-scale test. *Engineering Structures*, *239*, 112292. https://doi.org/10.1016/j.engstruct.2021.112292

Bondy, K. (2006). *POST-TENSIONED CONCRETE IN BUILDINGS PAST AND FUTURE AN INSIDER'S VIEW*. 10.

CEN. (2004). *NS-EN 1992-1-1:2004+A1:2014+NA:2021*. https://www.standard.no/no/Net tbutikk/produktkatalogen/Produktpresentasjon/?ProductID=1365302

CEN. (2021). *NS-EN 1992-1-1:2021*.

Concrete Society. (2016). *Concrete industrial ground floors: A guide to design and construction*.

de Albuquerque, A. T., El Debs, M. K., & Melo, A. M. C. (2012). A cost optimization-based design of precast concrete floors using genet ic algorithms. *Automation in Construction*, *22*, 348–356. https://doi.org/10.1016/j.autcon.2011.09.013

Destree, X. (2009). Steel-fibre-only reinforced concrete in free suspended elevated slabs. *Concrete Engineering International*, *13*, 47–49.

Eyre, J. R. (2006). Membrane action in ground-bearing concrete slabs. *Eyre, J.R. (2006) Membrane Action in Ground-Bearing Concrete Slabs. Structures & Buildings, 159 (3). Pp. 153-163. ISSN 09650911*, *159*. https://doi.org/10.1680/stbu.2006.159.3.153

Fernández Ruiz, M., Muttoni, A., & Kunz, J. (Eds.). (2010). Strengthening of flat slabs against punching shear using post-installed shear reinforcement. *ACI Structural Journal*. https://doi.org/10.14359/51663816

Focus Software. (2021, May 18). *Focus Konstruksjon 3D - Focus Software*. https://www.focus.no/en/products/focus-konstruksjon-3d/

Fürst, A., & Marti, P. (1997). Robert Maillart's Design Approach for Flat Slabs. *Journal of Structural Engineering*, *123*(8), 1102–1110. https://doi.org/10.1061/(ASCE)0733-9445(1997)123:8(1102)

Hagberg, T., Alexander, S., Aadnesen, L., & Vik, B. (2004). *Publikasjon nr. 33— Flatdekker: Beregning og konstruktiv utforming*.

Hirsch, J. (2009). *Accurate Long-Term Deflection Prediction in Flat Slabs Using Linear Elastic Global Analysis*. 11.

Hulett, T. (2011, September 11). *Design & Construction of Pile-Supported Concrete Industrial Floors*. Face Consultants. https://face-consultants.com/pile-supported-concrete-floors/

Kanstad, T., Døssland, Å. L., Vatnar, A., Mathisen, A. E., Brå, H., Hisdal, J. M., Leirud, N., Sandbakk, S., Sandaker, T. K., Bjøntegaard, Ø., & Sæter, Ø. (2020). Publikasjon nr 38, Fiberarmert betong i bærende konstruksjoner. *38*.

Kanstad, T., Juvik, D. A., & Vatnar, A. (2011). *Forslag til retningslinjer for dimensjonering, utførelse og kontroll av fiberarmerte betongkonstruksjoner SINTEF Bokhandel*. https://www.sintefbok.no/book/index/1010/forslag_til_retningslinjer_for_dimensjonering_utfoerelse_og_kontroll_av_fiberarmerte_betongkonstruksjoner

Kennedy, G., & Goodchild, C. (2004). *Practical Yield Line Design*. http://wsmurti.lecture.ub.ac.id/files/2012/10/Perencanaan-Praktis-Garis-Leleh1.pdf

Løset, Ø. (2021). *Dimensjonering med bruddlinjer – Bjelker og plater, kommentarutgave*.

Marcalikova, Z., Cajka, R., Bilek, V., Bujdos, D., & Sucharda, O. (2020). Determination of Mechanical Characteristics for Fiber-Reinforced Concrete with Straight and Hooked Fibers. *Crystals*, *10*(6), 545. https://doi.org/10.3390/cryst10060545

Mohaghegh, A. M., Silfwerbrand, J., & Årskog, V. (2015). *Properties of Fresh Macro Basalt Fibre (MiniBar) Self-Compacting Concrete (SCC) and Conventional Slump Concrete (CSC) Aimed for Marine Applications*.

Nawy, E. G. (2010). *Prestressed Concrete: A Fundamental Approach*. Prentice Hall.

Oikonomou-Mpegetis, S. (2013). *Behaviour and design of steel fibre reinforced concrete slabs*. https://doi.org/10.25560/23792

Ojo, T. O. (2021). *Performance of Steel Fiber Reinforced and Conventionally Reinforced Post-Tensioned Flat Plates*. https://vtechworks.lib.vt.edu/handle/10919/105008

Peel-Cross, J., Rankin, G. I. B., Gilbert, S. G., & Long, A. E. (2001). Compressive membrane action in composite floor slabs in the Cardington LBTF. *Proceedings of the Institution of Civil Engineers - Structures and Buildings*, *146*(2), 217–226. https://doi.org/10.1680/stbu.2001.146.2.217

Ramos, A., & Lucio, V. (2008). Post-punching behaviour of prestressed concrete flat slabs. *Magazine of Concrete Research - MAG CONCR RES*, *60*, 245–251. https://doi.org/10.1680/macr.2008.60.4.245

Sahab, M. G., Ashour, A. F., & Toropov, V. V. (2005). Cost optimisation of reinforced concrete flat slab buildings. *Engineering Structures*, *27*(3), 313–322. https://doi.org/10.1016/j.engstruct.2004.10.002

Sarma, K. C., & Adeli, H. (1998). Cost Optimization of Concrete Structures. *Journal of Structural Engineering*, *124*(5), 570–578. https://doi.org/10.1061/(ASCE)0733-9445(1998)124:5(570)

Silva, R. J. C., Regan, P. E., & Melo, G. S. S. A. (2007). Punching of Post-Tensioned Slabs—Tests and Codes. *Structural Journal*, *104*(2), 123–132. https://doi.org/10.14359/18524

Sørensen, S. I., & Øverli, J. A. (2013). *TKT4222 Concrete Structures 3—Compendium*. Department of Structural Engineering - NTNU.

Standard Norge. (2008). *Prøvingsmetode for betong med metalliske fibere—Måling av bøyestrekkfasthet (proporsjonalitetsgrense og restfastheter)*.

Trygestad, A. R. (2005). *Post-Tensioning for Two-Way Flat Plate Construction*. 8.

Van Gorder, R. A. (2012). Analytical method for the construction of solutions to the Föppl–von Kármán equations governing deflections of a thin flat plate. *International Journal of Non-Linear Mechanics*, *47*(3), 1–6. https://doi.org/10.1016/j.ijnonlinmec.2012.01.004

Vikan, H. (2007). *Concrete workability and fibre content*. https://www.sintef.no/globalassets/sintef-byggforsk/coin/sintef-reports/sbf-bk-a07029_concrete-workability-and-fibre-content.pdf

Appendix

Appendix A: Adjusted moment distributions from LFEA in FK.

Appendix B: Hand calculations.

Appendix A

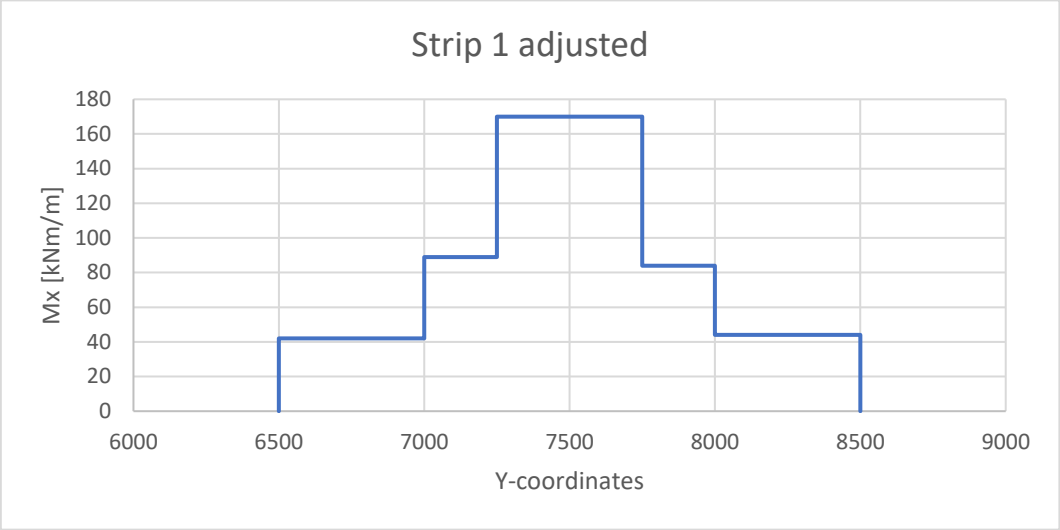
Strip 1 adjusted
Mx [kNm/m]
180
160
140
120
100
80
60
40
20
0
6000
6500
7000
7500
8000
8500
9000
Y-coordinates

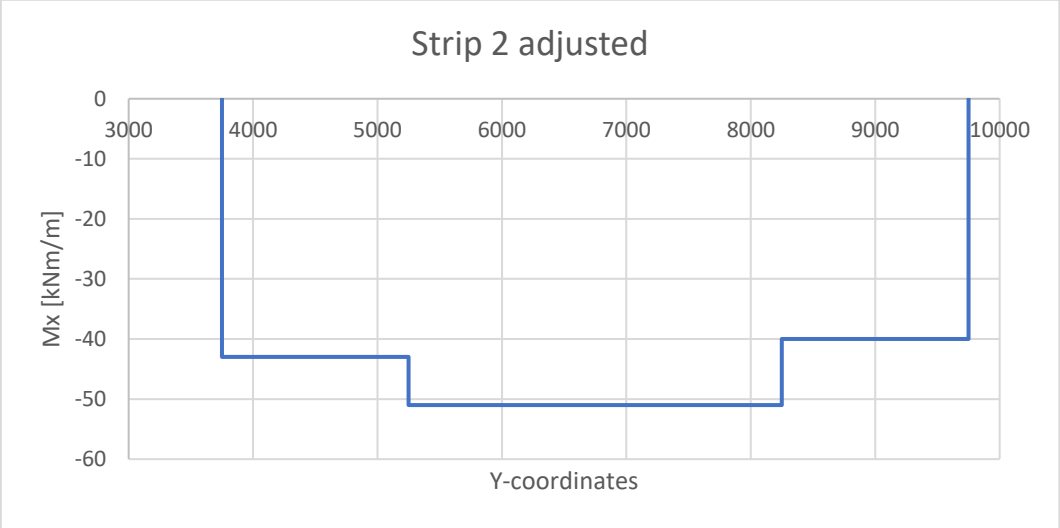
Strip 2 adjusted
Mx [kNm/m]
0
-10
-20
-30
-40
-50
-60
3000
4000
5000
6000
7000
8000
9000
10000
Y-coordinates

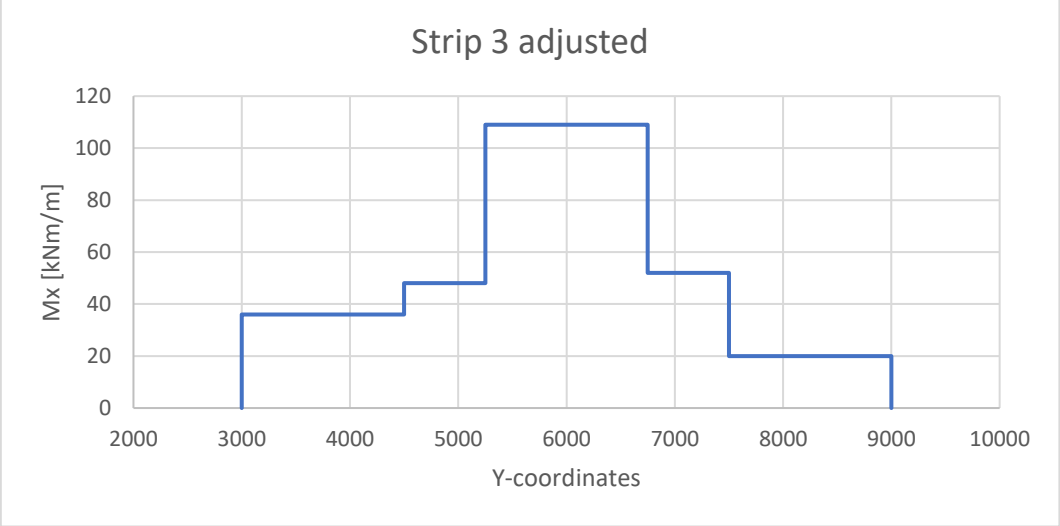
Strip 3 adjusted
Mx [kNm/m]
120
100
80
60
40
20
0
2000
3000
4000
5000
6000
7000
8000
9000
10000
Y-coordinates

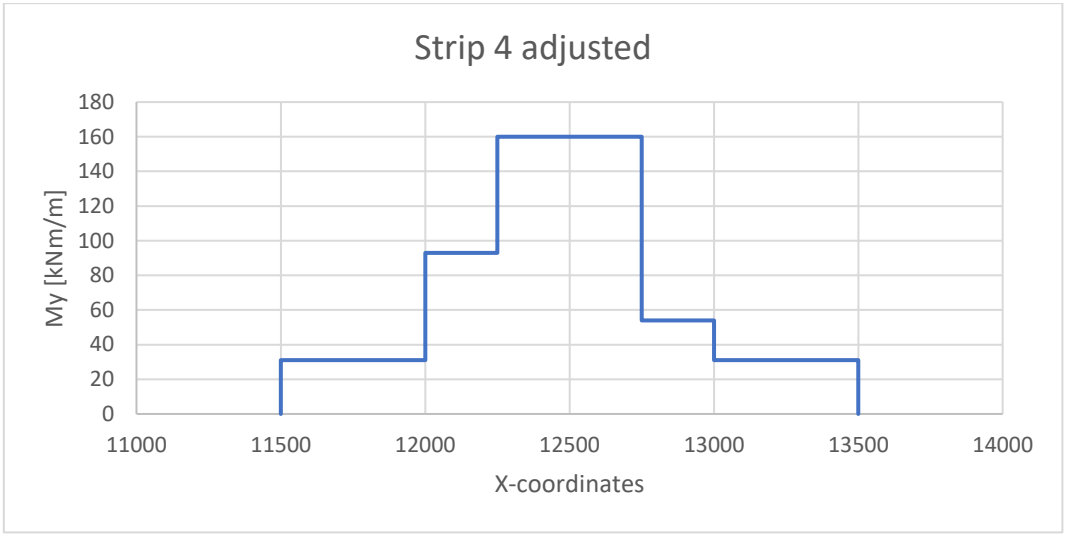
Strip 4 adjusted
My [kNm/m]
180
160
140
120
100
80
60
40
20
0
11000
11500
12000
12500
13000
13500
14000
X-coordinates

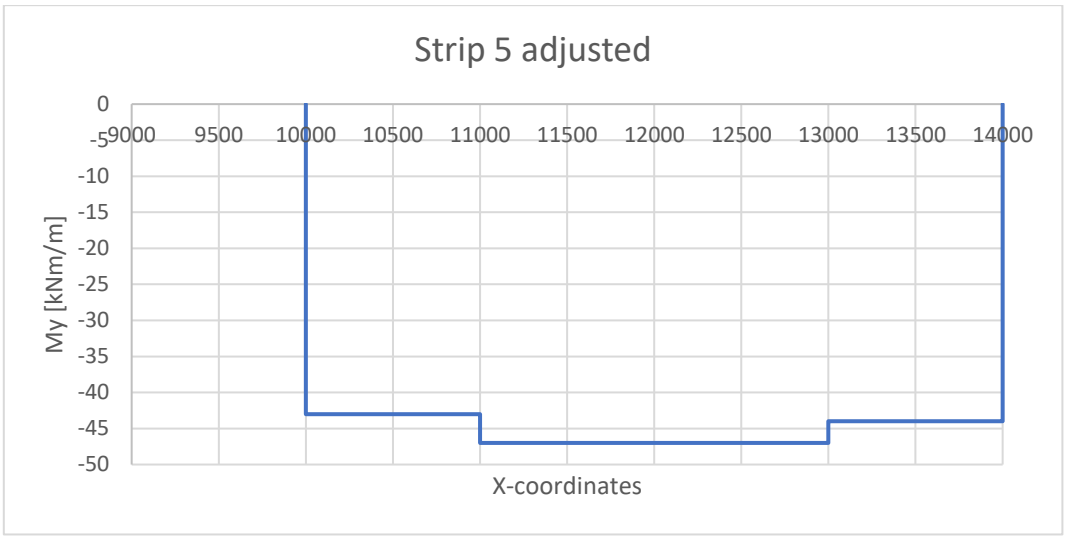
Strip 5 adjusted
My [kNm/m]
0
-5
-10
-15
-20
-25
-30
-35
-40
-45
-50
9000
9500
10000
10500
11000
11500
12000
12500
13000
13500
14000
X-coordinates

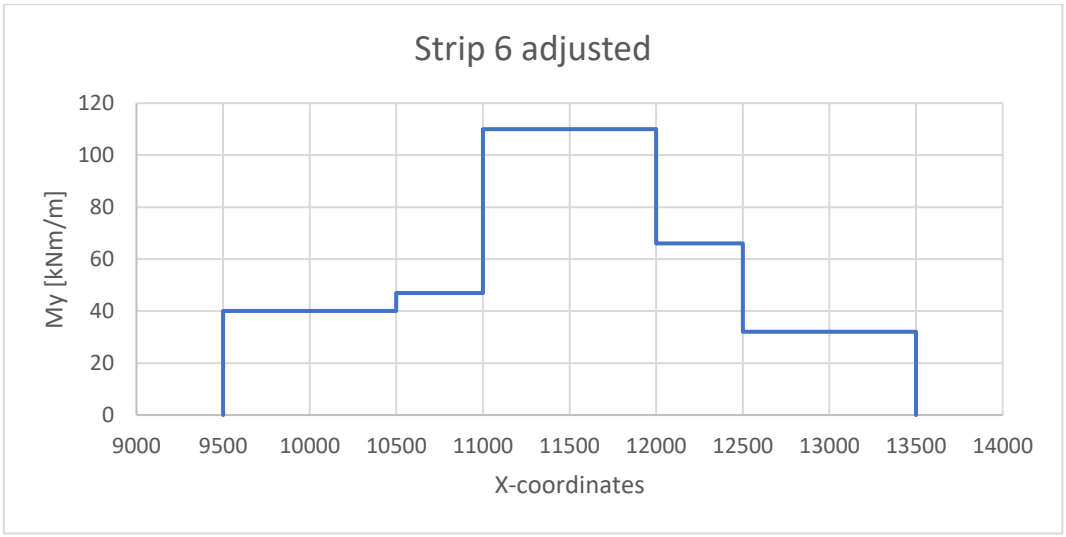
Strip 6 adjusted
My [kNm/m]
120
100
80
60
40
20
0
9000
9500
10000
10500
11000
11500
12000
12500
13000
13500
14000
X-coordinates

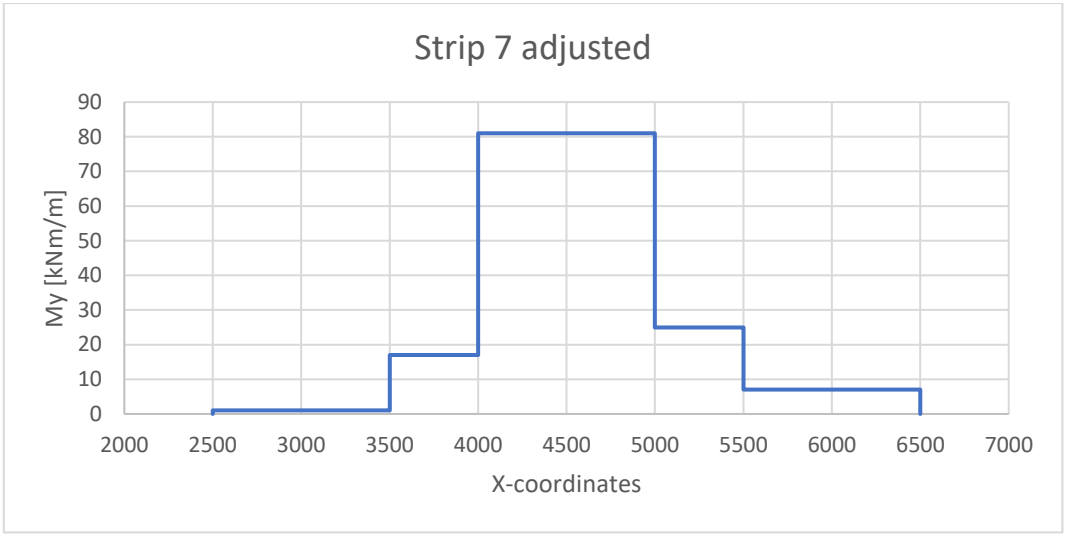
Strip 7 adjusted
My [kNm/m]
90
80
70
60
50
40
30
20
10
0
2000
2500
3000
3500
4000
4500
5000
5500
6000
6500
7000
X-coordinates

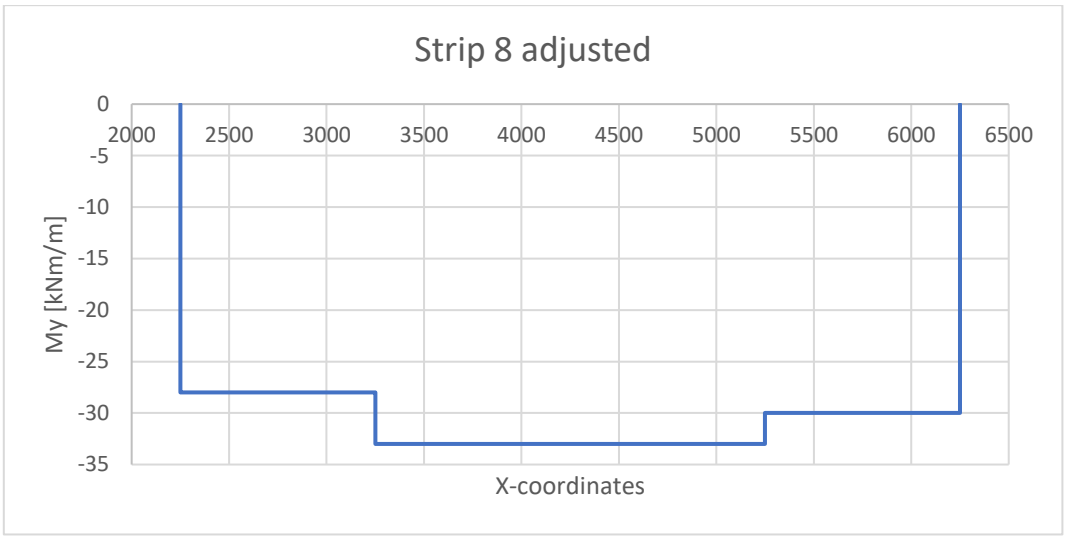
Strip 8 adjusted
My [kNm/m]
0
-5
-10
-15
-20
-25
-30
-35
2000
2500
3000
3500
4000
4500
5000
5500
6000
6500
X-coordinates

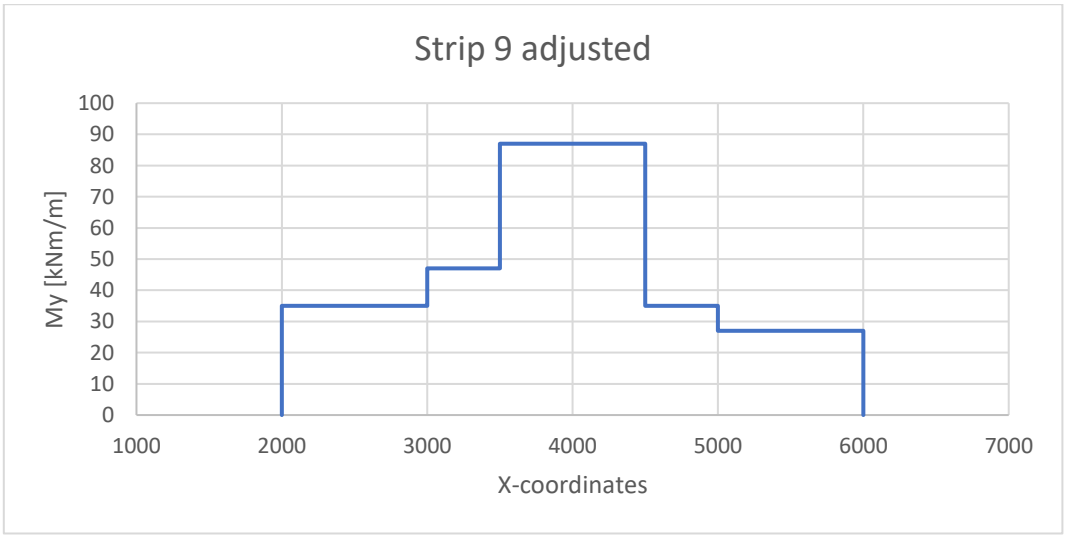
Strip 9 adjusted
My [kNm/m]
100
90
80
70
60
50
40
30
20
10
0
1000
2000
3000
4000
5000
6000
7000
X-coordinates

Appendix B

EFM and yield line theory

Loads and geometry

$h := 275\ mm$ Height of slab

$b := 1000\ mm$ Width of a given slab cross-section

$L := 8000\ mm$ Greatest span in slab

$\gamma := 2500\ \frac{kg}{m^3} \cdot 10\ \frac{m}{s^2} = \left(2.5 \cdot 10^4\right)\ \frac{N}{m^3}$ Unit weight of concrete

$g_{self} := \gamma \cdot h = 6.875\ \frac{kN}{m^2}$ Self weight of slab

$g_{outer} := 2.5\ \frac{kN}{m^2}$ Imposed dead load on slab

$p := 4\ \frac{kN}{m^2}$ Imposed live load on slab

$q := 1.2 \cdot \left(g_{self} + g_{outer}\right) + 1.5 \cdot p = 17.25\ \frac{kN}{m^2}$ Universally distributed load

Loads, reduced slab height

$h_C := 200\ mm$ Reduced slab height

$g_{selfc} := \gamma \cdot h_C = 5\ \frac{kN}{m^2}$ Reduced self weight of slab

$q_C := 1.2 \cdot \left(g_{selfc} + g_{outer}\right) + 1.5 \cdot p = 15\ \frac{kN}{m^2}$ Reduced load

Material properties

$f_{yk} := 500\ \frac{N}{mm^2}$ Characteristic yield strength for reinforcement steel

$f_{yd} := \frac{f_{yk}}{1.15} = 434.783\ \frac{N}{mm^2}$ Design yield strength for reinforcement steel

$f_{ck} := 35 \ \frac{N}{mm^2}$ Characteristic compression strength for the concrete in D3-2

$f_{cd} := 0.85 \cdot \frac{f_{ck}}{1.5} = 19.833 \ \frac{N}{mm^2}$ Design compression strength

$E_{cm} := 34 \ GPa$ Mean E-modulus for B35 concrete

$c_{nombot} := 50 \ mm$ Nominal cover depth at bottom

$c_{nomtop} := 35 \ mm$ Nominal cover depth at top

$A_{s383} := 383 \ mm^2$

$A_{s257} := 257 \ mm^2$ Chosen universal reinforcement amounts

EFM - design moments

Table 1: The adjusted moments in sections over columns.

	m_{SFL}	m^2_{SSL}	m^1_{SS}	m^2_{SSR}	m_{SFR}	
Section 1	42,00	89,00	170,00	84,00	44,00	Mx [kNm/m]
Section 3	36,00	48,00	109,00	52,00	20,00	Mx [kNm/m]
Section 4	31,00	93,00	160,00	54,00	31,00	My [kNm/m]
Section 6	40,00	47,00	110,00	66,00	32,00	My [kNm/m]
Section 7	1,00	17,00	81,00	25,00	7,00	My [kNm/m]
Section 9	35,00	47,00	87,00	35,00	27,00	My [kNm/m]

Table 2: The adjusted moments in field sections.

	m_{FFL}	m_{FS}	m_{FFR}	
Section 2	-43,00	-51,00	-40,00	Mx [kNm/m]
Section 5	-43,00	-47,00	-44,00	My [kNm/m]
Section 8	-28,00	-33,00	-30,00	My [kNm/m]

Table 3: Adjusted reduced moments over columns.

	m_{SFL}	m^2_{SSL}	m^1_{SS}	m^2_{SSR}	m_{SFR}	
Section 1	36,52	77,39	147,83	73,04	38,26	Mx [kNm/m]
Section 3	31,30	41,74	94,78	45,22	17,39	Mx [kNm/m]
Section 4	26,96	80,87	139,13	46,96	26,96	My [kNm/m]
Section 6	34,78	40,87	95,65	57,39	27,83	My [kNm/m]
Section 7	0,87	14,78	70,43	21,74	6,09	My [kNm/m]
Section 9	30,43	40,87	75,65	30,43	23,48	My [kNm/m]

Table 4: Adjusted reduced moments in field.

	m_{FFL}	m_{FS}	m_{FFR}	
Section 2	-37,39	-44,35	-34,78	Mx [kNm/m]
Section 5	-37,39	-40,87	-38,26	My [kNm/m]
Section 8	-24,35	-28,70	-26,09	My [kNm/m]

Yield line theory - design moments

$i_1 := 1$ $i_2 := 0.5$ $i_3 := 1$ $i_4 := 1$

$B := 8000\ mm$ $H := 13000\ mm$

$b_r := \frac{2 \cdot B}{\left(\sqrt{1+i_2}+\sqrt{1+i_4}\right)} = 6.063\ m$ Reduced breadth

$h_r := \frac{2 \cdot H}{\left(\sqrt{1+i_1}+\sqrt{1+i_3}\right)} = 9.192\ m$ Reduced height

$m_k := \frac{q \cdot b_r \cdot h_r}{8 \cdot \left(1+\frac{h_r}{b_r}+\frac{b_r}{h_r}\right)} = 37.842\ kN \cdot \frac{m}{m}$ Moment for the chosen yield line mechanism

$h_1 := \sqrt{6 \cdot \left(1+i_1\right) \cdot \frac{m_k}{q}} = 5.131\ m$ Height of area 1

$h_2 := \frac{b_r}{2} \cdot \sqrt{1+i_2} = 3.713\ m$ Height of area 2

$h_3 := \sqrt{6 \cdot \left(1+i_3\right) \cdot \frac{m_k}{q}} = 5.131\ m$ Height of area 3

$h_4 := \frac{b_r}{2} \cdot \sqrt{1+i_4} = 4.287\ m$ Height of area 4

$m_{yield} := 1.15 \cdot m_k = 43.518\ kN \cdot \frac{m}{m}$ Design moment for the chosen yield line mechanism

$m'_{yield} := i_1 \cdot m_{yield} = 43.518\ kN \cdot \frac{m}{m}$ Design moment for edges 1, 3 and 4

$m'_{yield2} := i_2 \cdot m_{yield} = 21.759\ kN \cdot \frac{m}{m}$ Design moment for edge 2

Solution C

$m_{yieldC} := 37.842\ kN \cdot \frac{m}{m}$ Design moment for the chosen yield line mechanism

$m'_{yieldC} := i_1 \cdot m_{yieldC} = 37.842\ kN \cdot \frac{m}{m}$ Design moment for edges 1, 3 and 4

$m'_{yield2C} := i_2 \cdot m_{yieldC} = 18.921\ kN \cdot \frac{m}{m}$ Design moment for edge 2

Post-tensioned reinforcement

$q_{long} := g_{self} + g_{outer} + 0.4 \cdot p = 10.975\ \frac{kN}{m^2}$ Long term load

$M_{long} := \frac{q_{long} \cdot L^2}{8} \cdot 1\ m = 87.8\ kN \cdot m$ Moment from long term load

$A_p := 150\ mm^2$ Area of post-tensioned cable

$E_p := 195\ GPa$ E-modulus for prestressing steel

$f_{p01k} := 1500\ \frac{N}{mm^2}$ 0.1% yield strength for tendons

$f_{pk} := 1600\ \frac{N}{mm^2}$ Characteristic tendon yield strength

$f_{pd} := \frac{f_{p01k}}{1.15} = \left(1.304 \cdot 10^3\right)\ MPa$ Design tendon yield strength

$\sigma_{pmax} := min\left(0.8 \cdot f_{pk}, 0.9 \cdot f_{p01k}\right) = \left(1.28 \cdot 10^3\right)\ MPa$ Maximum allowable stress applied to tendon, according to EC2.5.10.2.1(1)

$P_{max} := A_p \cdot \sigma_{pmax} = 192\ kN$ Maximum applied tensioning force to a tendon, according to EC2.eq. (5.41)

$\Delta\sigma_{pULS} := 100\ MPa$ Allowable stress increase due to deformation of concrete member, according to EC2.5.10.8(2)

$d_{pbot} := 177\ mm$ $d_{ptop} := 216\ mm$ Depth of prestressed reinforcement

$d_{sbot} := 206\ mm$ $d_{stop} := 233\ mm$ Depth of conventional reinforcement

$d := h - c_{nombot} - 20\ mm = 205\ mm$ Approximate depth of conventional reinforcement at bottom for combined solutions

Losses due to friction, according to EC2.5.10.5.2

$\mu := 0.19$ Friction coefficient

$k := \frac{0.01}{m}$ Estimated unintentional angular displacement

$e_{anchor} := \frac{h}{2} - (h - d_{ptop}) = 78.5\ mm$ Tendon eccentricity at anchor

$L_{dist} := 16000\ mm$ Length of longest distributed tendons

$\theta_{anchor} := \frac{(2 \cdot e_{anchor})}{0.5 \cdot L_{dist}} = 0.02$ Angle of tendons at anchor

$x := \frac{L_{dist}}{2} = (8 \cdot 10^3)\ mm$ Length to middle of tendon strip 32B

$\Delta P_{\mu} := P_{max} \cdot \left(1 - e^{(-\mu \cdot (\theta_{anchor} + k \cdot x))}\right) = 3.6\ kN$ Loss of prestress force due to friction

Losses at anchorage

$\Delta L_{anchor} := 6\ mm$ Estimated total loss at anchorage

$\varepsilon_{anchor} := \frac{\Delta L_{anchor}}{L_{dist}} = 3.75 \cdot 10^{-4}$ Strain loss due to loss at anchorage

$\Delta P_{anchor} := \varepsilon_{anchor} \cdot E_p \cdot A_p = 10.969\ kN$ Loss of prestress force due anchorage losses

Check for maximum allowable prestress force after tensioning, after EC2.5.10.3 (2)

Maximum allowable prestress force in tendon immediately after tensioning, after EC2.5.10.3(2)

$\sigma_{pm0} := min(0.75 \cdot f_{pk}, 0.85 \cdot f_{p01k}) = (1.2 \cdot 10^3)\ MPa$

$P_{mo} := \sigma_{pm0} \cdot A_p = 180\ \boldsymbol{kN}$

Estimated prestressing force immediately after tensioning

$P_{max} - \Delta P_{\mu} - \Delta P_{anchor} = 177.431\ \boldsymbol{kN}$

Check ok

Time dependent losses, simplified method according to EC2.5.10.6(2)

Total shrinkage strain, after EC2.3.1.4(6)

Drying shrinkage strain, EC2.B.2

$RH := 50\%$ Ambient relative humidity, indoors

$RH_0 := 100\%$ Maximum relative humidity

$\beta_{RH} := 1.55 \cdot \left(1 - \left(\frac{RH}{RH_0}\right)^3\right) = 1.356$ Coefficient relating to humidity

$f_{cm0} := 10\ \boldsymbol{MPa}$

$f_{cm} := 43\ \boldsymbol{MPa}$ Mean compressive strength for B35 concrete, from EC2. Table 3.1

$\alpha_{ds1} := 4$ Coefficients depending on cement type

$\alpha_{ds2} := 0.12$

$\varepsilon_{cd0} := 0.85 \cdot \left(\left(220 + 110 \cdot \alpha_{ds1}\right) \cdot e^{\left(-\alpha_{ds2} \cdot \frac{f_{cm}}{f_{cm0}}\right)}\right) \cdot 10^{-6} \cdot \beta_{RH} = 4.542 \cdot 10^{-4}$

$k_h := 0.78$ Coefficient from EC2. Table 3.3

$\varepsilon_{cd} := k_h \cdot \varepsilon_{cd0} = 3.542 \cdot 10^{-4}$ Drying shrinkage strain

Autogenous shrinkage strain, EC2. eq. (3.12)

$\varepsilon_{ca} := 2.5 \cdot \left(\frac{f_{ck}}{\boldsymbol{MPa}} - 10\right) \cdot 10^{-6} = 6.25 \cdot 10^{-5}$ Long term autogenous shrinkage strain

$\varepsilon_{cs} := \varepsilon_{cd} + \varepsilon_{ca} = 4.167 \cdot 10^{-4}$ Total shrinkage strain

Relaxation stress loss for Class 1 strands, after EC2. eq. (3.28)

$\sigma_{pi} := \sigma_{pm0} = \left(1.2 \cdot 10^{3}\right)\ \mathit{MPa}$ Absolute value of initial prestress

$\rho_{1000} := 2.5$ Relaxation loss after 1000 hours, in percent

$\mu_{relax} := \dfrac{\sigma_{pi}}{f_{pk}} = 0.75$

$t_{relax} := 500000$ After EC2.3.3.2(8)

$\Delta\sigma_{pr} := \sigma_{pi} \cdot 0.66 \cdot \rho_{1000} \cdot e^{\left(9.1 \cdot \mu_{relax}\right)} \cdot \left(\dfrac{t_{relax}}{1000}\right)^{\left(0.75 \cdot \left(1 - \mu_{relax}\right)\right)} \cdot 10^{(-5)} = 58.45\ \mathit{MPa}$

Creep

$\phi_{tt0} := 2.0$ Creep coefficient, after EC2. Figure 3.1a

$\eta := \dfrac{E_p}{E_{cm}} = 5.735$

$A_c := b \cdot h = 0.275\ m^2$ Area of concrete cross-section

$A_t := A_c + \left(\eta - 1\right) \cdot A_p = 0.276\ m^2$ Total cross-section area(?)

$e_{tendon} := d_{ptop} - \dfrac{h}{2} = 78.5\ mm$ Tendon eccentricity at top

$y_t := \dfrac{\left(\eta - 1\right) \cdot A_p \cdot e_{tendon}}{A_t} = 0.202\ mm$ Distance between center of gravity for concrete cross-section, and reinforced cross-section

$I_c := \dfrac{\left(b \cdot h^3\right)}{12} = 0.002\ m^4$ Second area of moment for concrete cross-section

$I_t := I_c + A_c \cdot {y_t}^2 + \left(\eta - 1\right) \cdot A_p \cdot \left(e_{tendon} - y_t\right)^2 = 0.002\ m^4$

$y := e_{tendon} = 78.5\ mm$

$M_p := P_{max} \cdot e_{tendon} \cdot 2 = 30.144\ \boldsymbol{kN \cdot m}$ Bending moment from tendons, per meter

$M_{long} = 87.8\ \boldsymbol{kN \cdot m}$

$M_{tl} := -M_p + M_{long} = 57.656\ \boldsymbol{kN \cdot m}$ Total long term moment

$\sigma_{cQP} := -\frac{P_{max}}{A_t} + \frac{M_{tl}}{I_t} \cdot \left(y - y_t\right) = 1.902\ \boldsymbol{MPa}$ Long term concrete stress

Simplified expression of stress loss from creep, shrinkage and relaxation. From eq. (5.46)

$z_{cp} := e_{tendon} = 78.5\ \boldsymbol{mm}$

$$\Delta\sigma_{pcsr} := \frac{\left(\varepsilon_{cs} \cdot E_p + 0.8 \cdot \Delta\sigma_{pr} + \frac{E_p}{E_{cm}} \cdot \phi_{tt0} \cdot \sigma_{cQP}\right)}{\left(1 + \frac{E_p}{E_{cm}} \cdot \frac{A_p}{A_c} \cdot \left(1 + \frac{A_c}{I_c} \cdot z_{cp}^{\ 2}\right) \cdot \left[1 + 0.8 \cdot \phi_{tt0}\right]\right)} = \left[147.468\right]\ \boldsymbol{MPa}$$

$\Delta P_{csr} := A_p \cdot \Delta\sigma_{pcsr} = \left[22.12\right]\ \boldsymbol{kN}$ Time dependent losses, per tendon

Prestressing force after all losses, including allowable stress increase

$P_{ULS} := P_{max} - \Delta P_{\mu} - \Delta P_{anchor} - \Delta P_{csr} + \Delta\sigma_{pULS} \cdot A_p = \left[170.311\right]\ \boldsymbol{kN}$

Solution A - Conventional reinforcement

$d_{bot} := h - c_{nombot} - 8\ mm = 217\ mm$ Depth to bottom reinforcement

$d_{top} := h - c_{nomtop} - 8\ mm = 232\ mm$ Depth to top reinforcement

$M_{Rdbot} := 0.275 \cdot f_{cd} \cdot b \cdot {d_{bot}}^2 = 256.831\ kN \cdot m$ Bending moment capacity, tension at bottom fiber

$M_{Rdtop} := 0.275 \cdot f_{cd} \cdot b \cdot {d_{top}}^2 = 293.565\ kN \cdot m$ Bending moment capacity, tension at top fiber

$z_{maxbot} := 0.95 \cdot d_{bot} = 206.15\ mm$

$z_{maxtop} := 0.95 \cdot d_{top} = 220.4\ mm$

Maximum internal lever arms, ensures sufficient height of concrete compressive area

EFM - necessary reinforcement amount

Section 1, left field column strip:

$M_{Ed1L} := 42\ kN \cdot m$ Design moment in section 1, left field column strip

$z_{chosen1L} := min\left(\left(1 - 0.17 \cdot \frac{M_{Ed1L}}{M_{Rdtop}}\right) \cdot d_{top}, z_{maxtop}\right) = 0.22\ m$ Chosen lever arm

$A_{scalc1L} := \frac{M_{Ed1L}}{z_{chosen1L} \cdot f_{yd}} = 438.294\ mm^2$ Calculated necessary reinforcement amount

By using the adjusted moment distributions and the formulae listed above, the necessary reinforcement amount was calculated for each section in like manner as section 1, left field column strip:

Table 5: Calculated necessary reinforcement over columns.

		m_{SFL}	m^2_{SSL}	m^1_{SS}	m^2_{SSR}	m_{SFR}	
$z_{calculated}$	**Section 1**	226	220	209	221	226	mm
z_{chosen}		220	220	209	220	220	mm
A_s		**438**	**930**	**1869**	**877**	**459**	mm^2/m
$z_{calculated}$	**Section 3**	227	226	217	225	229	mm
z_{chosen}		220	220	217	220	220	mm
A_s		**376**	**501**	**1153**	**543**	**209**	mm^2/m
$z_{calculated}$	**Section 4**	228	220	211	225	228	mm
z_{chosen}		220	206	206	206	206	mm
A_s		**324**	**1038**	**1785**	**602**	**346**	mm^2/m
$z_{calculated}$	**Section 6**	227	226	217	223	228	mm
z_{chosen}		220	220	217	220	220	mm
A_s		**417**	**490**	**1165**	**689**	**334**	mm^2/m
$z_{calculated}$	**Section 7**	232	230	221	229	231	mm
z_{chosen}		220	220	220	220	220	mm
A_s		**10**	**177**	**845**	**261**	**73**	mm^2/m
$z_{calculated}$	**Section 9**	227	226	220	227	228	mm
z_{chosen}		220	220	220	220	220	mm
A_s		**365**	**490**	**908**	**365**	**282**	mm^2/m

Table 6: Calculated necessary reinforcement in field.

		m_{FFL}	m_{FS}	m_{FFR}	
$z_{calculated}$		223	224	223	mm
z_{chosen}		206	206	206	mm
A_s	**Section 2**	**480**	**569**	**446**	mm^2/m
$z_{calculated}$		223	224	223	mm
z_{chosen}		206	206	206	mm
A_s	**Section 5**	**480**	**524**	**491**	mm^2/m
$z_{calculated}$		221	222	221	mm
z_{chosen}		206	206	206	mm
A_s	**Section 8**	**312**	**368**	**335**	mm^2/m

EFM - Summary of chosen reinforcement

Choosing $\phi 16$ reinforcement bars and comparing calculated reinforcement amount to minimum reinforcement amount, a reinforcement solution for each section was chosen.

Section 1, left field column strip:

$s_{max} := min(3 \cdot h, 400\ mm) = 400\ mm$ Maximum distance between reinforcement bars, EC2.NA.9.3.1.1(3)

$b_{strip} := 500\ mm$ Width of left field column strip in section 1

$A_{16} := \pi \cdot 8^2\ mm^2 = 201.062\ mm^2$ Area of a $\phi 16$ reinforcement bar

$$s_{calc1L} := min\left(s_{max}, A_{16} \cdot \frac{b_{strip}}{A_{scalc1L}}\right) = 229.369\ mm$$ Calculated bar spacing

$$s_{chosen1L} := 210\ mm$$ Chosen bar spacing

$$n := \frac{b_{strip}}{s_{chosen1L}} = 2.381$$

Necessary and chosen number of reinforcement bars

$$n_{1L} := 3$$

$$A_{s1L} := A_{16} \cdot \frac{b_{strip}}{s_{chosen1L}} = 478.719\ mm^2$$ Chosen reinforcement amount for left field column strip in section 1

This calculation was repeated for all strips in all sections. The chosen reinforcement thus became:

Table 7: Chosen reinforcement amounts in column strips calculated according to NB 33.

		m_{SFL}	m^2_{SSL}	m^1_{SS}	m^2_{SSR}	m_{SFR}	
b_{strip}	Section 1	500	250	500	250	500	mm
s_{calc}		229	54	54	57	219	mm
s_{chosen}		210	50	50	50	210	mm
n		3	5	10	5	3	
$A_{schosen}$		**603**	**1005**	**2011**	**1005**	**603**	mm^2
b_{strip}	Section 3	1500	750	1500	750	1500	mm
s_{calc}		400	301	261	278	400	mm
s_{chosen}		400	260	260	260	400	mm
n		4	3	6	3	4	
$A_{schosen}$		**804**	**603**	**1206**	**603**	**804**	mm^2
b_{strip}	Section 4	500	250	500	250	500	mm
s_{calc}		311	48	56	83	291	mm
s_{chosen}		270	50	50	50	270	mm
n		2	5	10	5	2	
$A_{schosen}$		**402**	**1005**	**2011**	**1005**	**402**	mm^2
b_{strip}	Section 6	1000	500	1000	500	1000	mm
s_{calc}		400	205	173	146	400	mm
s_{chosen}		400	200	140	140	400	mm
n		3	3	8	4	3	
$A_{schosen}$		**603**	**603**	**1608**	**804**	**603**	mm^2
b_{strip}	Section 7	1000	500	1000	500	1000	mm
s_{calc}		400	400	238	385	400	mm
s_{chosen}		400	400	200	380	400	mm
n		3	2	5	2	3	
$A_{schosen}$		**603**	**402**	**1005**	**402**	**603**	mm^2
b_{strip}	Section 9	1000	500	1000	500	1000	mm
s_{calc}		400	205	221	275	400	mm
s_{chosen}		400	200	200	270	400	mm
n		3	3	5	2	3	
$A_{schosen}$		**603**	**603**	**1005**	**402**	**603**	mm^2

Table 8: Chosen reinforcement amounts in field strips calculated according to NB 33.

		m_{FFL}	m_{FS}	m_{FFR}	
b_{strip}	**Section 2**	1500	3000	1500	mm
s_{calc}		400	400	400	mm
s_{chosen}		400	400	400	mm
n		4	8	4	
$A_{schosen}$		**804**	**1608**	**804**	mm^2
b_{strip}	**Section 5**	1000	2000	1000	mm
s_{calc}		400	400	400	mm
s_{chosen}		400	400	400	mm
n		3	5	3	
$A_{schosen}$		**603**	**1005**	**603**	mm^2
b_{strip}	**Section 8**	1000	2000	1000	mm
s_{calc}		400	400	400	mm
s_{chosen}		400	400	400	mm
n		3	5	3	
$A_{schosen}$		**603**	**1005**	**603**	mm^2

Yield line theory

$$z_{yield} := \left(1 - 0.17 \cdot \frac{m_{yield} \cdot 1000\ mm}{M_{Rdbot}}\right) \cdot d_{bot} = 210.749\ mm$$ Internal lever arm in field

$$z'_1 := \left(1 - 0.17 \cdot \frac{m'_{yield} \cdot 1000\ mm}{M_{Rdtop}}\right) \cdot d_{top} = 226.153\ mm$$ Internal lever arm in edge 1

$$z'_2 := \left(1 - 0.17 \cdot \frac{m'_{yield2} \cdot 1000\ mm}{M_{Rdtop}}\right) \cdot d_{top} = 229.077\ mm$$ Internal lever arm in edge 2

$$z'_3 := \left(1 - 0.17 \cdot \frac{m'_{yield} \cdot 1000\ mm}{M_{Rdtop}}\right) \cdot d_{top} = 226.153\ mm$$ Internal lever arm in edge 3

$$z'_4 := \left(1 - 0.17 \cdot \frac{m'_{yield} \cdot 1000\ mm}{M_{Rdtop}}\right) \cdot d_{top} = 226.153\ mm$$ Internal lever arm in edge 4

$$A_{syield} := \frac{m_{yield}}{z_{maxbot} \cdot f_{yd}} = 485.53\ \frac{mm^2}{m}$$ Necessary reinforcement area in field

$$A'_{syield1} := \frac{m'_{yield}}{z_{maxtop} \cdot f_{yd}} = 454.138\ \frac{mm^2}{m}$$ Necessary reinforcement area in edge 1

$A'_{syield2} := \frac{m'_{yield2}}{z_{maxtop} \cdot f_{yd}} = 227.069 \ \frac{mm^2}{m}$ Necessary reinforcement area in edge 2

$A'_{syield3} := \frac{m'_{yield}}{z_{maxtop} \cdot f_{yd}} = 454.138 \ \frac{mm^2}{m}$ Necessary reinforcement area in edge 3

$A'_{syield4} := \frac{m'_{yield}}{z_{maxtop} \cdot f_{yd}} = 454.138 \ \frac{mm^2}{m}$ Necessary reinforcement area in edge 4

$A_{smin} := 361 \ mm^2$ We see that $A'_{syield2} < A_{smin}$

Assume $\phi 16$:

$\phi 16 s550$ gives $A_s := 365 \ \frac{mm^2}{m}$

$s_{454} := A_{16} \cdot \left(\frac{1000}{A'_{syield1}} \right) = 442.733 \ m$

$s_{485} := A_{16} \cdot \frac{1000}{A_{syield}} = 414.108 \ m$

Necessary reinforcement bar spacing, the chosen value is rounded down

Solution B - Conventional and prestressed reinforcement

EFM

Section 1, left field column strip:

$M_{Ed1L} := 42\ kN \cdot m$ Design moment in the strip

$c_{1L} := \frac{M_{Ed1L}}{f_{cd} \cdot b \cdot {d_{top}}^2} = 0.039$ The constant for the strip

$\alpha_{1L} := \frac{0.8 - \sqrt{0.8^2 - 4 \cdot 0.32 \cdot c_{1L}}}{0.64} = 0.05$ Relative compression zone height for the strip

$n_{1L} := \frac{0.8 \cdot \alpha_{1L} \cdot f_{cd} \cdot b \cdot d_{top} - f_{yd} \cdot A_{s257}}{f_{pd} \cdot A_p} = 0.373$ Necessary number of tendons in the strip

The necessary number of tendons in each section, calculated as above, is presented in the following tables:

Table 9: Necessary number of tendons in the critical sections over columns.

		m_{SFL}	m^2_{SSL}	m^1_{SS}	m^2_{SSR}	m_{SFR}
$\frac{M_{Ed}}{f_{cd} b d^2}$	**Section 1**	0,0454	0,0962	0,1837	0,0908	0,0475
α		0,058	0,127	0,256	0,119	0,061
n		**0,45**	**1,65**	**3,91**	**1,52**	**0,50**
$\frac{M_{Ed}}{f_{cd} b d^2}$	**Section 3**	0,0389	0,0519	0,1178	0,0562	0,0216
α		0,050	0,067	0,157	0,072	0,027
n		**0,30**	**0,60**	**2,18**	**0,70**	**-0,09**
$\frac{M_{Ed}}{f_{cd} b d^2}$	**Section 4**	0,0335	0,1005	0,1729	0,0584	0,0335
α		0,043	0,133	0,239	0,075	0,043
n		**0,18**	**1,75**	**3,62**	**0,75**	**0,18**
$\frac{M_{Ed}}{f_{cd} b d^2}$	**Section 6**	0,0432	0,0508	0,1189	0,0713	0,0346
α		0,055	0,065	0,159	0,093	0,044
n		**0,40**	**0,57**	**2,21**	**1,05**	**0,20**
$\frac{M_{Ed}}{f_{cd} b d^2}$	**Section 7**	0,0011	0,0184	0,0875	0,0270	0,0076
α		0,001	0,023	0,115	0,034	0,009
n		**-0,55**	**-0,17**	**1,44**	**0,03**	**-0,40**
$\frac{M_{Ed}}{f_{cd} b d^2}$	**Section 9**	0,0378	0,0508	0,0940	0,0378	0,0292
α		0,048	0,065	0,124	0,048	0,037
n		**0,27**	**0,57**	**1,59**	**0,27**	**0,08**

Table 10: Necessary number of tendons in fields.

		m_{FFL}	m_{FS}	m_{FFR}
$\frac{M_{Ed}}{f_{cd} b d^2}$	**Section 2**	0,0692	0,0821	0,0644
α		0,090	0,107	0,083
n		**0,44**	**0,69**	**0,34**
$\frac{M_{Ed}}{f_{cd} b d^2}$	**Section 5**	0,0692	0,0756	0,0708
α		0,090	0,098	0,092
n		**0,44**	**0,56**	**0,47**
$\frac{M_{Ed}}{f_{cd} b d^2}$	**Section 8**	0,0451	0,0531	0,0483
α		0,058	0,068	0,062
n		**-0,02**	**0,13**	**0,04**

In order for the amount of tendons to be consistent through the sections that are aligned, a given number of tendons were chosen:

Table 11: Chosen number of tendons over columns.

		m_{SFL}	m^2_{SSL}	m^1_{SS}	m^2_{SSR}	m_{SFR}	
b_{step}	**Section 1**	500	250	500	250	500	mm
n_{chosen}		1	1	4	1	1	
n_{tot}				**8**			
b_{step}	**Section 3**	1500	750	1500	750	1500	mm
n_{chosen}		0	1	6	1	0	
n_{tot}				**8**			
b_{step}	**Section 4**	500	250	500	250	500	mm
n_{chosen}		0	2	3	1	0	
n_{tot}				**6**			
b_{step}	**Section 6**	1000	500	1000	500	1000	mm
n_{chosen}		0	0	6	0	0	
n_{tot}				**6**			
b_{step}	**Section 7**	1000	500	1000	500	1000	mm
n_{chosen}		0	1	1	1	0	
n_{tot}				**3**			
b_{step}	**Section 9**	1000	500	1000	500	1000	mm
n_{chosen}		0	1	1	1	0	
n_{tot}				**3**			

Table 12: Chosen number of tendons in fields.

		m_{FFL}	m_{FS}	m_{FFR}	
b_{step}	**Section 2**	1500	3000	1500	mm
n_{chosen}		0	8	0	
n_{tot}			**8**		
b_{step}	**Section 5**	1000	2000	1000	mm
n_{chosen}		0	6	0	
n_{tot}			**6**		
b_{step}	**Section 8**	1000	2000	1000	mm
n_{chosen}		0	3	0	
n_{tot}			**3**		

In order for the capacity in the critical sections to be sufficient, some additional conventional reinforcement was needed.

Section 1, left field column strip:

$n_{chosen1L} := 1$ Chosen number of tendons in the strip

The necessary amount of extra conventional reinforcement is then:

$$A_{sextra1L} := \max\left(0, \frac{0.8 \cdot \alpha_{1L} \cdot f_{cd} \cdot b \cdot d_{top} - n_{chosen1L} \cdot f_{pd} \cdot A_p}{f_{yd}} - A_{s257}\right) = 0\ m^2$$

Thus, the chosen amounts of both prestressed and extra conventional reinforcement for each section was chosen.

Table 13: Chosen prestressed reinforcement and extra conventional reinforcement over columns.

		m_{SFL}	m^2_{SSL}	m^1_{SS}	m^2_{SSR}	m_{SFR}	
$A_{pchosen}$	**Section 1**	150	150	600	150	150	mm^2
A_{ptot}				**1200**			mm^2
A_{sextra}		0	291	0	232	0	mm^2
A_{stot}				**523**			mm^2
$A_{pchosen}$	**Section 3**	0	150	900	150	0	mm^2
A_{ptot}				**1200**			mm^2
A_{sextra}		134	0	0	0	0	mm^2
A_{stot}				**134**			mm^2
$A_{pchosen}$	**Section 4**	0	300	450	150	0	mm^2
A_{ptot}				**900**			mm^2
A_{sextra}		79	0	277	0	79	mm^2
A_{stot}				**434**			mm^2
$A_{pchosen}$	**Section 6**	0	0	900	0	0	mm^2
A_{ptot}				**900**			mm^2
A_{sextra}		179	257	0	473	90	mm^2
A_{stot}				**998**			mm^2
$A_{pchosen}$	**Section 7**	0	150	150	150	0	mm^2
A_{ptot}				**450**			mm^2
A_{sextra}		0	0	197	0	0	mm^2
A_{stot}				**197**			mm^2
$A_{pchosen}$	**Section 9**	0	150	150	150	0	mm^2
A_{ptot}				**450**			mm^2
A_{sextra}		123	0	268	0	35	mm^2
A_{stot}				**425**			mm^2

Table 14: Chosen prestressed reinforcement and extra conventional reinforcement in fields.

		m_{FFL}	m_{FS}	m_{FFR}	
$A_{pchosen}$	**Section 2**	0	1200	0	mm^2
A_{ptot}			**1200**		mm^2
A_{sextra}		450	0	399	mm^2
A_{stot}			**849**		mm^2
$A_{pchosen}$	**Section 5**	0	900	0	mm^2
A_{ptot}			**900**		mm^2
A_{sextra}		450	0	467	mm^2
A_{stot}			**918**		mm^2
$A_{pchosen}$	**Section 8**	0	450	0	mm^2
A_{ptot}			**450**		mm^2
A_{sextra}		197	0	231	mm^2
A_{stot}			**428**		mm^2

Yield line theory

$L_y := 6.5\ m$

Moment capacity, y-direction:

$$c_{top} := \frac{m_{yield}}{f_{cd} \cdot b \cdot d_{top}^{\ 2}} \cdot m = 0.041 \qquad c_{bot} := \frac{m_{yield}}{f_{cd} \cdot b \cdot d_{bot}^{\ 2}} \cdot m = 0.047$$

$$\alpha_{top} := \frac{0.8 - \sqrt{0.8^2 - 4 \cdot 0.32 \cdot c_{top}}}{0.64} = 0.052 \qquad \alpha_{bot} := \frac{0.8 - \sqrt{0.8^2 - 4 \cdot 0.32 \cdot c_{bot}}}{0.64} = 0.06$$

$$n_{disttop} := \frac{0.8 \cdot \alpha_{top} \cdot f_{cd} \cdot b \cdot d_{top} - f_{yd} \cdot A_{s257}}{f_{pd} \cdot A_p} = 0.408$$

Necessary amount of distributed tendons in the top of cross-section, per meter

$$n_{distbot} := \frac{0.8 \cdot \alpha_{bot} \cdot f_{cd} \cdot b \cdot d_{bot} - f_{yd} \cdot A_{s383}}{f_{pd} \cdot A_p} = 0.199$$

Necessary amount of distributed tendons in the bottom of cross-section, per meter

Moment capacity, x-direction:

Strips 32A and 32C:

$$c_{top} := \frac{m_{yield}}{f_{cd} \cdot b \cdot d_{top}^{\ 2}} \cdot m = 0.041 \qquad c_{bot} := \frac{m_{yield}}{f_{cd} \cdot b \cdot d_{bot}^{\ 2}} \cdot m = 0.047$$

$$\alpha_{top} := \frac{0.8 - \sqrt{0.8^2 - 4 \cdot 0.32 \cdot c_{top}}}{0.64} = 0.052 \qquad \alpha_{bot} := \frac{0.8 - \sqrt{0.8^2 - 4 \cdot 0.32 \cdot c_{bot}}}{0.64} = 0.06$$

$$n_{disttop} := \frac{0.8 \cdot \alpha_{top} \cdot f_{cd} \cdot b \cdot d_{top} - f_{yd} \cdot A_{s257}}{f_{pd} \cdot A_p} \cdot \frac{L_y}{2\ m} = 1.326$$

Necessary number of tendons in the top of cross-section, strip 32A and 32C

$$n_{distbot} := \frac{0.8 \cdot \alpha_{bot} \cdot f_{cd} \cdot b \cdot d_{bot} - f_{yd} \cdot A_{s383}}{f_{pd} \cdot A_p} \cdot \frac{L_y}{2 \cdot m} = 0.647$$

Necessary number of tendons in the bottom of cross-section, strip 32A and 32C

Strip 32B:

$$c_{top} := \frac{m_{yield}}{f_{cd} \cdot b \cdot d_{top}^{\ 2}} \cdot m = 0.041 \qquad c_{bot} := \frac{m_{yield}}{f_{cd} \cdot b \cdot d_{bot}^{\ 2}} \cdot m = 0.047$$

$$\alpha_{top} := \frac{0.8 - \sqrt{0.8^2 - 4 \cdot 0.32 \cdot c_{top}}}{0.64} = 0.052 \qquad \alpha_{bot} := \frac{0.8 - \sqrt{0.8^2 - 4 \cdot 0.32 \cdot c_{bot}}}{0.64} = 0.06$$

$$n_{disttop} := \frac{0.8 \cdot \alpha_{top} \cdot f_{cd} \cdot b \cdot d_{top} - f_{yd} \cdot A_{s257}}{f_{pd} \cdot A_p} \cdot \frac{L_y}{m} = 2.652$$

Necessary number of tendons in the top of cross-section, strip 32B

$$n_{distbot} := \frac{0.8 \cdot \alpha_{bot} \cdot f_{cd} \cdot b \cdot d_{bot} - f_{yd} \cdot A_{s383}}{f_{pd} \cdot A_p} \cdot \frac{L_y}{m} = 1.293$$

Necessary number of tendons in the bottom of cross-section, strip 32B

Chosen reinforcement amount

In addition to the conventional reinforcement in the slab, the chosen number of prestressed tendons after yield line analysis as follows:

Table 15: Chosen number of prestressed tendons according to yield line theory.

Tendon strip	Chosen number per meter	Strip width [m]	Total area
Distributed	0,5	8	600
32A	2	3,25	300
32B	3	6,5	450
32C	2	3,25	300

Solution C - Conventional and prestressed reinforcement, reduced slab height

$d_{sbot} := h - c_{nombot} - 7\ mm = 218\ mm$ — Depth of reinforcement at bottom, assuming $\phi = 7\ mm$

$d_{stop} := h - c_{nomtop} - 7\ mm = 233\ mm$ — Depth of reinforcement at top, assuming $\phi = 7\ mm$

$d_{pbot} := d_{sbot} - 10\ mm = 208\ mm$ — Depth of tendons at bottom

$d_{ptop} := d_{stop} - 10\ mm = 223\ mm$ — Depth of tendons at top

$A_{sminred} := 0.26 \cdot \frac{3.2}{500} \cdot b \cdot d_{sbot} = 362.752\ mm^2$ — Minimum reinforcement amount for slimmer cross-section according to EC2.NA.9.2.1.1(1)

$A_{sred} := 257\ mm^2$ — Conventional reinforcement amount, both top and bottom, in slimmer cross-section

EFM

Necessary number of tendons

Section 1, left field column strip:

$M_{Ed1L} := 36.52\ kN \cdot m$ — Design moment in the strip

$c_{1L} := \frac{M_{Ed1L}}{f_{cd} \cdot b \cdot d_{ptop}^2} = 0.037$ — The constant for the strip

$\alpha_{1L} := \frac{0.8 - \sqrt{0.8^2 - 4 \cdot 0.32 \cdot c_{1L}}}{0.64} = 0.047$ — Relative compression zone height for the strip

$n_{1L} := \frac{0.8 \cdot \alpha_{1L} \cdot f_{cd} \cdot b \cdot d_{ptop} - f_{yd} \cdot A_{sred}}{f_{pd} \cdot A_p} = 0.282$ — Necessary number of tendons in the strip

The necessary number of tendons, calculated as shown above, is presented below:

Table 16: Necessary number of tendons over columns.

		m_{SFL}	m_{SSL}^{2}	m_{SS}^{1}	m_{SSR}^{2}	m_{SFR}
$\frac{M_{Ed}}{f_{cd}bd^2}$	**Section 1**	0,0841	0,1781	0,3403	0,1681	0,0881
α		0,110	0,247	0,544	0,232	0,115
n		**0,75**	**2,39**	**5,95**	**2,21**	**0,81**
$\frac{M_{Ed}}{f_{cd}bd^2}$	**Section 3**	0,0721	0,0961	0,2182	0,1041	0,0400
α		0,094	0,126	0,312	0,138	0,051
n		**0,55**	**0,95**	**3,17**	**1,08**	**0,04**
$\frac{M_{Ed}}{f_{cd}bd^2}$	**Section 4**	0,0621	0,1862	0,3203	0,1081	0,0621
α		0,080	0,260	0,501	0,143	0,080
n		**0,39**	**2,55**	**5,44**	**1,15**	**0,39**
$\frac{M_{Ed}}{f_{cd}bd^2}$	**Section 6**	0,0801	0,0941	0,2202	0,1321	0,0641
α		0,104	0,124	0,315	0,178	0,083
n		**0,68**	**0,91**	**3,21**	**1,56**	**0,42**
$\frac{M_{Ed}}{f_{cd}bd^2}$	**Section 7**	0,0020	0,0340	0,1621	0,0500	0,0140
α		0,003	0,043	0,222	0,064	0,018
n		**-0,54**	**-0,05**	**2,10**	**0,20**	**-0,36**
$\frac{M_{Ed}}{f_{cd}bd^2}$	**Section 9**	0,0701	0,0941	0,1741	0,0701	0,0540
α		0,091	0,124	0,241	0,091	0,069
n		**0,52**	**0,91**	**2,32**	**0,52**	**0,26**

Table 17: Necessary number of tendons in fields.

		m_{FFL}	m_{FS}	m_{FFR}
$\frac{M_{Ed}}{f_{cd}bd^2}$	**Section 2**	0,1066	0,1264	0,0991
α		0,141	0,170	0,131
n		**0,95**	**1,26**	**0,84**
$\frac{M_{Ed}}{f_{cd}bd^2}$	**Section 5**	0,1066	0,1165	0,1091
α		0,141	0,155	0,145
n		**0,95**	**1,10**	**0,99**
$\frac{M_{Ed}}{f_{cd}bd^2}$	**Section 8**	0,0694	0,0818	0,0744
α		0,090	0,107	0,097
n		**0,40**	**0,58**	**0,47**

Chosen number of tendons

The chosen number of tendons is presented below.

Table 18: Chosen number of tendons over columns.

		m_{SFL}	m^2_{SSL}	m^1_{SS}	m^2_{SSR}	m_{SFR}	
b_{step}	**Section 1**	500	250	500	250	500	mm
n_{chosen}		1	2	6	2	1	
n_{tot}		**12**					
b_{step}	**Section 3**	1500	750	1500	750	1500	mm
n_{chosen}		0	1	10	1	0	
n_{tot}		**12**					
b_{step}	**Section 4**	500	250	500	250	500	mm
n_{chosen}		1	2	5	1	1	
n_{tot}		**10**					
b_{step}	**Section 6**	1000	500	1000	500	1000	mm
n_{chosen}		0	1	8	1	0	
n_{tot}		**10**					
b_{step}	**Section 7**	1000	500	1000	500	1000	mm
n_{chosen}		0	1	2	1	0	
n_{tot}		**4**					
b_{step}	**Section 9**	1000	500	1000	500	1000	mm
n_{chosen}		0	1	2	1	0	
n_{tot}		**4**					

Table 19: Chosen number of tendons in fields.

		m_{FFL}	m_{FS}	m_{FFR}	
b_{step}	**Section 2**	1500	3000	1500	mm
n_{chosen}		0	12	0	
n_{tot}		**12**			
b_{step}	**Section 5**	1000	2000	1000	mm
n_{chosen}		0	10	0	
n_{tot}		**10**			
b_{step}	**Section 8**	1000	2000	1000	mm
n_{chosen}		0	4	0	
n_{tot}		**4**			

Area of chosen prestressing tendons and extra conventional reinforcement

Section 1, left field column strip:

$b_{strip} := 500\ mm$ Width of strip

$n_{1L} := 1$ Chosen number of tendons in strip

$A_{p1L} := n_{1L} \cdot A_p = 150\ mm^2$ Area of tendons in strip

The necessary area of extra conventional reinforcement is:

$$A_{sextra1L} := \max\left(0, \frac{0.8 \cdot \alpha_{1L} \cdot f_{cd} \cdot b \cdot d_{ptop} - A_{p1L} \cdot f_{pd}}{f_{yd}} - A_{sred}\right) = 0\ m^2$$

The total amount of post-tensioned tendons and additional conventional reinforcement, calculated as shown above, is presented below.

Table 20: Reinforcement amount over columns.

		m_{SFL}	m^2_{SSL}	m^1_{SS}	m^2_{SSR}	m_{SFR}	
$A_{pchosen}$	Section 1	150	300	900	300	150	mm^2
A_{ptot}				**1800**			mm^2
A_{sextra}		0	178	0	94	0	mm^2
A_{stot}				**272**			mm^2
$A_{pchosen}$	Section 3	0	150	1500	150	0	mm^2
A_{ptot}				**1800**			mm^2
A_{sextra}		248	0	0	37	0	mm^2
A_{stot}				**285**			mm^2
$A_{pchosen}$	Section 4	150	300	750	150	150	mm^2
A_{ptot}				**1500**			mm^2
A_{sextra}		0	245	196	67	0	mm^2
A_{stot}				**509**			mm^2
$A_{pchosen}$	Section 6	0	150	1200	150	0	mm^2
A_{ptot}				**1500**			mm^2
A_{sextra}		307	0	0	253	190	mm^2
A_{stot}				**751**			mm^2
$A_{pchosen}$	Section 7	0	150	300	150	0	mm^2
A_{ptot}				**600**			mm^2
A_{sextra}		0	0	45	0	0	mm^2
A_{stot}				**45**			mm^2
$A_{pchosen}$	Section 9	0	150	300	150	0	mm^2
A_{ptot}				**600**			mm^2
A_{sextra}		234	0	144	0	118	mm^2
A_{stot}				**496**			mm^2

Table 21: Reinforcement amount in fields.

		m_{FFL}	m_{FS}	m_{FFR}	
$A_{pchosen}$	Section 2	0	1800	0	mm^2
A_{ptot}			**1800**		mm^2
A_{sextra}		428	0	378	mm^2
A_{stot}			**806**		mm^2
$A_{pchosen}$	Section 5	0	1500	0	mm^2
A_{ptot}			**1500**		mm^2
A_{sextra}		428	0	445	mm^2
A_{stot}			**874**		mm^2
$A_{pchosen}$	Section 8	0	600	0	mm^2
A_{ptot}			**600**		mm^2
A_{sextra}		180	0	212	mm^2
A_{stot}			**392**		mm^2

Yield line theory

Moment capacity, y-direction:

$$c_{top} := \frac{m_{yield}}{f_{cd} \cdot b \cdot d_{ptop}^{\ 2}} \cdot \boldsymbol{m} = 0.044 \qquad c_{bot} := \frac{m_{yield}}{f_{cd} \cdot b \cdot d_{pbot}^{\ 2}} \cdot \boldsymbol{m} = 0.051$$

$$\alpha_{top} := \frac{0.8 - \sqrt{0.8^2 - 4 \cdot 0.32 \cdot c_{top}}}{0.64} = 0.056 \qquad \alpha_{bot} := \frac{0.8 - \sqrt{0.8^2 - 4 \cdot 0.32 \cdot c_{bot}}}{0.64} = 0.065$$

$$n_{disttop} := \frac{0.8 \cdot \alpha_{top} \cdot f_{cd} \cdot b \cdot d_{ptop} - f_{yd} \cdot A_{sred}}{f_{pd} \cdot A_p} = 0.449$$

Necessary amount of distributed tendons in the top of cross-section, per meter

$$n_{distbot} := \frac{0.8 \cdot \alpha_{bot} \cdot f_{cd} \cdot b \cdot d_{pbot} - f_{yd} \cdot A_{sred}}{f_{pd} \cdot A_p} = 0.527$$

Necessary amount of distributed tendons in the bottom of cross-section, per meter

Moment capacity, x-direction:

Strips 32A and 32C:

$$c_{top} := \frac{m_{yield}}{f_{cd} \cdot b \cdot d_{ptop}^{\ 2}} \cdot \boldsymbol{m} = 0.044 \qquad c_{bot} := \frac{m_{yield}}{f_{cd} \cdot b \cdot d_{pbot}^{\ 2}} \cdot \boldsymbol{m} = 0.051$$

$$\alpha_{top} := \frac{0.8 - \sqrt{0.8^2 - 4 \cdot 0.32 \cdot c_{top}}}{0.64} = 0.056 \qquad \alpha_{bot} := \frac{0.8 - \sqrt{0.8^2 - 4 \cdot 0.32 \cdot c_{bot}}}{0.64} = 0.065$$

$$n_{disttop} := \frac{0.8 \cdot \alpha_{top} \cdot f_{cd} \cdot b \cdot d_{ptop} - f_{yd} \cdot A_{sred}}{f_{pd} \cdot A_p} \cdot \frac{L_y}{2\ \boldsymbol{m}} = 1.46$$

Necessary number of tendons in the top of cross-section, strip 32A and 32C

$$n_{distbot} := \frac{0.8 \cdot \alpha_{bot} \cdot f_{cd} \cdot b \cdot d_{pbot} - f_{yd} \cdot A_{sred}}{f_{pd} \cdot A_p} \cdot \frac{L_y}{2 \cdot \boldsymbol{m}} = 1.712$$

Necessary number of tendons in the bottom of cross-section, strip 32A and 32C

Strip 32B:

$$c_{top} := \frac{m_{yield}}{f_{cd} \cdot b \cdot d_{ptop}^{\ 2}} \cdot \boldsymbol{m} = 0.044 \qquad c_{bot} := \frac{m_{yield}}{f_{cd} \cdot b \cdot d_{pbot}^{\ 2}} \cdot \boldsymbol{m} = 0.051$$

$$\alpha_{top} := \frac{0.8 - \sqrt{0.8^2 - 4 \cdot 0.32 \cdot c_{top}}}{0.64} = 0.056 \qquad \alpha_{bot} := \frac{0.8 - \sqrt{0.8^2 - 4 \cdot 0.32 \cdot c_{bot}}}{0.64} = 0.065$$

$$n_{disttop} := \frac{0.8 \cdot \alpha_{top} \cdot f_{cd} \cdot b \cdot d_{ptop} - f_{yd} \cdot A_{sred}}{f_{pd} \cdot A_p} \cdot \frac{L_y}{m} = 2.921$$

Necessary number of tendons in the top of cross-section, strip 32B

$$n_{distbot} := \frac{0.8 \cdot \alpha_{bot} \cdot f_{cd} \cdot b \cdot d_{pbot} - f_{yd} \cdot A_{sred}}{f_{pd} \cdot A_p} \cdot \frac{L_y}{m} = 3.424$$

Necessary number of tendons in the bottom of cross-section, strip 32B

Chosen reinforcement amount

In addition to the conventional reinforcement in the slab, the chosen number of prestressed tendons after yield line analysis as follows:

Table 22: Chosen amount of tendons after yield line theory analysis.

Tendon strip	Chosen number per meter	Strip width [m]	Total area
Distributed	1	8	1200
32A	3	3,25	450
32B	6	6,5	900
32C	3	3,25	450

Solution D - Conventional, prestressed reinforcement and fibers

For n=0:

$f_{Ftud} := 1.2 \ \frac{N}{mm^2}$ — Steel fiber strength in ULS

$n := 0$ — Number of tendons per meter

$x_f := 30.6 \ mm$ — Compression zone in fields, obtained from equilibrium in longitudinal forces

$x_c := 26.9 \ mm$ — Compression zone over columns

$S_{ff} := (h - x_f) \cdot b \cdot f_{Ftud} = 293.28 \ kN$ — Force contributed by fiber reinforcement in fields

$S_{fc} := (h - x_c) \cdot b \cdot f_{Ftud} = 297.72 \ kN$ — Force contributed by fiber reinforcement in columns

$S_p := n \cdot P_{ULS} = [0] \ kN$ — Force contributed by post-tensioned reinforcement

$S_{sf} := f_{yk} \cdot A_{s383} = 191.5 \ kN$ — Force contributed by conventional reinforcement in fields

$S_{sc} := f_{yk} \cdot A_{s257} = 128.5 \ kN$ — Force contributed by conventional reinforcement over columns

Moment capacity in fields and columns:

$$M_{Rdf} := S_{ff} \cdot (0.5 \ h + 0.1 \ x_f) + S_p \cdot (d_{pbot} - 0.4 \ x_f) + S_{sf} \cdot (d_{sbot} - 0.4 \ x_f) = [80.626] \ kN \cdot m$$

$$M_{Rdc} := S_{fc} \cdot (0.5 \ h + 0.1 \ x_c) + S_p \cdot (d_{ptop} - 0.4 \ x_c) + S_{sc} \cdot (d_{stop} - 0.4 \ x_c) = [70.295] \ kN \cdot m$$

For n=1:

$n := 1$ — Number of tendons per meter

$x_f := 40.5\ mm$ — Compression zone in fields, obtained from equilibrium in longitudinal forces

$x_c := 36.9\ mm$ — Compression zone over columns

$S_{ff} := (h - x_f) \cdot b \cdot f_{Ftud} = 281.4\ kN$ — Force contributed by fiber reinforcement in fields

$S_{fc} := (h - x_c) \cdot b \cdot f_{Ftud} = 285.72\ kN$ — Force contributed by fiber reinforcement in columns

$S_p := n \cdot P_{ULS} = [170.311]\ kN$ — Force contributed by post-tensioned reinforcement

$S_{sf} := f_{yk} \cdot A_{s383} = 191.5\ kN$ — Force contributed by conventional reinforcement in fields

$S_{sc} := f_{yk} \cdot A_{s257} = 128.5\ kN$ — Force contributed by conventional reinforcement over columns

Moment capacity in fields and columns:

$$M_{Rdf} := S_{ff} \cdot (0.5\ h + 0.1\ x_f) + S_p \cdot (d_{pbot} - 0.4\ x_f) + S_{sf} \cdot (d_{sbot} - 0.4\ x_f) = [111.143]\ kN \cdot m$$

$$M_{Rdc} := S_{fc} \cdot (0.5\ h + 0.1\ x_c) + S_p \cdot (d_{ptop} - 0.4\ x_c) + S_{sc} \cdot (d_{stop} - 0.4\ x_c) = [103.85]\ kN \cdot m$$

For n=2:

$n := 2$ Number of tendons per meter

$x_f := 50.5\ mm$ Compression zone in fields, obtained from equilibrium in longitudinal forces

$x_c := 46.8\ mm$ Compression zone over columns

$S_{ff} := (h - x_f) \cdot b \cdot f_{Ftud} = 269.4\ kN$ Force contributed by fiber reinforcement in fields

$S_{fc} := (h - x_c) \cdot b \cdot f_{Ftud} = 273.84\ kN$ Force contributed by fiber reinforcement in columns

$S_p := n \cdot P_{ULS} = [340.622]\ kN$ Force contributed by post-tensioned reinforcement

$S_{sf} := f_{yk} \cdot A_{s383} = 191.5\ kN$ Force contributed by conventional reinforcement in fields

$S_{sc} := f_{yk} \cdot A_{s257} = 128.5\ kN$ Force contributed by conventional reinforcement over columns

Moment capacity in fields and columns:

$$M_{Rdf} := S_{ff} \cdot (0.5\ h + 0.1\ x_f) + S_p \cdot (d_{pbot} - 0.4\ x_f) + S_{sf} \cdot (d_{sbot} - 0.4\ x_f) = [140.25]\ kN \cdot m$$

$$M_{Rdc} := S_{fc} \cdot (0.5\ h + 0.1\ x_c) + S_p \cdot (d_{ptop} - 0.4\ x_c) + S_{sc} \cdot (d_{stop} - 0.4\ x_c) = [136.052]\ kN \cdot m$$

For n=3:

$n := 3$ Number of tendons per meter

$x_f := 60.5\ mm$ Compression zone in fields, obtained from equilibrium in longitudinal forces

$x_c := 56.8\ mm$ Compression zone over columns

$S_{ff} := (h - x_f) \cdot b \cdot f_{Ftud} = 257.4\ kN$ Force contributed by fiber reinforcement in fields

$S_{fc} := (h - x_c) \cdot b \cdot f_{Ftud} = 261.84\ kN$ Force contributed by fiber reinforcement in columns

$S_p := n \cdot P_{ULS} = [510.933]\ kN$ Force contributed by post-tensioned reinforcement

$S_{sf} := f_{yk} \cdot A_{s383} = 191.5\ kN$ Force contributed by conventional reinforcement in fields

$S_{sc} := f_{yk} \cdot A_{s257} = 128.5\ kN$ Force contributed by conventional reinforcement over columns

Moment capacity in fields and columns:

$$M_{Rdf} := S_{ff} \cdot (0.5\ h + 0.1\ x_f) + S_p \cdot (d_{pbot} - 0.4\ x_f) + S_{sf} \cdot (d_{sbot} - 0.4\ x_f) = [167.972]\ kN \cdot m$$

$$M_{Rdc} := S_{fc} \cdot (0.5\ h + 0.1\ x_c) + S_p \cdot (d_{ptop} - 0.4\ x_c) + S_{sc} \cdot (d_{stop} - 0.4\ x_c) = [166.841]\ kN \cdot m$$

For n=4:

$n := 4$ — Number of tendons per meter

$x_f := 70.5\ mm$ — Compression zone in fields, obtained from equilibrium in longitudinal forces

$x_c := 66.8\ mm$ — Compression zone over columns

$S_{ff} := (h - x_f) \cdot b \cdot f_{Ftud} = 245.4\ kN$ — Force contributed by fiber reinforcement in fields

$S_{fc} := (h - x_c) \cdot b \cdot f_{Ftud} = 249.84\ kN$ — Force contributed by fiber reinforcement in columns

$S_p := n \cdot P_{ULS} = [681.244]\ kN$ — Force contributed by post-tensioned reinforcement

$S_{sf} := f_{yk} \cdot A_{s383} = 191.5\ kN$ — Force contributed by conventional reinforcement in fields

$S_{sc} := f_{yk} \cdot A_{s257} = 128.5\ kN$ — Force contributed by conventional reinforcement over columns

Moment capacity in fields and columns:

$$M_{Rdf} := S_{ff} \cdot (0.5\ h + 0.1\ x_f) + S_p \cdot (d_{pbot} - 0.4\ x_f) + S_{sf} \cdot (d_{sbot} - 0.4\ x_f) = [194.307]\ kN \cdot m$$

$$M_{Rdc} := S_{fc} \cdot (0.5\ h + 0.1\ x_c) + S_p \cdot (d_{ptop} - 0.4\ x_c) + S_{sc} \cdot (d_{stop} - 0.4\ x_c) = [196.243]\ kN \cdot m$$

Solution E - Prestressed reinforcement and fibers

For n=0:

$n := 0$ — Number of tendons

$x := 19.3\ mm$ — Compression zone

$S_f := (h - x) \cdot b \cdot f_{Ftud} = 306.84\ kN$ — Force contributed by fiber reinforcement

$S_p := n \cdot P_{ULS} = [0]\ kN$ — Force contributed by post-tensioned reinforcement

Moment capacity in fields and columns:

$M_{Rdf} := S_f \cdot (0.5\ h + 0.1\ x) + S_p \cdot (d_{pbot} - 0.4\ x) = [42.783]\ kN \cdot m$

$M_{Rdc} := S_f \cdot (0.5\ h + 0.1\ x) + S_p \cdot (d_{ptop} - 0.4\ x) = [42.783]\ kN \cdot m$

For n=1:

$n := 1$ — Number of tendons

$x := 29.3\ mm$ — Compression zone

$S_f := (h - x) \cdot b \cdot f_{Ftud} = 294.84\ kN$ — Force contributed by fiber reinforcement

$S_p := n \cdot P_{ULS} = [170.311]\ kN$ — Force contributed by post-tensioned reinforcement

Moment capacity in fields and columns:

$M_{Rdf} := S_f \cdot (0.5\ h + 0.1\ x) + S_p \cdot (d_{pbot} - 0.4\ x) = [74.833]\ kN \cdot m$

$M_{Rdc} := S_f \cdot (0.5\ h + 0.1\ x) + S_p \cdot (d_{ptop} - 0.4\ x) = [77.388]\ kN \cdot m$

For n=2:

$n := 2$ Number of tendons

$x := 39.3\ mm$ Compression zone

$S_f := (h - x) \cdot b \cdot f_{Ftud} = 282.84\ kN$ Force contributed by fiber reinforcement

$S_p := n \cdot P_{ULS} = [340.622]\ kN$ Force contributed by post-tensioned reinforcement

Moment capacity in fields and columns:

$M_{Rdf} := S_f \cdot (0.5\ h + 0.1\ x) + S_p \cdot (d_{pbot} - 0.4\ x) = [105.497]\ kN \cdot m$

$M_{Rdc} := S_f \cdot (0.5\ h + 0.1\ x) + S_p \cdot (d_{ptop} - 0.4\ x) = [110.606]\ kN \cdot m$

For n=3:

$n := 3$ Number of tendons

$x := 49.3\ mm$ Compression zone

$S_f := (h - x) \cdot b \cdot f_{Ftud} = 270.84\ kN$ Force contributed by fiber reinforcement

$S_p := n \cdot P_{ULS} = [510.933]\ kN$ Force contributed by post-tensioned reinforcement

Moment capacity in fields and columns:

$M_{Rdf} := S_f \cdot (0.5\ h + 0.1\ x) + S_p \cdot (d_{pbot} - 0.4\ x) = [134.774]\ kN \cdot m$

$M_{Rdc} := S_f \cdot (0.5\ h + 0.1\ x) + S_p \cdot (d_{ptop} - 0.4\ x) = [142.438]\ kN \cdot m$

For n=4:

$n := 4$ Number of tendons

$x := 59.3\ mm$ Compression zone

$S_f := (h - x) \cdot b \cdot f_{Ftud} = 258.84\ kN$ Force contributed by fiber reinforcement

$S_p := n \cdot P_{ULS} = [681.244]\ kN$ Force contributed by post-tensioned reinforcement

Moment capacity in fields and columns:

$M_{Rdf} := S_f \cdot (0.5\ h + 0.1\ x) + S_p \cdot (d_{pbot} - 0.4\ x) = [162.665]\ kN \cdot m$

$M_{Rdc} := S_f \cdot (0.5\ h + 0.1\ x) + S_p \cdot (d_{ptop} - 0.4\ x) = [172.884]\ kN \cdot m$

For n=5:

$n := 5$ Number of tendons

$x := 69.2\ mm$ Compression zone

$S_f := (h - x) \cdot b \cdot f_{Ftud} = 246.96\ kN$ Force contributed by fiber reinforcement

$S_p := n \cdot P_{ULS} = [851.555]\ kN$ Force contributed by post-tensioned reinforcement

Moment capacity in fields and columns:

$$M_{Rdf} := S_f \cdot (0.5\ h + 0.1\ x) + S_p \cdot (d_{pbot} - 0.4\ x) = [189.218]\ \mathbf{kN \cdot m}$$

$$M_{Rdc} := S_f \cdot (0.5\ h + 0.1\ x) + S_p \cdot (d_{ptop} - 0.4\ x) = [201.992]\ \mathbf{kN \cdot m}$$

Solution F - Fiber reinforcement

$x := 19.3\ mm$ Compression zone

$S_f := (h - x) \cdot b \cdot f_{Ftud} = 306.84\ kN$ Force contributed by fiber reinforcement

Force contributed by fiber reinforcement in columns

Moment capacity in fields and columns:

$M_{Rd} := S_f \cdot (0.5\ h + 0.1\ x) = 42.783\ kN \cdot m$

Yield line - all fiber solutions

$m_{yield} = 43.518\ kN \cdot \frac{m}{m}$

There is (almost) no need for more reinforcement than fiber according to yield line solution

Punching shear

Geometry and data, current Eurocode 2

$c_{int} := 700\ mm$ Side length of loaded area at internal pile

$c_{edge} := 600\ mm$ Side length of loaded area at edge pile

$V_{Edint} := 387\ kN$ Shear force on internal pile

$V_{Ededge} := 203\ kN$ Shear force on edge pile

$V_{EdintC} := \frac{15}{17.25} \cdot V_{Edint} = 336.522\ kN$ Reduced shear force for reduced slab height

$V_{EdedgeC} := \frac{15}{17.25} \cdot V_{Ededge} = 176.522\ kN$ Reduced shear force on edge pile

$\beta_{internal} := 1.15$

$\beta_{edge} := 1.4$

Coefficient handling the transfer of bending moment at column-slab connections (NA.6.4.3(6))

$C_{Rdc} := \frac{0.18}{1.5} = 0.12$

$f_{ck} := 35\ MPa$ Characteristic concrete strength

$f_{cd} := 0.85 \cdot \frac{f_{ck}}{1.5} = 19.833\ MPa$ Design concrete strength

$v_{Rdmax} := 0.4 \cdot 0.6 \cdot \left(1 - \frac{f_{ck}}{250\ MPa}\right) \cdot f_{cd} = 4.094\ MPa$ Maximum allowable shear stress at column face, NA.6.4.5

$P_{ULS} := 170.311\ kN$ Design post-tensioning force

$s_r := 100\ mm$ Assumed link shear link spacing

$u_{0internal} := 4 \cdot c_{int} = \left(2.8 \cdot 10^3\right)\ mm$ Length of area adjacent to internal pile-head

$b := 1000\ mm$ Width of cross-section

$h := 275\ mm$ Height of cross-section

$h_{red} := 200\ mm$ Height of reduced cross-section

$k_1 := 0.1$

$f_{yd} := \frac{500 \cdot MPa}{1.15} = 434.783\ MPa$ Design yield strength of reinforcing steel

Geometry and data, new Eurocode 2

$D_{lower} := 22\ mm$ Assumed value

$d_{dg} := 16\ mm + D_{lower} = 38\ mm$ Size parameter describing failure zone roughness

$f_{ywd} := f_{yd} = 434.783\ MPa$ Design yield strength of shear reinforcement

$\mu_{pinternal} := 8$

$\mu_{pedge} := 4$ Coefficient regarding shear force gradient and bending moment within control perimeter

$\gamma_V := 1.4$ Partial factor for shear design

$b_{0int} := 4 \cdot c_{int} = \left(2.8 \cdot 10^3\right)\ mm$

$b_{0edge} := 2 \cdot c_{edge} + c_{int} = \left(1.9 \cdot 10^3\right)\ mm$ Length of control perimeters at pile heads

Fiber reinforcement

$f_{Ftud} = 1.2\ MPa$ Characteristic and design residual flexural tensile strength

$f_{Ftuk} := f_{Ftud} \cdot 1.5 = 1.8\ MPa$

$d_{vp} := 216\ mm$ Mean reinforcement depth

Solution A - Conventional reinforcement

EC2:2004

$d_{topA} := 232\ mm$ Reinforcement depth over piles

$u_{1edge} := 2 \cdot \pi \cdot d_{topA} + 2 \cdot c_{edge} + c_{int} = \left(3.358 \cdot 10^3\right)\ mm$

$u_{1internal} := 4 \cdot \pi \cdot d_{topA} + 4 \cdot c_{int} = \left(5.715 \cdot 10^3\right)\ mm$ Control section lengths

$k_A := 1 + \sqrt{\frac{200\ mm}{d_{topA}}} = 1.928$

$v_{minA} := 0.035 \cdot k_A^{\frac{3}{2}} \cdot \sqrt{f_{ck} \cdot MPa} = 0.555\ MPa$ Minimum concrete shear capacity (NA.6.3N)

$u_{0edge} := min\left(c_{int} + 3 \cdot d_{topA}, c_{int} + 2 \cdot c_{edge}\right) = \left(1.396 \cdot 10^3\right)\ mm$ Length of area adjacent to corner pile-head

$f_{ywdefA} := min\left(250 \cdot MPa + \frac{0.25}{mm} \cdot d_{topA} \cdot MPa, f_{yd}\right) = 308\ MPa$ Effective design strength of punching shear reinforcement

$b_s := c_{int} + 6 \cdot d_{topA} = 2.092\ m$ Extended width

$A_{cA} := h \cdot b_s = 0.575\ m^2$ Concrete area

Internal pile:

$v_{Ed0A} := \frac{\beta_{internal} \cdot V_{Edint}}{u_{0internal} \cdot d_{topA}} = 0.685\ MPa$ Maximum shear stress at pile-head. Eq.(6.38)

$v_{Ed1A} := \frac{\beta_{internal} \cdot V_{Edint}}{u_{1internal} \cdot d_{topA}} = 0.336\ MPa$ Maximum shear stress at control section. Eq.(6.38)

$A_{sintA} := 1994\ mm^2$ Bonded tension steel area in the area around the pile-head plus 3d on each side

$\rho_{lintA} := \frac{A_{sintA}}{\left(c_{int} + 6 \cdot d_{topA}\right) \cdot d_{topA}} = 0.004$

The concrete shear capacity at the inner pile is (6.47):

$$v_{RdcintA} := \max\left(C_{Rdc} \cdot k_A \cdot \left(100 \cdot \rho_{lintA} \cdot f_{ck}\right)^{\frac{1}{3}} \cdot MPa^{\frac{2}{3}}, v_{minA}\right) = 0.563\ MPa$$

The utilisation factors are: $\frac{v_{Ed1A}}{v_{RdcintA}} = 0.596$ $\frac{v_{Ed0A}}{v_{Rdmax}} = 0.167$

The necessary amount of shear reinforcement is then (6.52):

$$A_{swintA} := \max\left(\frac{\left(v_{Ed1A} - 0.75 \cdot v_{RdcintA}\right) \cdot u_{1internal} \cdot s_r}{1.5 \cdot f_{ywdefA}}, 0\right) = 0\ mm^2$$

Edge pile:

$v_{Ed0A} := \frac{\beta_{edge} \cdot V_{Ededge}}{u_{0edge} \cdot d_{topA}} = 0.878\ MPa$ Maximum shear stress at pile-head. Eq.(6.38)

$v_{Ed1A} := \frac{\beta_{edge} \cdot V_{Ededge}}{u_{1edge} \cdot d_{topA}} = 0.365\ MPa$ Maximum shear stress at control section. Eq.(6.38)

$A_{sedgeA} := 386\ mm^2$ Bonded tension steel area in the area around the pile-head plus 3d on each side

$$\rho_{ledgeA} := \frac{A_{sedgeA}}{\left(c_{edge} + 6 \cdot d_{topA}\right) \cdot d_{topA}} = 8.352 \cdot 10^{-4}$$

The concrete shear capacity at the corner pile is (6.47):

$$v_{RdcedgeA} := \max\left(C_{Rdc} \cdot k_A \cdot \left(100 \cdot \rho_{ledgeA} \cdot f_{ck}\right)^{\frac{1}{3}} \cdot MPa^{\frac{2}{3}}, v_{minA}\right) = 0.555\ MPa$$

The utilisation factors area: $\frac{v_{Ed1A}}{v_{RdcedgeA}} = 0.658$ $\frac{v_{Ed0A}}{v_{Rdmax}} = 0.214$

The necessary amount of shear reinforcement is then (6.52):

$$A_{swedgeA} := \max\left(\frac{\left(v_{Ed1A} - 0.75 \cdot v_{RdcedgeA}\right) \cdot u_{1edge} \cdot s_r}{1.5 \cdot f_{ywdefA}}, 0\right) = 0\ mm^2$$

EC2:2021

$b_{05edge} := \frac{\pi \cdot d_{topA}}{2} + 2 \cdot c_{edge} + c_{int} = \left(2.264 \cdot 10^3\right)\ mm$ Length of control perimeter for edge pile

$b_{05internal} := \pi \cdot d_{topA} + 4 \cdot c_{int} = \left(3.529 \cdot 10^3\right)\ mm$ Length of control perimeter for internal piles

$\tau_{Rdcmin} := \frac{11 \cdot MPa}{\gamma_V} \cdot \sqrt{\frac{f_{ck} \cdot d_{dg}}{f_{yd} \cdot d_{topA}}} = 0.902\ MPa$ Minimum shear stress resistance

$\tau_{Ededge} := \frac{\beta_{edge} \cdot V_{Ededge}}{b_{05edge} \cdot d_{topA}} = 0.541\ MPa$ Design shear stress acting on edge pile

$\tau_{Edint} := \frac{\beta_{internal} \cdot V_{Edint}}{b_{05internal} \cdot d_{topA}} = 0.544\ MPa$ Design shear stress acting on internal pile

The first check according to Eq.(8.71):

$\frac{\tau_{Ededge}}{\tau_{Rdcmin}} = 0.6$ $\frac{\tau_{Edint}}{\tau_{Rdcmin}} = 0.603$

Check ok, shear resistance of concrete cross-section nevertheless calculated for the purpose of comparison

$k_{pbint} := 3.6 \cdot \sqrt{1 - \frac{b_{0int}}{b_{05internal}}} = 1.636$ $k_{pbedge} := 3.6 \cdot \sqrt{1 - \frac{b_{0edge}}{b_{05edge}}} = 1.444$

$\rho_{lintA} = 0.004$ $\rho_{ledgeA} = 8.352 \cdot 10^{-4}$

$\tau_{Rdcint} := \frac{0.6 \cdot k_{pbint}}{\gamma_V} \cdot \left(100 \cdot \rho_{lintA} \cdot f_{ck} \cdot \frac{d_{dg}}{d_{topA}}\right)^{\left(\frac{1}{3}\right)} \cdot MPa^{\left(\frac{2}{3}\right)} = 0.933\ MPa$

$\tau_{Rdcedge} := \frac{0.6 \cdot k_{pbedge}}{\gamma_V} \cdot \left(100 \cdot \rho_{ledgeA} \cdot f_{ck} \cdot \frac{d_{dg}}{d_{topA}}\right)^{\left(\frac{1}{3}\right)} \cdot MPa^{\left(\frac{2}{3}\right)} = 0.484\ MPa$

Solution B - Conventional and post-tensioned reinforcement

EC2:2004

$d_{topB} := 216\ mm$ Reinforcement depth over piles

$u_{1edge} := 2 \cdot \pi \cdot d_{topB} + 2 \cdot c_{edge} + c_{int} = (3.257 \cdot 10^3)\ mm$

$u_{1internal} := 4 \cdot \pi \cdot d_{topB} + 4 \cdot c_{int} = (5.514 \cdot 10^3)\ mm$ Control section lengths

$k_B := 1 + \sqrt{\frac{200\ mm}{d_{topB}}} = 1.962$

$v_{minB} := 0.035 \cdot k_B^{\frac{3}{2}} \cdot \sqrt{f_{ck} \cdot MPa} = 0.569\ MPa$ Minimum concrete shear capacity (NA.6.3N)

$u_{0edge} := min\left(c_{int} + 3 \cdot d_{topB}, c_{int} + 2 \cdot c_{edge}\right) = (1.348 \cdot 10^3)\ mm$ Length of area adjacent to corner pile-head

$f_{ywdefB} := min\left(250 \cdot MPa + \frac{0.25}{mm} \cdot d_{topB} \cdot MPa, f_{yd}\right) = 304\ MPa$ Effective design strength of punching shear reinforcement

$b_s := c_{int} + 6 \cdot d_{topB} = 1.996\ m$ Extended width

$A_{cB} := h \cdot b_s = 0.549\ m^2$ Concrete area

Internal pile:

$v_{Ed0B} := \frac{\beta_{internal} \cdot V_{Edint}}{u_{0internal} \cdot d_{topB}} = 0.736\ MPa$ Maximum shear stress at pile-head. Eq.(6.38)

$v_{Ed1B} := \frac{\beta_{internal} \cdot V_{Edint}}{u_{1internal} \cdot d_{topB}} = 0.374\ MPa$ Maximum shear stress at control section. Eq.(6.38)

$A_{sintB} := 750\ mm^2$ Bonded tension steel area in the area around the pile-head plus 3d on each side

$\rho_{lintB} := \frac{A_{sintB}}{\left(c_{int} + 6 \cdot d_{topB}\right) \cdot d_{topB}} = 0.002$

$N_{xB} := 6 \cdot P_{ULS} = \left(1.022 \cdot 10^3\right)\ kN$

$N_{yB} := 2 \cdot P_{ULS} = 340.622\ kN$

Axial forces from post-tensioned tendons

$\sigma_{cintB} := \frac{N_{xB} + N_{yB}}{2 \cdot A_{cB}} = 1.241\ MPa$ Axial stress from post-tensioned tendons

The concrete shear capacity at the inner pile is (6.47):

$$v_{RdcintB} := \max\left(C_{Rdc} \cdot k_B \cdot \left(100 \cdot \rho_{lintB} \cdot f_{ck}\right)^{\frac{1}{3}} \cdot MPa^{\frac{2}{3}} + k_1 \cdot \sigma_{cintB},\ v_{minB} + k_1 \cdot \sigma_{cintB}\right) = 0.693\ MPa$$

The utilisation factors are: $\frac{v_{Ed1B}}{v_{RdcintB}} = 0.539$ $\frac{v_{Ed0B}}{v_{Rdmax}} = 0.18$

The necessary amount of shear reinforcement is then (6.52):

$$A_{swintB} := \max\left(\frac{\left(v_{Ed1B} - 0.75 \cdot v_{RdcintB}\right) \cdot u_{1internal} \cdot s_r}{1.5 \cdot f_{ywdefB}}, 0\right) = 0\ mm^2$$

Edge pile:

$v_{Ed0B} := \frac{\beta_{edge} \cdot V_{Ededge}}{u_{0edge} \cdot d_{topB}} = 0.976\ MPa$ Maximum shear stress at pile-head. Eq.(6.38)

$v_{Ed1B} := \frac{\beta_{edge} \cdot V_{Ededge}}{u_{1edge} \cdot d_{topB}} = 0.404\ MPa$ Maximum shear stress at control section. Eq.(6.38)

$A_{sedgeB} := 386\ mm^2$ Bonded tension steel area in the area around the pile-head plus 3d on each side

$\rho_{ledgeB} := \frac{A_{sedgeB}}{\left(c_{edge} + 6 \cdot d_{topB}\right) \cdot d_{topB}} = 9.425 \cdot 10^{-4}$

$N_{xB} := 2 \cdot P_{ULS} = 340.622\ kN$

$N_{yB} := 2 \cdot P_{ULS} = 340.622\ kN$

Axial forces from post-tensioned tendons

$\sigma_{cedgeB} := \frac{N_{xB} + N_{yB}}{2 \cdot A_{cB}} = 0.621\ MPa$ Axial stress from post-tensioned tendons

The concrete shear capacity at the corner pile is (6.47):

$$v_{RdcedgeB} := \max\left(C_{Rdc}\cdot k_B\cdot\left(100\cdot\rho_{ledgeB}\cdot f_{ck}\right)^{\frac{1}{3}}\cdot MPa^{\frac{2}{3}} + k_1\cdot\sigma_{cedgeB}, v_{minB} + k_1\cdot\sigma_{cedgeB}\right) = 0.631\ MPa$$

The utilisation factors area: $\frac{v_{Ed1B}}{v_{RdcedgeB}} = 0.64$ $\frac{v_{Ed0B}}{v_{Rdmax}} = 0.238$

The necessary amount of shear reinforcement is then (6.52):

$$A_{swedgeB} := \max\left(\frac{\left(v_{Ed1B} - 0.75\cdot v_{RdcedgeB}\right)\cdot u_{1edge}\cdot s_r}{1.5\cdot f_{ywdefB}}, 0\right) = 0\ mm^2$$

EC2:2021

$b_{05edge} := \frac{\pi\cdot d_{topB}}{2} + 2\cdot c_{edge} + c_{int} = \left(2.239\cdot 10^3\right)\ mm$ Length of control perimeter for edge pile

$b_{05internal} := \pi\cdot d_{topB} + 4\cdot c_{int} = \left(3.479\cdot 10^3\right)\ mm$ Length of control perimeter for internal piles

$\tau_{Rdcmin} := \frac{11\cdot MPa}{\gamma_V}\cdot\sqrt{\frac{f_{ck}\cdot d_{dg}}{f_{yd}\cdot d_{topB}}} = 0.935\ MPa$ Minimum shear stress resistance

$\tau_{Eedge} := \frac{\beta_{edge}\cdot V_{Eedge}}{b_{05edge}\cdot d_{topB}} = 0.588\ MPa$ Design shear stress acting on edge pile

$\tau_{Eint} := \frac{\beta_{internal}\cdot V_{Eint}}{b_{05internal}\cdot d_{topB}} = 0.592\ MPa$ Design shear stress acting on internal pile

The first check according to Eq.(8.71):

$\frac{\tau_{Eedge}}{\tau_{Rdcmin}} = 0.628$ $\frac{\tau_{Eint}}{\tau_{Rdcmin}} = 0.633$

Check ok, shear resistance of concrete cross-section nevertheless calculated for the purpose of comparison

$k_{pbint} := 3.6\cdot\sqrt{1 - \frac{b_{0int}}{b_{05internal}}} = 1.59$ $k_{pbedge} := 3.6\cdot\sqrt{1 - \frac{b_{0edge}}{b_{05edge}}} = 1.401$

$\rho_{lintB} = 0.002$ $\rho_{ledgeB} = 9.425\cdot 10^{-4}$

$$\tau_{Rdcint} := \frac{0.6 \cdot k_{pbint}}{\gamma_V} \cdot \left(100 \cdot \rho_{lintB} \cdot f_{ck} \cdot \frac{d_{dg}}{d_{topB}}\right)^{\left(\frac{1}{3}\right)} \cdot MPa^{\left(\frac{2}{3}\right)} = 0.697\ MPa$$

$$\tau_{Rdcedge} := \frac{0.6 \cdot k_{pbedge}}{\gamma_V} \cdot \left(100 \cdot \rho_{ledgeB} \cdot f_{ck} \cdot \frac{d_{dg}}{d_{topB}}\right)^{\left(\frac{1}{3}\right)} \cdot MPa^{\left(\frac{2}{3}\right)} = 0.501\ MPa$$

Solution C - Conventional and post-tensioned reinforcement, reduced slab height

EC2:2004

$d_{topC} := 158\ mm$ Reinforcement depth over piles

$u_{1edge} := 2 \cdot \pi \cdot d_{topC} + 2 \cdot c_{edge} + c_{int} = \left(2.893 \cdot 10^3\right)\ mm$

$u_{1internal} := 4 \cdot \pi \cdot d_{topC} + 4 \cdot c_{int} = \left(4.785 \cdot 10^3\right)\ mm$ Control section lengths

$$k_C := min\left(1 + \sqrt{\frac{200\ mm}{d_{topC}}}, 2\right) = 2$$

$v_{minC} := 0.035 \cdot k_C^{\frac{3}{2}} \cdot \sqrt{f_{ck} \cdot MPa} = 0.586\ MPa$ Minimum concrete shear capacity (NA.6.3N)

$u_{0edge} := min\left(c_{int} + 3 \cdot d_{topC}, c_{int} + 2 \cdot c_{edge}\right) = \left(1.174 \cdot 10^3\right)\ mm$ Length of area adjacent to corner pile-head

$f_{ywdefC} := min\left(250 \cdot MPa + \frac{0.25}{mm} \cdot d_{topC} \cdot MPa, f_{yd}\right) = 289.5\ MPa$ Effective design strength of punching shear reinforcement

$b_s := c_{int} + 6 \cdot d_{topC} = 1.648\ m$ Extended width

$A_{cC} := h_{red} \cdot b_s = 0.33\ m^2$ Concrete area

Internal pile:

$$v_{Ed0C} := \frac{\beta_{internal} \cdot V_{EdintC}}{u_{0internal} \cdot d_{topC}} = 0.875\ MPa$$ Maximum shear stress at pile-head. Eq.(6.38)

$$v_{Ed1C} := \frac{\beta_{internal} \cdot V_{EdintC}}{u_{1internal} \cdot d_{topC}} = 0.512\ MPa$$ Maximum shear stress at control section. Eq.(6.38)

$A_{sintC} := 477\ mm^2$ Bonded tension steel area in the area around the pile-head plus 3d on each side

$$\rho_{lintC} := \frac{A_{sintC}}{\left(c_{int} + 6 \cdot d_{topC}\right) \cdot d_{topC}} = 0.002$$

$N_{xC} := 9 \cdot P_{ULS} = \left(1.533 \cdot 10^3\right)\ kN$

$N_{yC} := 2 \cdot P_{ULS} = 340.622\ kN$

Axial forces from post-tensioned tendons

$\sigma_{cintC} := \frac{N_{xC} + N_{yC}}{2 \cdot A_{cC}} = 2.842\ MPa$ Axial stress from post-tensioned tendons

The concrete shear capacity at the inner pile is (6.47):

$$v_{RdcintC} := \max\left(C_{Rdc} \cdot k_C \cdot \left(100 \cdot \rho_{lintC} \cdot f_{ck}\right)^{\frac{1}{3}} \cdot MPa^{\frac{2}{3}} + k_1 \cdot \sigma_{cintC},\ v_{minC} + k_1 \cdot \sigma_{cintC}\right) = 0.87\ MPa$$

The utilisation factors are: $\frac{v_{Ed1C}}{v_{RdcintC}} = 0.588$ $\frac{v_{Ed0C}}{v_{Rdmax}} = 0.214$

The necessary amount of shear reinforcement is then (6.52):

$$A_{swintC} := \max\left(\frac{\left(v_{Ed1C} - 0.75 \cdot v_{RdcintC}\right) \cdot u_{1internal} \cdot s_r}{1.5 \cdot f_{ywdefC}}, 0\right) = 0\ mm^2$$

Edge pile:

$v_{Ed0C} := \frac{\beta_{edge} \cdot V_{EdedgeC}}{u_{0edge} \cdot d_{topC}} = 1.332\ MPa$ Maximum shear stress at pile-head. Eq.(6.38)

$v_{Ed1C} := \frac{\beta_{edge} \cdot V_{EdedgeC}}{u_{1edge} \cdot d_{topC}} = 0.541\ MPa$ Maximum shear stress at control section. Eq.(6.38)

$A_{sedgeC} := 386\ mm^2$ Bonded tension steel area in the area around the pile-head plus 3d on each side

$\rho_{ledgeC} := \frac{A_{sedgeC}}{\left(c_{edge} + 6 \cdot d_{topC}\right) \cdot d_{topC}} = 0.002$

$N_{xC} := 2 \cdot P_{ULS} = 340.622\ kN$

$N_{yC} := 2 \cdot P_{ULS} = 340.622\ kN$

Axial forces from post-tensioned tendons

$\sigma_{cedgeC} := \frac{N_{xC} + N_{yC}}{2 \cdot A_{cC}} = 1.033\ MPa$ Axial stress from post-tensioned tendons

The concrete shear capacity at the corner pile is (6.47):

$$v_{RdcedgeC} := \max\left(C_{Rdc}\cdot k_C\cdot\left(100\cdot\rho_{ledgeC}\cdot f_{ck}\right)^{\frac{1}{3}}\cdot MPa^{\frac{2}{3}} + k_1\cdot\sigma_{cedgeC}, v_{minC} + k_1\cdot\sigma_{cedgeC}\right) = 0.689\ MPa$$

The utilisation factors area: $\frac{v_{Ed1C}}{v_{RdcedgeC}} = 0.785$ $\frac{v_{Ed0C}}{v_{Rdmax}} = 0.325$

The necessary amount of shear reinforcement is then (6.52):

$$A_{swedgeC} := \max\left(\frac{\left(v_{Ed1C} - 0.75\cdot v_{RdcedgeC}\right)\cdot u_{1edge}\cdot s_r}{1.5\cdot f_{ywdefC}}, 0\right) = 15.954\ mm^2$$

EC2:2021

$b_{05edge} := \frac{\pi\cdot d_{topC}}{2} + 2\cdot c_{edge} + c_{int} = \left(2.148\cdot 10^3\right)\ mm$ — Length of control perimeter for edge pile

$b_{05internal} := \pi\cdot d_{topC} + 4\cdot c_{int} = \left(3.296\cdot 10^3\right)\ mm$ — Length of control perimeter for internal piles

$\tau_{Rdcmin} := \frac{11\cdot MPa}{\gamma_V}\cdot\sqrt{\frac{f_{ck}\cdot d_{dg}}{f_{yd}\cdot d_{topC}}} = 1.093\ MPa$ — Minimum shear stress resistance

$\tau_{Ededge} := \frac{\beta_{edge}\cdot V_{EdedgeC}}{b_{05edge}\cdot d_{topC}} = 0.728\ MPa$ — Design shear stress acting on edge pile

$\tau_{Edint} := \frac{\beta_{internal}\cdot V_{EdintC}}{b_{05internal}\cdot d_{topC}} = 0.743\ MPa$ — Design shear stress acting on internal pile

The first check according to Eq.(8.71):

$\frac{\tau_{Ededge}}{\tau_{Rdcmin}} = 0.666$ $\frac{\tau_{Edint}}{\tau_{Rdcmin}} = 0.68$

Check ok, shear resistance of concrete cross-section nevertheless calculated for the purpose of comparison

$k_{pbint} := 3.6\cdot\sqrt{1 - \frac{b_{0int}}{b_{05internal}}} = 1.397$ $k_{pbedge} := 3.6\cdot\sqrt{1 - \frac{b_{0edge}}{b_{05edge}}} = 1.224$

$\rho_{lintC} := 0.0008$ $\rho_{ledgeC} := 0.0007$

$$\tau_{Rdcint} := \frac{0.6 \cdot k_{pbint}}{\gamma_V} \cdot \left(100 \cdot \rho_{lintC} \cdot f_{ck} \cdot \frac{d_{dg}}{d_{topC}}\right)^{\left(\frac{1}{3}\right)} \cdot MPa^{\left(\frac{2}{3}\right)} = 0.525\ MPa$$

$$\tau_{Rdcedge} := \frac{0.6 \cdot k_{pbedge}}{\gamma_V} \cdot \left(100 \cdot \rho_{ledgeC} \cdot f_{ck} \cdot \frac{d_{dg}}{d_{topC}}\right)^{\left(\frac{1}{3}\right)} \cdot MPa^{\left(\frac{2}{3}\right)} = 0.44\ MPa$$

Solution D - Conventional, post-tensioned and fiber reinforcement

$d_{mtop} := 224\ mm$

$d_v := d_{mtop} = 0.224\ m$ — Shear resisting effective depth

$b_{0i} := 4 \cdot c_{int} = 2.8\ m$ — Perimeter of the loaded area for inner columns

$b_{0.5i} := b_{0i} + \pi \cdot d_v = 3.504\ m$ — Control perimeter for inner columns

$b_{0e} := c_{int} + 2 \cdot c_{edge} = 1.9\ m$ — Perimeter of the loaded area for edge columns

$b_{0.5e} := b_{0e} + \pi \cdot \frac{d_v}{2} = 2.252\ m$ — Control perimeter for edge columns

$\tau_{Edi} := \beta_{internal} \cdot \frac{V_{Edint}}{b_{0.5i} \cdot d_v} = 0.567\ MPa$ — Design shear stress

$\tau_{Ede} := \beta_{edge} \cdot \frac{V_{Ededge}}{b_{0.5e} \cdot d_v} = 0.563\ MPa$ — Design shear stress

$\tau_{Rdcmin} := \frac{11}{\gamma_V} \cdot \sqrt{\frac{f_{ck}}{f_{yd}} \cdot \frac{d_{dg}}{d_v}} \cdot MPa = 0.918\ MPa$ — Minimum shear stress capacity

The minimum value is sufficient, but the capacities are still calculated for better comparing, even though it is not needed according to new Eurocode

$\rho_l := \frac{A_s}{b \cdot d_v} \cdot m = 0.002$ — Reinforcement ratios of bonded flexural reinforcement

$k_{pbi} := 3.6 \cdot \sqrt{1 - \frac{b_{0i}}{b_{0.5i}}} = 1.613$ — Punching shear gradient enhancement coefficient

$k_{pbe} := 3.6 \cdot \sqrt{1 - \frac{b_{0e}}{b_{0.5e}}} = 1.423$ — Punching shear gradient enhancement coefficient

$1.0 < k_{pb} > 2.5$

$\tau_{Rdcmax} := \frac{0.6}{\gamma_V} \cdot \sqrt{f_{ck} \cdot \mathit{MPa}} = 2.535\ \mathit{MPa}$ Max shear stress capacity

Shear stress capacity

$$\tau_{Rdci} := \frac{0.6}{\gamma_V} \cdot k_{pbi} \cdot \left(100 \cdot \rho_l \cdot f_{ck} \cdot \frac{d_{dg}}{d_v} \cdot \frac{1}{\mathit{MPa}}\right)^{\frac{1}{3}} \cdot \mathit{MPa} = 0.684\ \mathit{MPa}$$

$$\tau_{Rdce} := \frac{0.6}{\gamma_V} \cdot k_{pbe} \cdot \left(100 \cdot \rho_l \cdot f_{ck} \cdot \frac{d_{dg}}{d_v} \cdot \frac{1}{\mathit{MPa}}\right)^{\frac{1}{3}} \cdot \mathit{MPa} = 0.603\ \mathit{MPa}$$

$\tau_{Rdci} := \tau_{Rdcmin} = 0.918\ \mathit{MPa}$ Shear stress capacity when minimum value is considered

$\tau_{Rdce} := \tau_{Rdcmin} = 0.918\ \mathit{MPa}$ Shear stress capacity when minimum value is considered

$\eta_{ci} := \frac{\tau_{Rdci}}{\tau_{Edi}} = 1.619$ $\eta_{ce} := \frac{\tau_{Rdce}}{\tau_{Ede}} = 1.63$ $\eta_c \leq 1.0$ (L.23)

$\eta_{ci} := 1.0$ $\eta_{ce} := 1.0$

$\tau_{RdcFi} := \eta_{ci} \cdot \tau_{Rdci} + f_{Ftud} = 2.118\ \mathit{MPa}$ Shear stress capacity with fiber contribution

$\tau_{RdcFe} := \eta_{ce} \cdot \tau_{Rdce} + f_{Ftud} = 2.118\ \mathit{MPa}$ Shear stress capacity with fiber contribution

Solution E - Post-tensioned and fiber reinforcement

$d_v := 216\ mm$ Shear resisting effective depth

$A_s := 0\ mm^2$ Bonded reinforcement

$b_{0i} := 4 \cdot c_{int} = 2.8\ m$ Perimeter of the loaded area for inner columns

$b_{0.5i} := b_{0i} + \pi \cdot d_v = 3.479\ m$ Control perimeter for inner columns

$b_{0e} := c_{int} + 2 \cdot c_{edge} = 1.9\ m$ Perimeter of the loaded area for edge columns

$b_{0.5e} := b_{0e} + \pi \cdot \frac{d_v}{2} = 2.239\ m$ Control perimeter for edge columns

$\tau_{Edi} := \beta_{internal} \cdot \frac{V_{Edint}}{b_{0.5i} \cdot d_v} = 0.592\ MPa$ Design shear stress

$\tau_{Ede} := \beta_{edge} \cdot \frac{V_{Ededge}}{b_{0.5e} \cdot d_v} = 0.588\ MPa$ Design shear stress

$\tau_{Rdcmin} := \frac{11}{\gamma_V} \cdot \sqrt{\frac{f_{ck}}{f_{yd}} \cdot \frac{d_{dg}}{d_v}} \cdot MPa = 0.935\ MPa$ Minimum shear stress capacity

No further check is needed

$\rho_l := \frac{A_s}{b \cdot d_v} = 0$ Reinforcement ratios of bonded flexural reinforcement

$k_{pbi} := 3.6 \cdot \sqrt{1 - \frac{b_{0i}}{b_{0.5i}}} = 1.59$ Punching shear gradient enhancement coefficient

$k_{pbe} := 3.6 \cdot \sqrt{1 - \frac{b_{0e}}{b_{0.5e}}} = 1.401$ Punching shear gradient enhancement coefficient

$1.0 < k_{pb} > 2.5$

$\tau_{Rdcmax} := \frac{0.6}{\gamma_V} \cdot \sqrt{f_{ck} \cdot MPa} = 2.535\ MPa$ Max shear stress capacity

$$\tau_{Rdci} := \frac{0.6}{\gamma_V} \cdot k_{pbi} \cdot \left(100 \cdot \rho_l \cdot f_{ck} \cdot \frac{d_{dg}}{d_v} \cdot \frac{1}{MPa}\right)^{\frac{1}{3}} \cdot MPa = 0\ MPa$$ Shear stress capacity

$$\tau_{Rdce} := \frac{0.6}{\gamma_V} \cdot k_{pbe} \cdot \left(100 \cdot \rho_l \cdot f_{ck} \cdot \frac{d_{dg}}{d_v} \cdot \frac{1}{MPa}\right)^{\frac{1}{3}} \cdot MPa = 0\ MPa$$ Shear stress capacity

$\tau_{Rdci} := \tau_{Rdcmin} = 0.935\ MPa$ Shear stress capacity when minimum value is considered

$\tau_{Rdce} := \tau_{Rdcmin} = 0.935\ MPa$ Shear stress capacity when minimum value is considered

$\eta_{ci} := \frac{\tau_{Rdci}}{\tau_{Edi}} = 1.579$ $\eta_{ce} := \frac{\tau_{Rdce}}{\tau_{Ede}} = 1.591$ $\eta_c \leq 1.0$ (L.23)

$\eta_{ci} := 1.0$ $\eta_{ce} := 1.0$

$\tau_{RdcFi} := \eta_{ci} \cdot \tau_{Rdci} + f_{Ftud} = 2.135\ MPa$ Shear stress capacity with fiber contribution

$\tau_{RdcFe} := \eta_{ce} \cdot \tau_{Rdce} + f_{Ftud} = 2.135\ MPa$ Shear stress capacity with fiber contribution

Solution F - Fiber reinforcement

NB 38:

$\tau_{RdcF} := f_{Ftud} = 1.2\ MPa$ Shear stress capacity with fiber contribution

For this solution, there is no d, so the formulae given in New Eurocode is not usable. However, the punching shear capacity given above is higher than the design punching shear for the other solutions.

Lars Dalhaug & Torgeir Tveraaen

Effect of fiber and post-tensioned reinforcement on pile supported ground slabs

NTNU
Kunnskap for en bedre verden